Title
Massively Parallel Delivery of Large-sized Cargo into Mammalian Cells with Light Pulses

Author
Wu, Yi-Chien

Publication Date
2014

Peer reviewed|Thesis/dissertation

UNIVERSITY OF CALIFORNIA

Los Angeles

Massively Parallel Delivery of Large-sized Cargo into Mammalian Cells with Light Pulses

A dissertation submitted in partial satisfaction of the

requirements for the degree Doctor of Philosophy

in Mechanical Engineering

by

Yi-Chien Wu

2014

ABSTRACT OF THE DISSERTATION

Massively Parallel Delivery of Large-sized Cargo into Mammalian Cells

with Light Pulses

by

Yi-Chien Wu

Doctor of Philosophy in Mechanical Engineering

University of California, Los Angeles, 2014

Professor Pei-Yu Chiou, Chair

Enabling technologies that transfer micron-sized objects into mammalian cells are needed to advance key applications in cell engineering. High-throughput delivery of organelles, modified intracellular pathogens, enzymes, proteins, and other types of cargo is required to obtain reliable data in settings of cellular heterogeneity. Delivered objects must also avoid entrapment in cell vacuoles or endosomes to retain functionality. Here, we report a massively parallel photothermal microfluidic platform for high-throughput delivery of large cargo directly into the cytosol of mammalian cells. Micron-sized cargo is reproducibly delivered in up to 100,000 cells on the platform in a minute, with parameters for cargo delivery tunable for each cell and cargo type. The delivery platform is a compact silicon chip on which hundreds of thousands of micron-sized cavitation bubbles expand and collapse within nanoseconds in response to pulsed laser excitation. Cavitation bubbles are formed by rapid heat transfer from nearby metallic nanostructures via a

photothermal process enhanced by the lightning-rod effect. High speed, localized fluid flows near cavitation bubbles puncture contacting cell membranes with precision, resulting in micron-sized transient membrane pores. Applied pressure provides an active driving force to speed slow diffusing large cargo through these transient pores before membrane repair and resealing. We have reproducibly delivered large cargo including micron-sized bacteria, enzymes, antibodies, and functional nanoparticles into a variety of cell lines, including three different types of primary cells, with high efficiency and high cell viability. Our experiments involving delivery of functional enzymes, antibodies and vacuole escape-incompetent bacteria prove that cargo is delivered directly into the cell cytosol on this platform, bypassing endocytosis. Massively parallel and nearly simultaneous delivery of cargo into cells under the same physiological conditions enables reliable statistical measurements of cargo interactions with cells over time. To demonstrate its utility, we used this platform to explore the intracellular lifestyle of *Francisella novicida* and discovered that the *iglC* gene is unexpectedly required for intracellular replication even after vacuolar escape into the cell cytosol. Our photothermal platform approach, termed BLAST (*B*iophotonic *L*aser *A*ssisted *S*urgery *T*ool), provides a reliable mechanism for high-throughput engineering of cells with micron-sized natural and man-made materials.

The dissertation of Yi-Chien Wu is approved.

Chih-Ming Ho

Yong Chen

Michael A. Teitell

Pei-Yu Chiou, Committee Chair

University of California, Los Angeles

2014

Contents

List of Figures

Acknowledgments

First, I would like to thank my advisor, Prof. Pei-Yu Chiou, for his patience, guidance and support on my research in the past five years. I would also like to thank Prof. Michael Teitell for his countless discussion about biological knowledge. This dissertation would not be completed without their fully support. Besides, I also thank Prof. Chih-Ming Ho and Prof. Yong Chen for all of their time spent in reading my dissertation and providing professional suggestion.

During my doctoral study, I got lots of help from my colleagues in Optofluidics Systems Lab. I especially thank Dr. Ting-Hsiang Wu for all of her invaluable help. Dr. Daisuke Yamane, Dr. Kuo-Wei Huang, Dr. Yu-Jui Fan, Dr. Ming-Yu Lin, Dr. Thomas Zangle, Yu-Chun Kung and Ximiao Wen are also contributing their efforts to my research projects. I would like to thank Dr. Daniel Clemens and Dr. Bai-Yu Lee from Prof. Horwtz's Lab for their cheerful cooperation with several pioneering experiments. I also thank Dr. Kayvan Niazi and Dr. Shahrooz Rabizadeh from CNSI for their helpful discussion. It is my great pleasure to work with these excellent researchers.

Last, I would like to thank my family, especially my parents and my grandmother, for their understanding and selfless devotion. It is impossible for me to fully focus on my research as long as seven years without their endless support.

Vita

Education

2008-2010 M.S., Electrical and Computer Engineering
University of California at San Diego (UCSD), La Jolla, California

2001-2005 B.S., Engineering and System Science
National Tsing-Hua University, Hsinchu, Taiwan

Publications and Presentations

[1] **Y.-C. Wu**, T.-H. Wu, D. L. Clemens, B.-Y. Lee, X. Wen, M. A. Horwitz, M. A. Teitell, P.-Y. Chiou, "Massively parallel delivery of large-sized cargo into mammalian cells with light pulses," *Nat. Methods* (under review)

[2] D. Yamane, **Y.-C. Wu**, T.-H. Wu, H. Toshiyoshi, M. A. Teitell, P.-Y. Chiou, "Electrical impedance monitoring of photothermal porated mammalian cells," *J. Lab. Autom.*, 19, pp. 50-59, 2014

[3] Y.-J. Fan, **Y.-C. Wu**, Y. Chen, Y.-C. Kung, T.-H. Wu, K.-W. Huang, H.-J. Sheen, P.-Y. Chiou, "Three dimensional microfluidics with implanted microball lens array for parallel and high throughput multicolor fluorescence detection," *Biomicrofluidics*, 7, 044121, 2013

[4] T.-H. Wu, **Y.-C. Wu**, E. Sagullo, M. A. Teitell, P.-Y. Chiou," Direct nuclear delivery of DNA macromolecules using the photothermal nanoblade," IEEE/LEOS International Conference on Optical MEMS and Nanophotonics, pp. 77-78, Aug. 2013

[5] K.-W. Huang, Y.-C. Kung, **Y.-C. Wu**, Y.-J. Fan, P.-Y. Chiou," Optoelectronic tweezers integrated with 3D microfluidic networks," IEEE/LEOS International Conference on Optical MEMS and Nanophotonics, pp. 79-80, Aug. 2013

[6] Y.-J. Fan, Y. Chen, **Y.-C. Wu**, T.-H. Wu, H.-J. Sheen, P.-Y. Chiou, "Multicolor ultrahigh throughput parallel microfluidic flow cytometer," IEEE International Conference on Solid-State Sensors, Actuators and Microsystems (Transducers '13), pp. 2556 - 2559, Jun. 2013

[7] K.-W. Huang, **Y.-C. Wu**, J.-A. Lee, P.-Y. Chiou," Microfluidic integrated optoelectronic tweezers for single-cell preparation and analysis," *Lab Chip*, 13, pp. 3721 - 3727, 2013

[8] Y.-J. Fan, Y.-C. Kung, **Y.-C. Wu**, K.-W. Huang, T.-H. Wu, Y. Chen, H.-J. Sheen, P.-Y. Chiou, "High throughput fluorescence based flow cytometer using 3D microfluidics for parallel

sheath flow focusing and embedded high N.A. microlens," The 15th International Conference on Miniaturized Systems for Chemistry and Life Sciences (μTAS), pp.1-3, Oct. 2012

[9] K.-W. Huang, **Y.-C. Wu**, S. Sattar, J.-A. Lee, P.-Y. Chiou, "Microfluidic integrated optoelectronic tweezers for single cell sample prepation and analysis," The 15th International Conference on Miniaturized Systems for Chemistry and Life Sciences (μTAS), pp.1-3, Oct. 2012

[10] D. Yamane, **Y.-C. Wu**, T.-H. Wu, H. Toshiyoshi, M. A. Teitell, P.-Y. Chiou, " Real-time monitoring of photothermally porated mammalian cells by electric impedance sensors," IEEE/LEOS International Conference on Optical MEMS and Nanophotonics, pp. 1-2, Aug. 2012.

[11] Y.-T. Tseng, Y.-J. Chuang, **Y.-C. Wu**, C.-S. Yang, M.-C. Wang, F.-G. Tseng, "A gold-nanoparticle-enhanced immune sensor based on fiber optic interferometry", *Nanotechnology*, 19, 345501, 2008

[12] Y.-T. Tseng, **Y.-C. Wu**, C.-S. Yang, M.-C. Wang, F.-G. Tseng, "Gold-nanoparticle enhanced in-situ immunosensor based on fiber-optical Fabry-Perot interferometry", IEEE Conference on Nanotechnology, pp. 845-848, Jul. 2005

[13] Y.-T. Tseng, **Y.-C. Wu**, C.-S. Yang, M.-C. Wang, F.-G. Tseng, "Gold-nanoparticle enhanced fiber sensor based on Fabry-Perot interferometry," IEEE International Conference on Solid-State Sensors, Actuators and Microsystems (Transducers '05), pp. 1764-1767, Jun. 2005

Patents

[1] **Y.-C. Wu**, T.-H. Wu, P.-Y. Chiou, M. A. Teitell, "High-Throughput Cargo Delivery into Live Cells Using Photothermal Platforms," U.S. Patent Application No. 61/799,222, March 15th, 2013

Chapter 1

Introduction

Efficient large cargo delivery into living cells is an extremely desirable technique for many fields of biological research, especially the cell engineering, intracellular biology and gene therapy. However, no matter biological, chemical or physical methodologies for introducing large cargo, such as organelles and intracellular pathogens, into mammalian cells do not exist[1]. Biological approaches such as viruses can provide high transfer efficiency[2-5] but are restricted to kb-sized nucleic acids. Besides, immunogenicity and cytotoxcity are the major drawbacks of virus-mediated transfection. An inflammatory reaction and mutation might be caused when the viral vectors randomly integrate with the host genome. Chemical methods, such as non-viral gene therapy techniques[6-12], utilizing lipids[13], cationic polymers[14], or insoluble precipitates are the most widely used techniques in biological research. These methods frequently show undesirable endosome trapping of delivered cargo and their transfection efficiency is dependent on cell type. The efficiency can be improved by the help of magnetic force, called megnetofection[15]. Delivery vectors are associated with magnetic nanoparticles and concentrated on the target cells by an external magnetic field.

Most physical approaches[16-23] bypass endocytosis and require two-steps: (1) disruption of the plasma membrane to create one or more transient pores and (2) delivery of cargo across pores

into the cytosol. To create transient pores, electroporation[24-43] utilizes electrostatic pressure to disrupt the cell membrane; sonoporation[44-47] generates acoustic waves that induce cavitation bubbles with strong fluid flows; optoporation[48-64] utilizes nonlinear optical absorption triggered by short laser pulses to transiently break down the cell membrane at a focal point or induces photothermal bubbles to damage cell membrane; nanomechanical needles[65-69] and tubes[70-74] utilize sharp nanoscale tips; and other mechanical forces utilize microchannels[75] and beads[76, 77]. All of these mechanisms are limited to delivery of small cargo since they can only create small pores on cell membrane or rely on thermal diffusion for cargo transit across transient membrane pores. Slowly diffusing large cargo has little chance to transit pores before membrane resealing. Microinjection[78-85] uses a sharp glass tip to insert target cell for delivery. However, the tip size is typically smaller than 500 nm in diameter to penetrate the flexible cell membrane[66]. Otherwise, this technique is very labor-intensive and throughput is low even controlled by automatic robot system.

A recent hybrid approach called a photothermal nanoblade utilizes a metal-coated glass pipette to harvest laser energy and generate localized cavitation bubble to cut cell membrane[86-89]. It opens large 2 – 3 μm membrane pores with providing active pressure to drive slow diffusing large cargo into the cytosol. The wide range of deliverable cargo, including DNA, RNA, 200 nm plystyrene beads and 2 μm bacteria, was delivered into several mammalian cell types. However, this micropipette-based method suffers from low throughput limiting their usefulness for applications that require large numbers of cells or for rare, stochastic intracellular events.

To overcome this field block, we developed a massively parallel photothermal microfluidic platform, termed BLAST (Biophotonic Laser Assisted Surgery Tool), to deliver micron-sized cargo into ~100,000 cells in 10 seconds, providing a ~10^5- fold enhanced throughput compared

with the photothermal nanoblade[86]. A wide range of cargo including live micron-sized bacteria, enzymes, antibodies, and functional nanoparticles have been successfully delivered into a variety of cell types, including three types of primary cells [human peripheral blood monocyte-derived macrophages (PB-MDMs), primary normal human dermal fibroblasts (NHDFs), and human primary renal proximal tubule epithelial cells (RPTECs)] and one cancer cell line (HeLa), at high efficiency and high cell viability.

As a demonstration of the utility of the BLAST platform, we have used it to examine whether the *iglC* gene of *Francisella novicida*, a gene on the Francisella Pathogenicity Island (FPI)[90] known to be required for vacuolar permeabilization and escape into the cytosol, is also required for cytosolic replication of the bacteria following escape. By synchronous and efficient cytosolic delivery of these micron-sized bacteria in a way that bypasses the vacuolar stage, we were able to demonstrate the surprising finding that *iglC* is required not just for vacuolar escape but also for cytosolic replication.

Chapter 2

BLAST Platform for Large Cargo Delivery into Mammalian Cells

A silicon-based device integrated with fluid pumping system, named Biophotonic Laser Assisted Surgery Tool (BLAST), was developed for micron-sized cargo delivery into mammalian cells. The device mechanism, design, fabrication and operation were described. Three types of primary cells, including normal human dermal fibroblasts (NHDFs), human peripheral blood monocyte-derived macrophages (PB-MDMs), and human primary renal proximal tubule epithelial cells (RPTECs) and one cancer cell line (HeLa) were used to demonstrate the outstanding performance (high delivery efficiency and high cell viability) of BLAST platform.

2.1 Device principle and structure

2.1.1 Principle

BLAST utilizes laser energy harvested by the metallic titanium thin films in each trans-film hole to induce rapid heating and vaporization of adjacent thin water layers to trigger cavitation bubbles that cause disruption of a contacting cell membrane[91-95]. Electromagnetic waves to excite the oscillation of electrons in the well-deposited titanium nanostructures, whose kinetic

energy is converted into lattice heat, which rapidly raises their temperature. This heat propagates into the surrounding aqueous media through thermal conduction. When a thin layer of water adjacent to the metal hot spots is heated to near its critical temperature, rapidly expanding cavitation bubbles are triggered. These small bubbles can cut the cell membrane locally and minimize the damages of the cells. After membrane cutting, the external fluidic pumping system drives the delivered cargo into cell cytosol before transient membrane pores recovering (Fig. 2.1). This active flow can highly improve the delivery efficiency of large samples, especially micron-sized cargo, due to their slow diffusion speed.

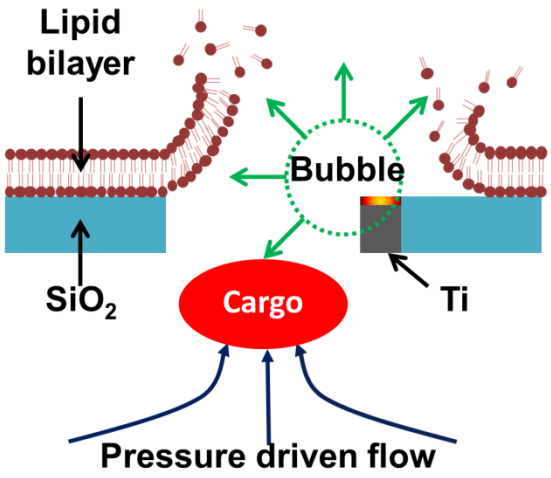

Figure 2.1 | Mechanism of a photothermal platform for large cargo delivery. Rapid pulsed laser shining the titanium-coated region on the chip triggers cavitation bubbles in all holes that disrupt contacting cell membranes. Following hole opening, an external pressure driven flow to push cargo into the cytosol of cells via transient membrane pores.

2.1.2 Platform structure

Figure 2.2 illustrates the BLAST platform structure. The platform consists of a silicon chip with a 1.5 μm thick porous SiO_2 membrane on top providing an array of micron-wide, trans-film

holes. Crescent-shaped titanium films are asymmetrically coated on the sidewalls of these holes through a directional electron beam evaporation method to harvest laser pulse energy. Rapid

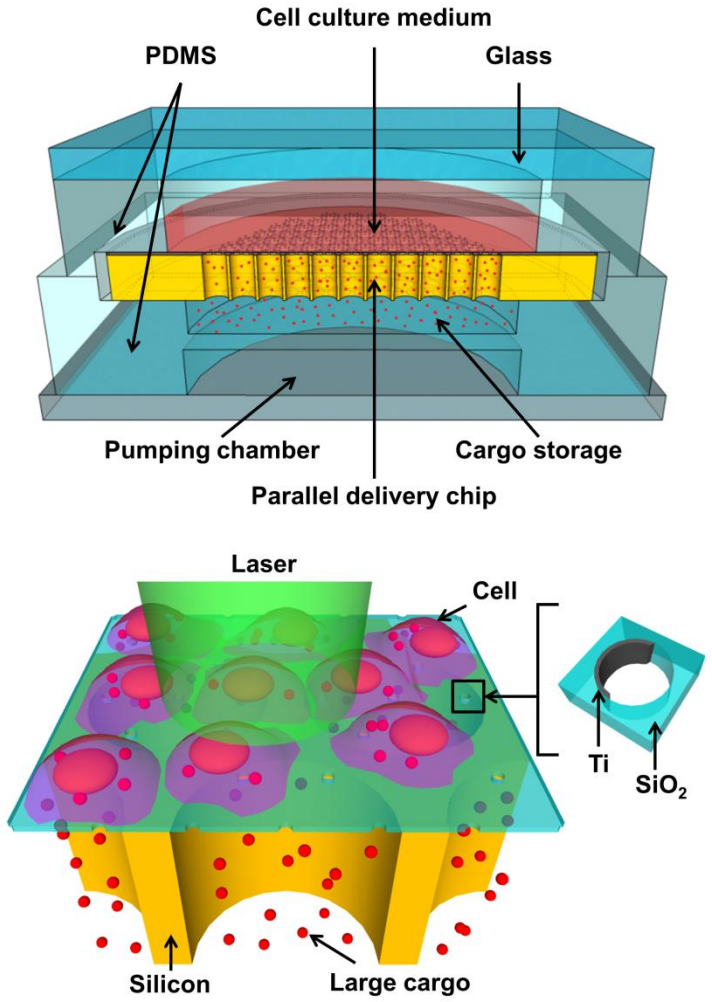

Figure 2.2 | Schematic of a massively parallel photothermal platform for large cargo delivery.

pulsed laser scanning of the entire active photothermal region on the chip triggers cavitation bubbles in all holes that disrupt contacting cell membranes. Following hole opening, an external pressure source is applied to fill the bottom pumping chamber and deform the flexible polydimethylsiloxane (PDMS, Dow Corning) storage chamber to push cargo into the cytosol of cells via transient membrane pores. A chip with an active area of 1 cm^2 can provide parallel

delivery to 100,000 cells in 1 minute. A green light (λ = 532 nm) nanosecond pulse laser (Minilite, Continuum) with a pulse energy at 10 mJ and a repetition rate of 15 Hz in utilized in the current setup for laser pulsing the BLAST chip.

The size of BLAST chip is a little bit smaller than a quarter (2 cm in diameter). In order to handle the chip easier, there is a 5 mm solid silicon ring area outside the fragile delivery region (Fig. 2.3). SEM images show a 100 nm thick titanium thin film coated on the inner sidewall of a 3 μm hole on the SiO_2 membrane through a lift-off process using the e-beam evaporation method. The two ends of this film are tapered and form sharp tips.

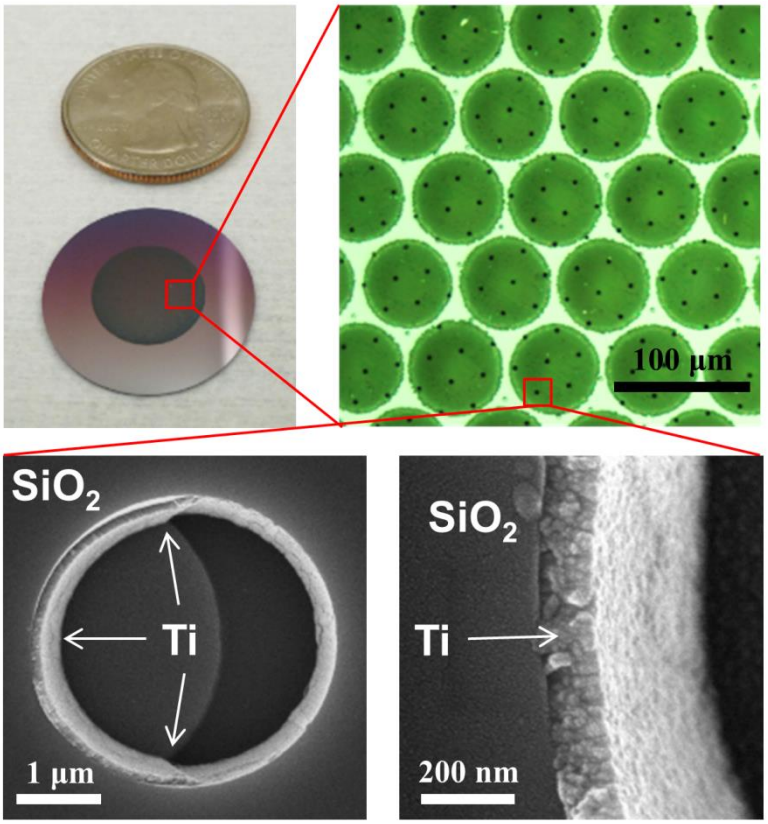

Figure 2.3 | Microscope and SEM images for BLAST chip.

2.1.3 Hot spots generated on the titanium thin film

To characterize the laser-induced cavitation bubbles on BLAST chip, a 3D finite element analysis (FEA) method was used to simulate the distribution of heat generation nearby the delivery hole (COMSOL). In Figure 2.4, the structure was drawn based on the real dimension of delivery hole shown in Figure 2.3. Three materials, including 100 nm thick titanium coating (n_{Ti} = 1.86 + 2.56 i)[96], SiO_2 thin film (n_{glass} = 1.46) and surrounding water region (n_{water} = 1.34), were defined in the regions shown in Figure 2.4. The structure is symmetric perfectly. So half of the region included for simulation is enough to describe the complete phenomenon and the software can be run under finer mesh due to smaller calculated domain.

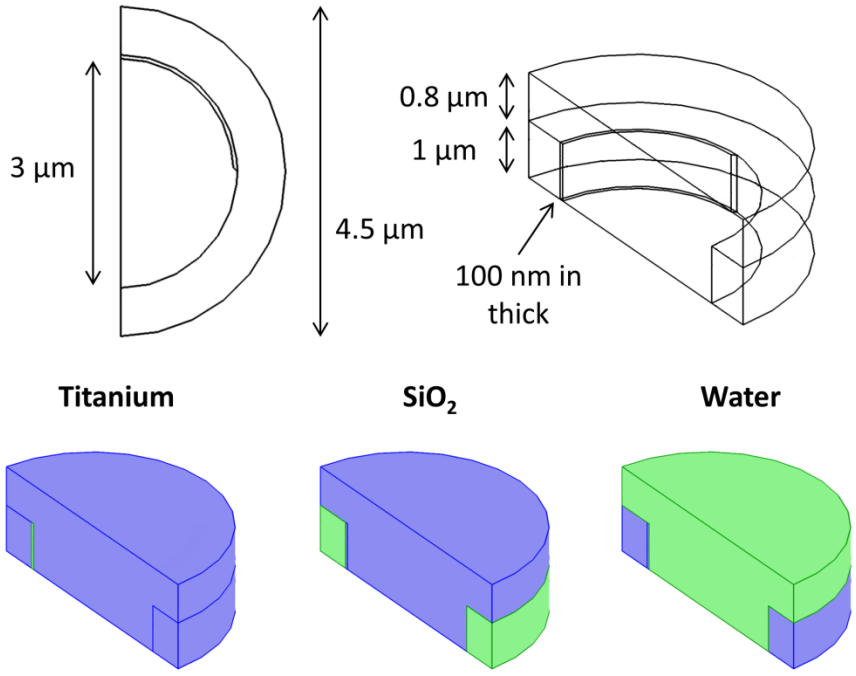

Figure 2.4 | 3D structures and parameters for FEA simulation.

Plane wave with wavelength of 532 nm propagated in the direction perpendicular to the surface of SiO_2 thin film. In Figure 2.5, two directions of polarization were used and the distributions of heat generation by laser shining were calculated. The hottest spots for both of

polarizing directions were located at two tips of the crescent-shaped titanium film. The rest of thin film was heated up quite uniform by the absorption of the laser light. In our case, the shape and size of cavitation bubbles are not sensitive for the direction of laser polarization.

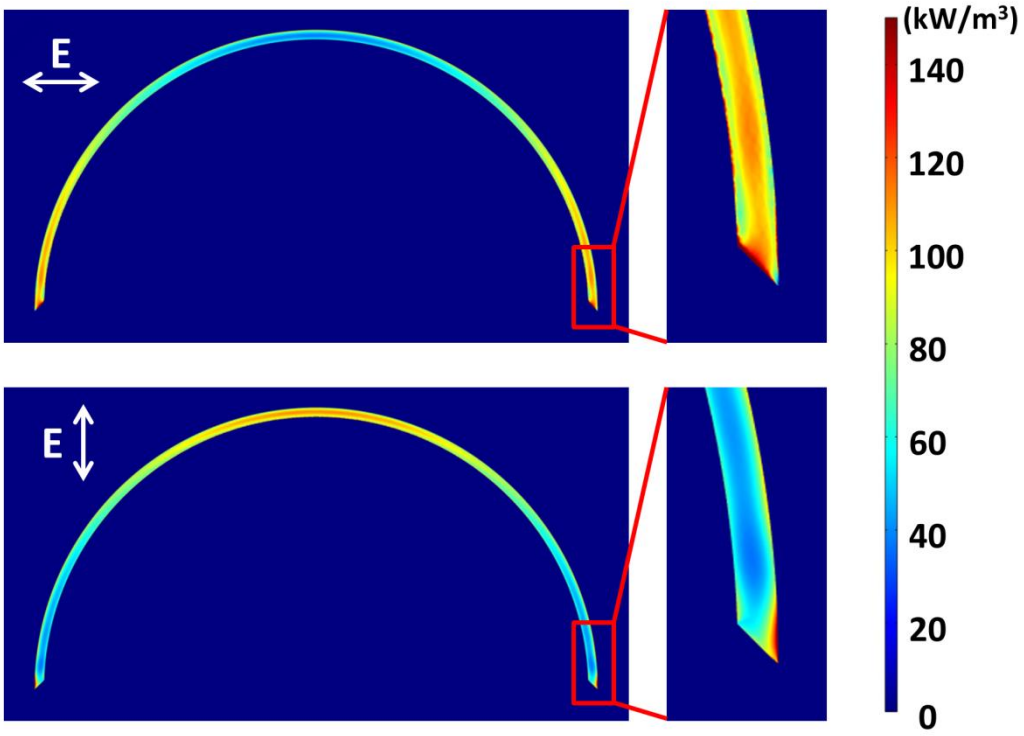

Figure 2.5 | 3D FEA simulation to get the distribution of heat generation by laser shining.

2.1.4 Cavitation bubble dynamics

The laser-induced cavitation bubbles on BLAST chip are in the size of a few microns depending on the laser energy. These small bubbles expand and collapse within hundreds of nanoseconds. The regular camera has no chance to capture this kind of ultra-fast bubble dynamic images. The time-resolved imaging system shown in Figure 2.6 was built for observation of these cavitation bubbles. The BLAST chip was sandwiched between two cover glasses with

water immersed and located on an inverted microscope stage. The pulsed laser beam was split into two light paths, one for bubble excitation and another for illumination, by a polarizing beam splitter. The laser pulse for bubble excitation was guided into the inverted microscope and went through the objective lens (40X or 100X) to focus on the sample plane. The light for illumination passed through a fluorescent dye cell and the emission light (λ = 698 nm) was collected into a multimode optical fiber (Thorlabs). A nanosecond time delay between the excitation laser pulsing and captured bubble image is controlled by the length of the optical fiber. The delay time per one meter fiber can be calculated by the light speed in optical fiber. The speed of light in the fiber is around 2×10^8 m/sec and we can get 5 nanoseconds delay per one meter fiber length.

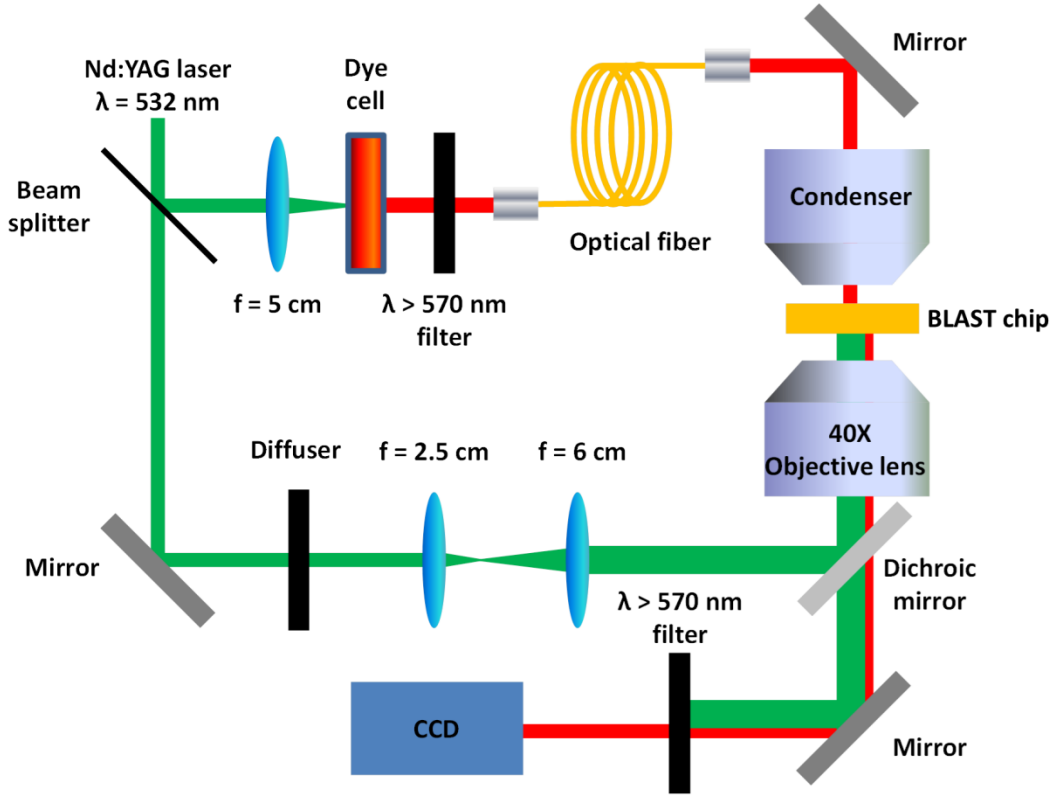

Figure 2.6 | Experiment setup for time-resolved imaging. A nanosecond time delay images for the photothermal induced bubble after laser pulsing were captured by controlling the length of the optical fiber.

Figure 2.7 shows the time-resolved images capturing rapidly expanding cavitation bubbles triggered in a 3 μm hole from 10 to 110 nanoseconds after laser pulsing. At 10-50 nanoseconds, two bubbles form and enlarge at the upper and lower poles of the hole; at 55 nanoseconds, the bubbles coalesce; and by 110 nanoseconds, the bubbles collapse. Cavitation bubbles initiate at the two tips of the crescent shaped titanium film, which is the location of the hottest spots (Ch 2.1.3). Local electric field enhancement occurs due to the lightning-rod effect, a non-resonant (broadband) phenomenon that originates near a sharp metal corner.

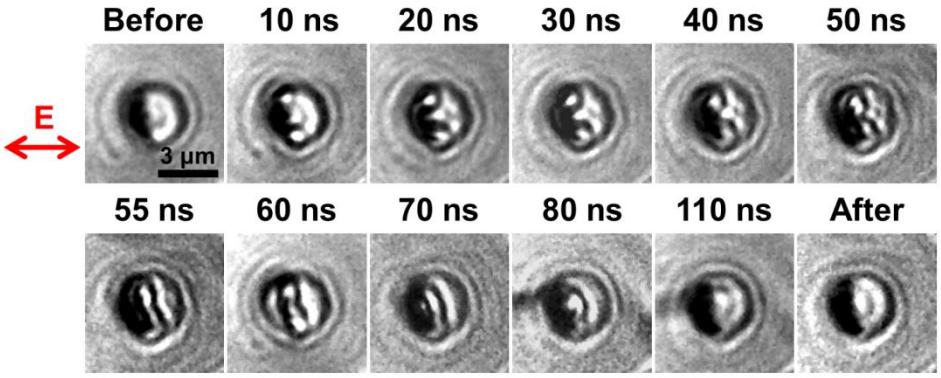

Figure 2.7 | Time-resolved images showing a laser triggered, rapidly expanding cavitation bubble in a platform hole.

Cavitation bubbles are initiated at the two tips of the tapered titanium film due to the lighting-rod enhancement effect near sharp metal tips. This is a non-resonant broadband effect and is also insensitive to light polarization on our platform. Figure 2.8 shows the bubble size is dependent on the laser fluence and not related to the polarization. Higher pulse energy generates larger sized cavitation bubbles with longer lifetimes. The lifetime of bubbles triggered by nanosecond laser pulses typically lasts for a few hundred nanoseconds.

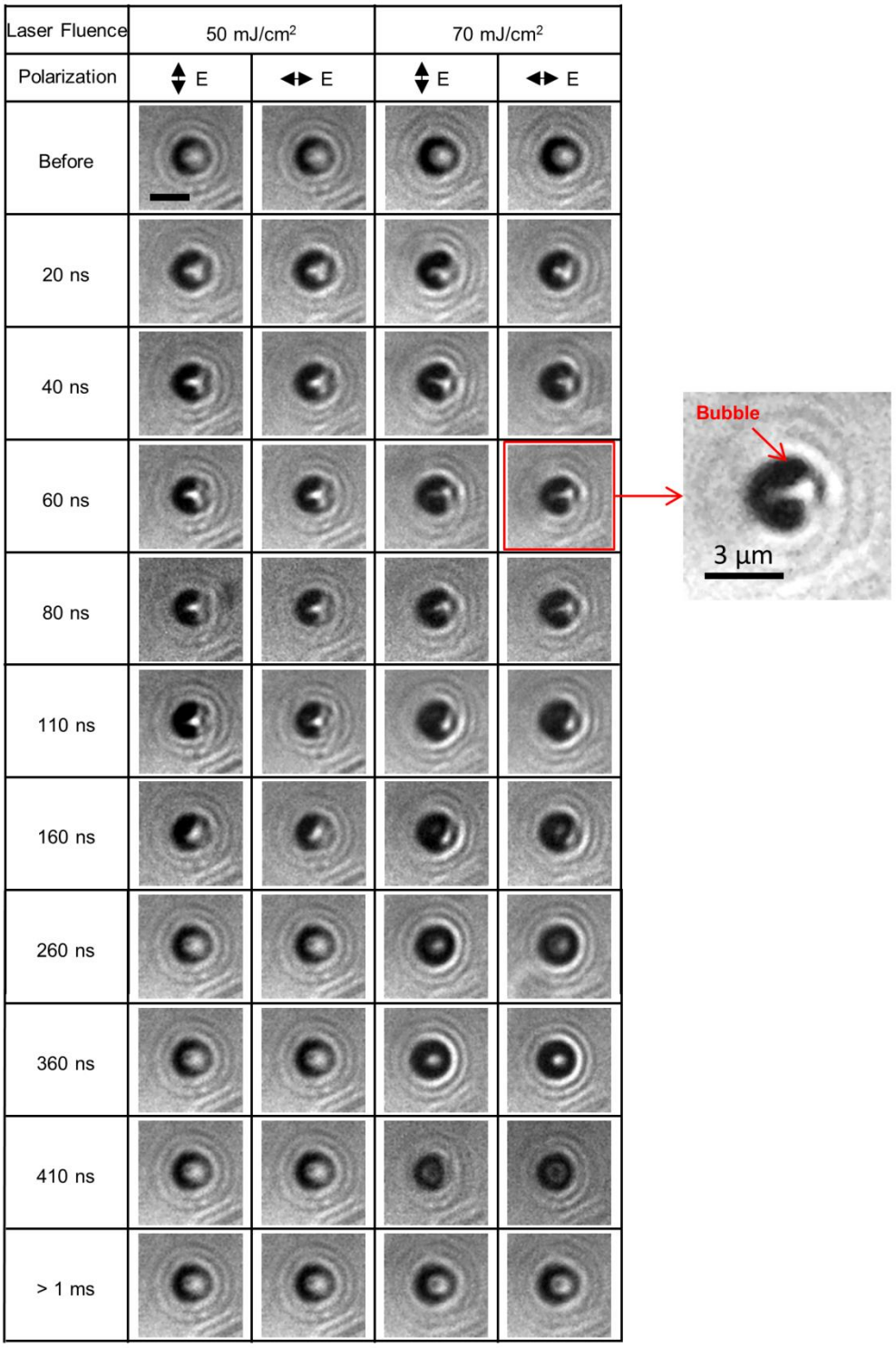

Figure 2.8 | Time-resolved images showing the dynamics of rapidly expanding bubbles triggered under different laser fluence and polarization.

2.1.5 Cell membrane cut by cavitation bubble

Figure 2.9 shows a confocal fluorescence image of a pore formed in a plasma membrane. To avoid membrane resealing after bubble cutting, HeLa cells cultured on BLAST chip were fixed by the 4% paraformaldehyde before laser pulsing. Cell membrane was stained by WGA594 (Invitrogen) and shown the red fluorescence. A 3 μm opening on the membrane right above the BLAST delivery hole was found from the top view and cross-section view of the confocal image. It proves that cell membrane cut by BLAST is highly localized and that the part of a cell outside the SiO_2 holes is not affected.

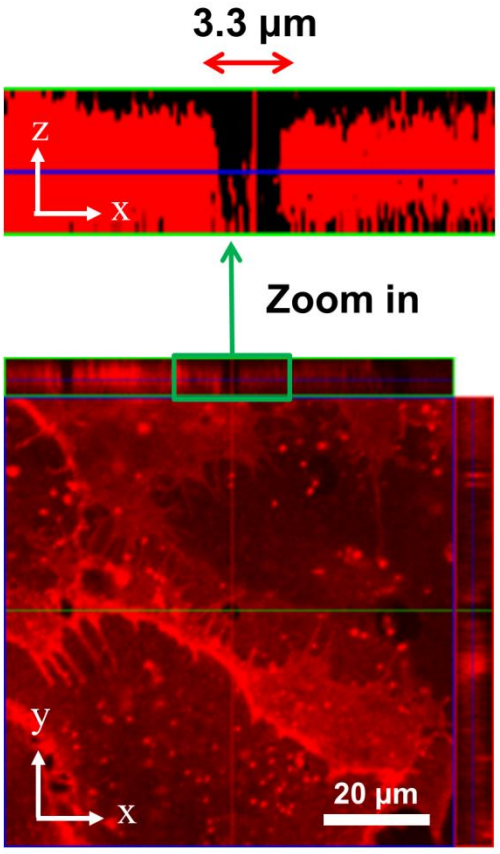

Figure 2.9 | Confocal images showing the cell membrane cut by photothermal bubbles.

2.2 Device fabrication

2.2.1 BLAST chip fabrication

As shown in Figure 2.10, the silicon-based device was fabricated on 2” double-sided polished silicon wafers of 300 μm thickness as follows. Step 1: A 1.5 μm thick thermal oxide layer was grown on both sides of a wafer. Step 2: After surface treatment with hexamethyldisilazane (HMDS) for 10 minutes, photoresist AZ4620 (AZ Electronic Materials) was spin-coated on one side of the wafer and exposed to UV light through a chrome mask with the design of fluid channels. The patterns were developed in 1:4 dilute AZ400K (AZ Electronic Materials) solution for 5 minutes. Step 3: After 100℃ baking for 10 minutes, the wafer was etched by advanced oxide etching (Surface Technology Systems) to remove the oxide layer and by deep reactive ion etching (Unaxis USA) to etch through the silicon substrate. Step 4: Another photolithography process was repeated on the opposite side of the wafer to pattern a 3 μm hole array and aligned to the channel structures. Step 5: Advanced oxide etching was used again to etch through holes on the oxide thin film. There was still a residue photoresist layer on the top surface. Step 6&7: A 100 nm thick titanium thin film was deposited at a tilted angle by an e-beam evaporator (CHA Industries). Step 8: Finally, the device was immersed in acetone to detach the titanium thin film on the photoresist such that only the sidewalls of the small holes retained the metal coating.

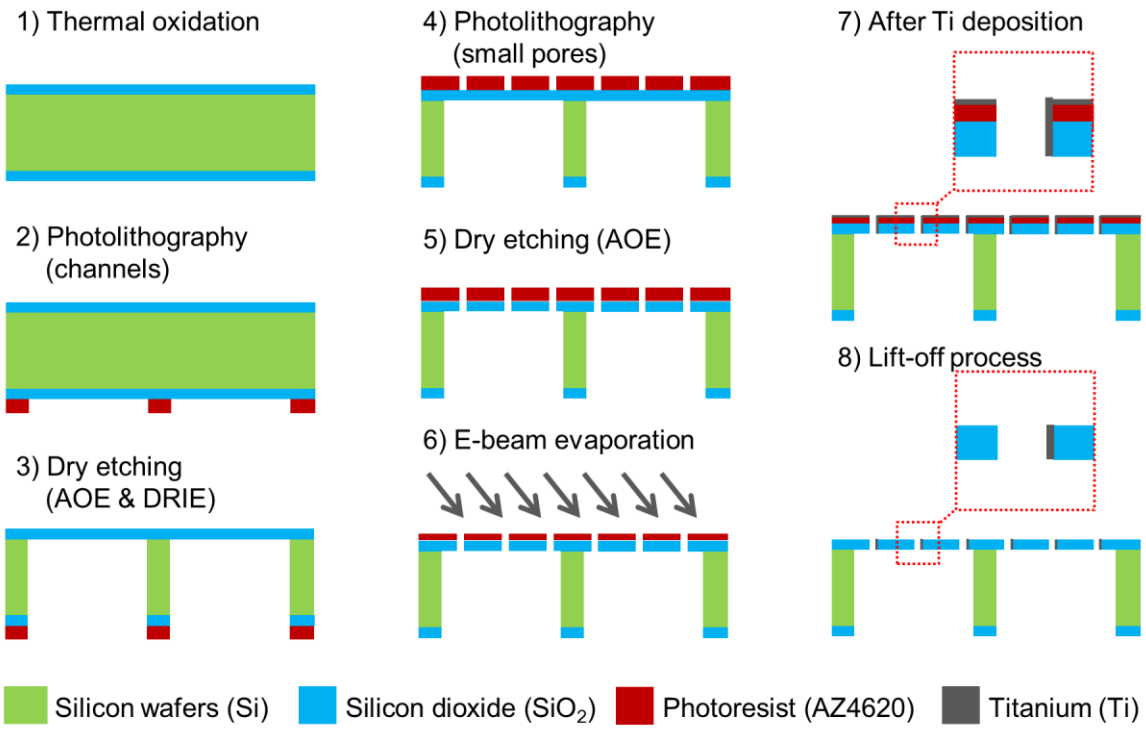

Figure 2.10 | Fabrication procedure of BLAST chip.

2.2.2 PDMS pump fabrication

The fluidic pump for BLAST system was assembled by three PDMS components. The fabrication processes are shown in Figure 2.11. Step 1: The molds for soft lithography were fabricated by SU-8 (MicroChem) photolithography process on 4" silicon wafers. SU-8 is an idea photoresist to fabricate high aspect ratio structures. Step 2: The gel-type polydimethylsiloxane (PDMS), mixed Sylgard 184 silicone elastomer and curing agent (Dow Corning) with 10:1 ratio, was poured on each SU-8 mold. Step 3: After 2 hours baking at 60℃, the PDMS was cured and easy to be removed from the molds. Step 4: Two of the PDMS components need to be cut a through chamber by using the blade.

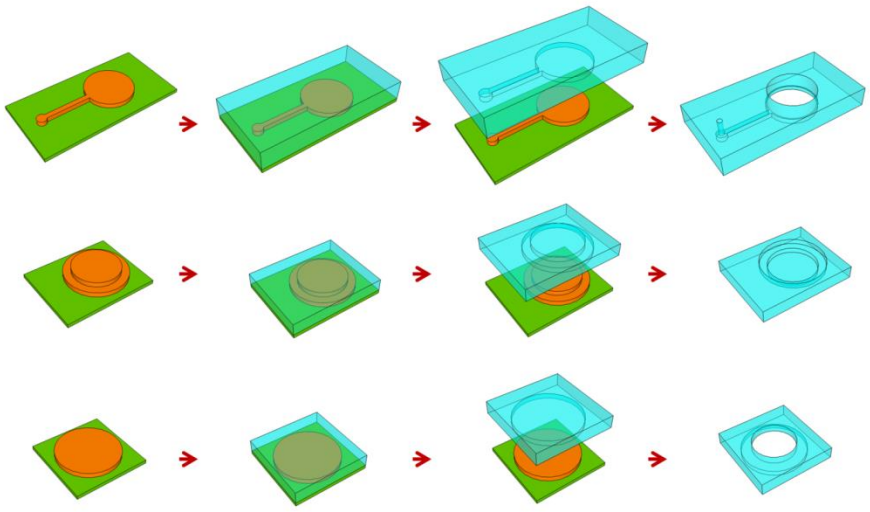

Figure 2.11 | Fabrication procedure of BLAST fluid pumping system.

O_2 plasma treatment was used to permanent bond PDMS-PDMS or PDMS-Glass interface. The assembling process was shown in Figure 2.12. First and second layer PDMS components were bonded each other and then bonded to a 1 mm thick glass slide. There is no bonding treatment for the top PDMS component. After BLAST chip loaded on the sample storage chamber, the top component was aligned and clamped the chip to create a fully sealed chamber.

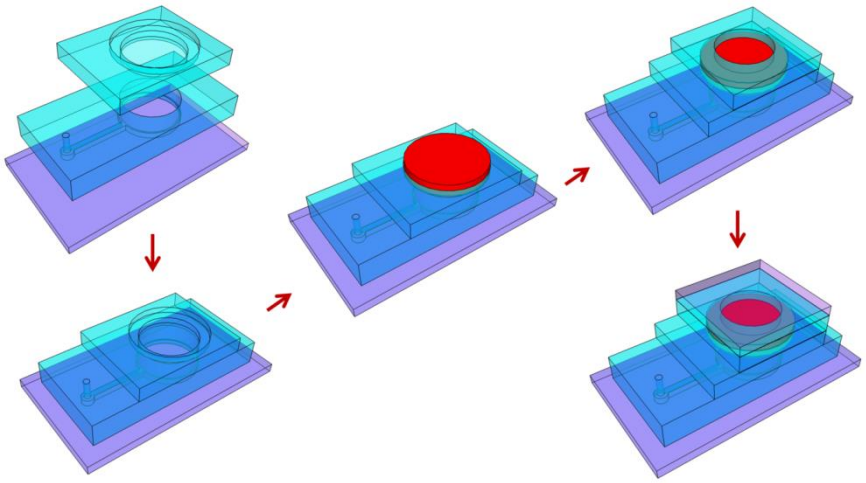

Figure 2.12 | Assembling of BLAST fluid pumping system.

2.3 Device design

2.3.1 Design of injection holes

To decide the dimension of delivery holes, sample size and cell viability are the most important issues. This platform was designed for micron-sized cargo delivery. So the size of delivery holes must be larger than 1 μm in diameter to avoid the clogging. Ideally, devices with bigger holes should have wider range of cargo delivery. However, keeping high cell viability limits the maximum hole opening. Wu *et al.* shown cells are able to survive by using photothermal nanoblade to cut a micron-sized transient pores on membrane[86, 87]. Otherwise, Waleed *et al.* used tightly focused near-infrared femtosecond laser pulse to puncture a hole on cell membrane and observed the membrane healed condition by optical microscope[61]. They found the optoporated cells with hole opening above 3.5 μm caused permanent damage on membrane. Based on our experimental results, the BLAST chips with 4 μm or larger delivery holes could lower the cell viability seriously. Hence, 3 μm in diameter was selected as the standard size of the delivery holes.

To deposit titanium thin film on the inner sidewall of delivery holes, several parameters need to be considered during fabrication processes. As shown in Figure 2.13, the thickness of spin-coated photoresist after oxide etching (t), the diameter of the delivery hole (d) and the tilt angle of e-beam evaporation (θ) will affect the quality of metal coating and then change the shape of laser-induced bubbles. The titanium thin film should cover whole 1.5 μm deep sidewall to minimize the variations in bubbles generation from each batch of BLAST chips. These parameters can be calculated by basic geometry and trigonometric function.

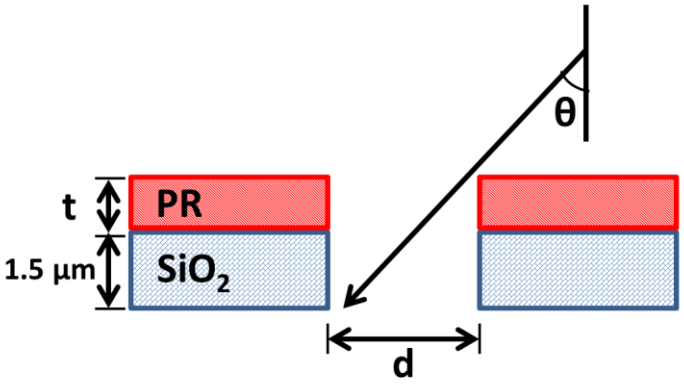

Figure 2.13 | A titanium thin film coated on the inner sidewall of a small hole.

2.3.2 Design of delivery channels

To design the delivery channels on BLAST chips, the efficient sample transportation from storage chamber to target cells is the basic requirement. One advantage of big channel design is decreasing the opportunity of sample clogging even in very high sample concentration. These big openings on silicon chips are also benefit for the microfabrication process. For the fabrication step to etch through silicon wafer, etching rate and uniformity are proportional to the dimension of channels due to the property of etching machine. However, the structure with big openings has much weak supporting for the SiO_2 thin film stood on the top. It is necessary to make a compromise between easy fabrication and strong enough supporting structure.

Based on the real fabrication tests, 50 μm in diameter is the perfect size for delivery channels (Fig. 2.14 (a)). 1.5 μm thick SiO_2 thin film can keep flat on this supporting structure and there is no problem to etch through 300 μm thick silicon wafers by regular DRIE machine. The uniformity for etching process is also acceptable for 1 cm^2 chip area. Besides, this dimension is much bigger than all of the biology samples that we are interested in and there is no chance for delivered cargo to clog inside these channels. In Figure 2.14 (b), the SiO_2 thin film

was deformed before using and would be broken after liquid pumping when the channels enlarged to 100 µm in diameter.

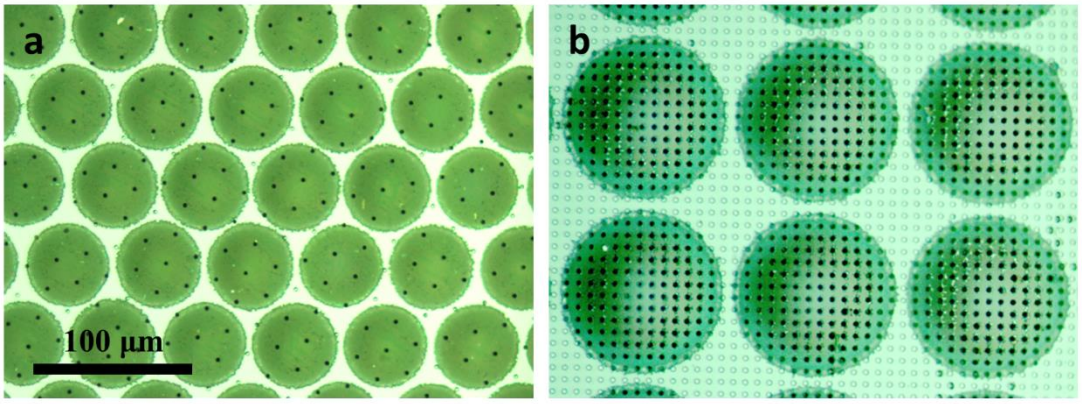

Figure 2.14 | Size effect of the delivery channel. The images show the delivery channels with (**a**) 50 µm and (**b**) 100 µm in diameter.

2.3.3 Design of fluidic pump

For high-throughput delivery, applying uniform pumping flow for each cell is the most challenging part for the design of BLAST integrated fluid system. The total amount of loading volume for each delivery is usually limited, especially some precious biological samples. Besides, the platform which is easy to operate for biological researchers is also an important concern.

The schematic of fluidic pumping system for BLAST chips is shown in Figure 2.15 (the detailed device drawing has been shown in Fig. 2.2). Compared with other microfluidic devices, this design is simple and there is no micro-channel, connected tubing and external fluidic pump in this system. A hundreds microns thick PDMS membrane integrated with a pressure chamber is the key component to trigger the uniform flow. The samples prepared for delivery inside the storage chamber are squeezed to another side (cell side) of the BLAST chip when an applied air pressure deforms the membrane and the liquid pressure is almost equal to whole delivery area.

The delivery volume is controlled by the depth of sample storage chamber (h). The chamber we usually use is 50 μm in depth and 9 μL sample solution is quite enough to fill it. Hence, this platform has the potential to deliver extremely precious samples because the sample prepared for the usage of 100,000 cells is less than 10 μL. Another powerful design is the user-friendly operation. A regular pipette can finish the steps of sample loading in a few seconds (the detail shown in Ch 2.4).

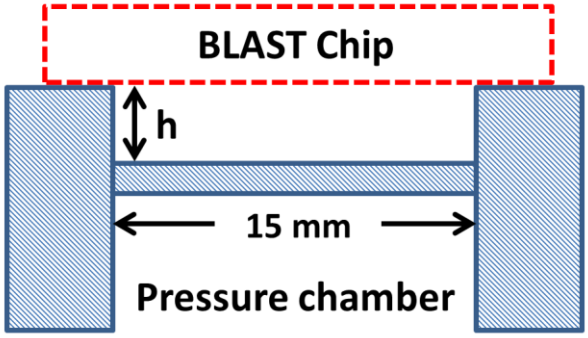

Figure 2.15 | Design of PDMS fluidic pumping system.

2.3.4 Design of laser scanning system

As shown in Figure 2.16, the laser scanning and pressure pumping were controlled by the computer software (LabVIEW). The laser pulsing energy was adjusted by a linear polarizer. And then the expand laser beam was guided by a 2D scanning mirror (Thorlabs) and the scanning trace was defined by the software to fit the delivery area on BLAST chips. The program was set to trigger an external pressure source (FemtoJet, Eppendorf) right after whole chip laser scanning. The whole process took around 10 seconds to complete.

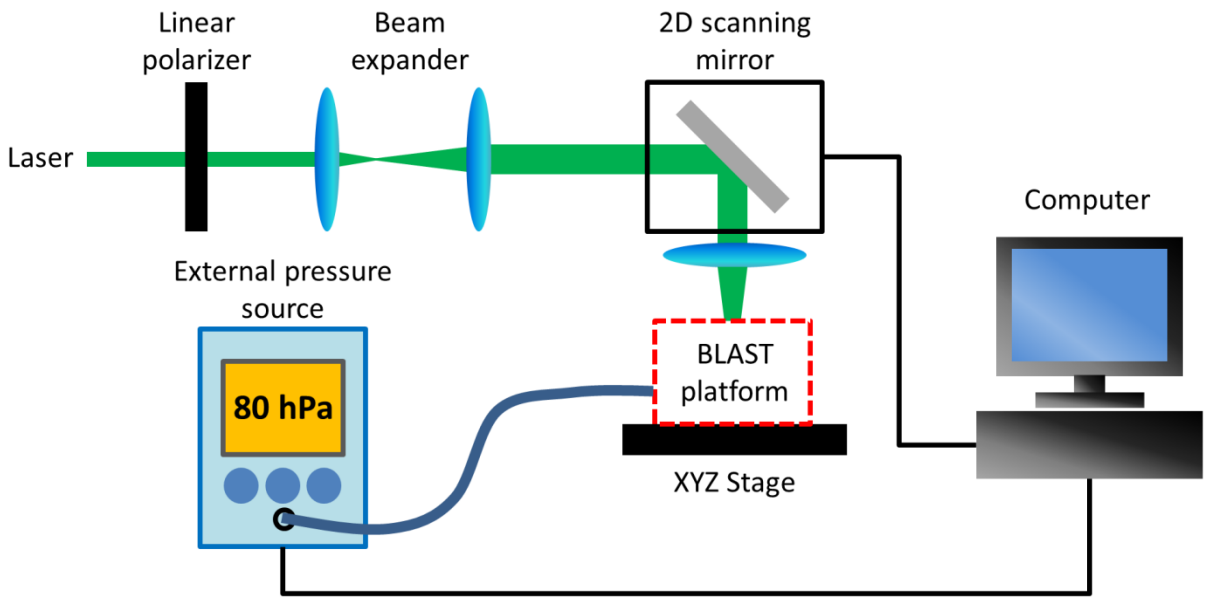

Figure 2.16 | Control of laser scanning and fluid pumping.

2.4 Device operation

In order to satisfy the requirements from most of the biologists, easy to operate is the guideline for the BLAST platform design. Users handle these chips as they would handle microscope cover slips. The procedure for cargo delivery on a BLAST platform is shown in Figure 2.17. Step 1: Drop proper amount of sample solution on the center of the storage chamber (Fig. 2.17 (a)). Step 2: Load the cell-cultured BLAST chip on the top of the storage chamber (Fig. 2.17 (b)). Step 3: Assemble a PDMS well on BLAST chip to fully seal the pumping system (Fig. 2.17 (c)). Step 4: Add cell culture medium into the well to avoid cell dried during delivery (Fig. 2.17 (d)). Step 5: Put a glass slide on the top of PDMS well to block any possible contamination from outside environment (Fig. 2.17 (e)). And then the BLAST platform is ready for cargo delivery.

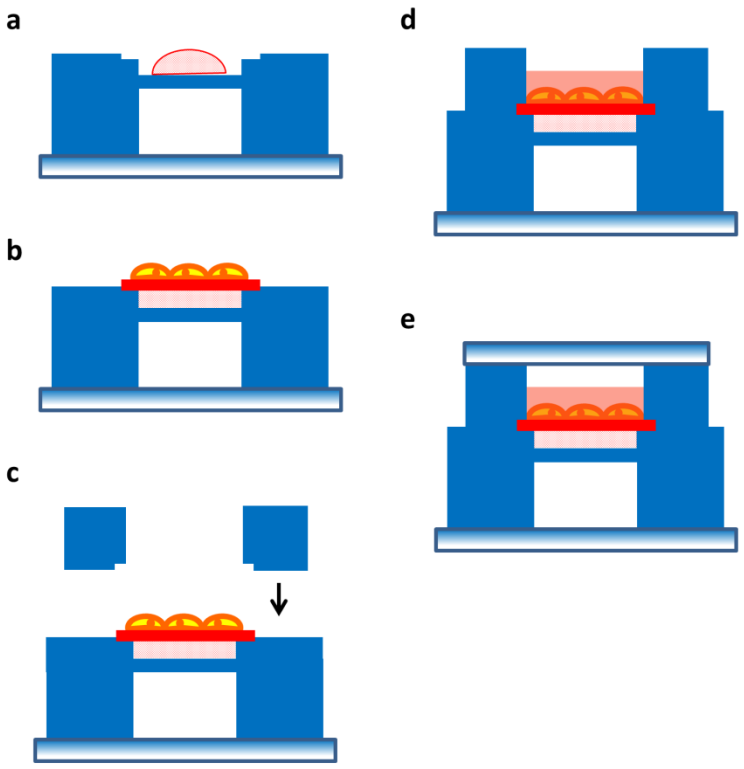

Figure 2.17 | Operation procedure of BLAST platform.

2.5 Device characterization

2.5.1 Hole density and laser energy

Delivery efficiency and cell viability are highly dependent upon hole density of BLAST chip and laser pulse energy. The number of pores opened on each cell is critical for cell viability and it depends on cell type and chip design. For example, Figure 2.18 shows that HeLa cells can cover 6.22, 3.78, 2.11, 1.26 and 0.68 holes/cell on average when the hole densities on a chip are 1.15, 0.51, 0.29, 0.18 and 0.12 holes/10μm^2, respectively. Different cell lines may require individualized designs for platform delivery holes and patterns to achieve optimized delivery efficiency and cell viability. In our fabrication process, only one photolithography step needs to be customized for specific delivery hole design.

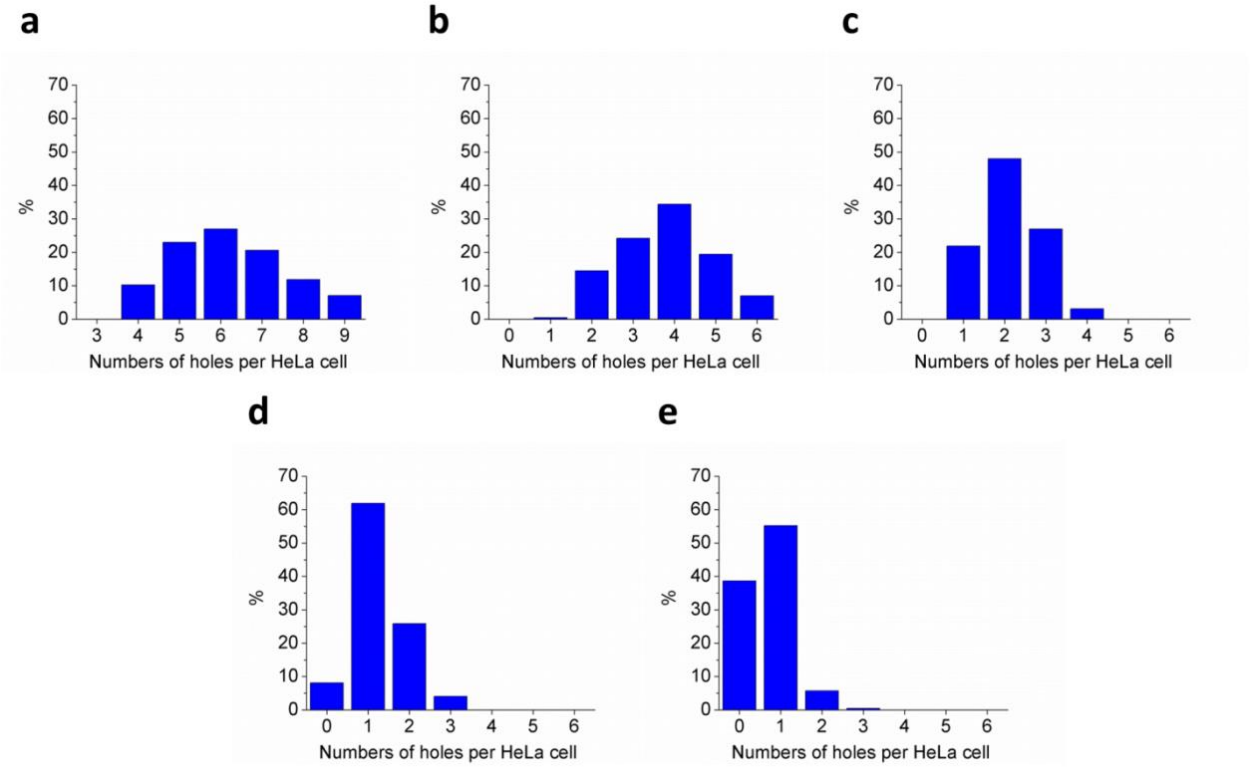

Figure 2.18 | Hole density on chips and distribution of number of holes covered by a cell. The bars in each plot represent the percentage of cells covering certain number of holes. Their hole density are (**a**) 1,154,700 (**b**) 513,200 (**c**) 288,700 (**d**) 184,800 (**e**) 128,300 holes/cm^2**.**

Laser energy is another parameter to affect the cell viability. Figure 2.19 shows the laser-induced cavitation bubbles captured at 60 ns after different laser energy pulsing. Higher laser energy can generate bigger size cavitation bubble and create a bigger pore on cell membrane. It would be helpful for large cargo delivery. However, cutting a big opening on the membrane might exceed the tolerance of cell re-sealing ability and cause the cell to die.

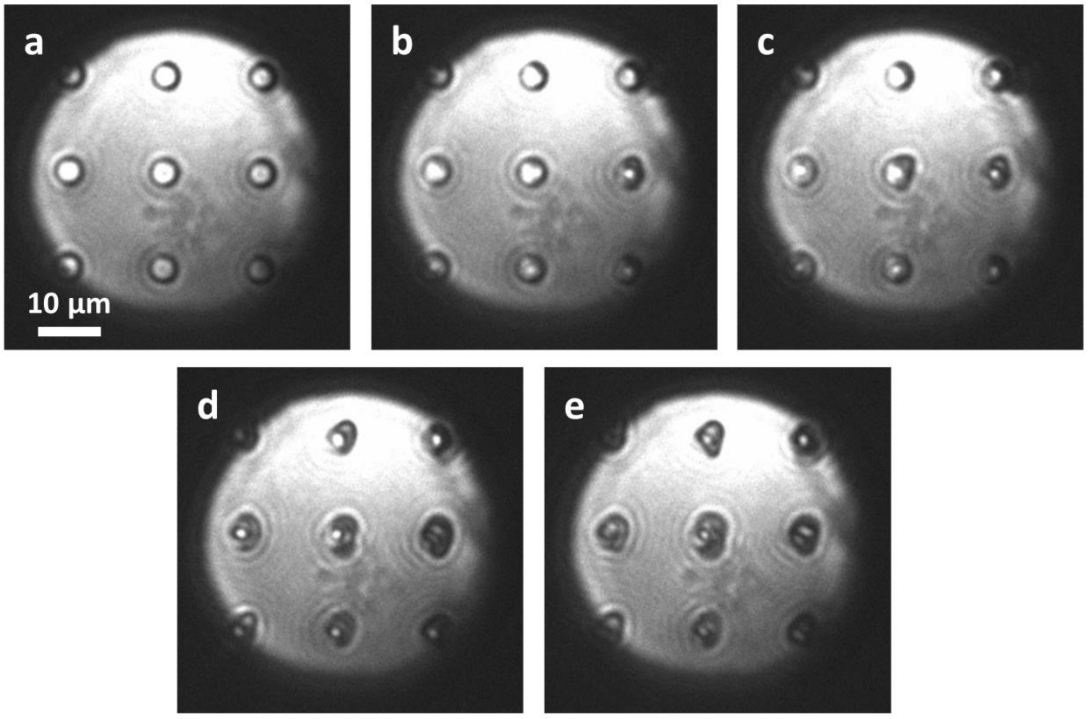

Figure 2.19 | Cavitation bubbles triggered by different laser energy. (**a**) 0, (**b**) 35, (**c**) 50, (**d**) 70 and (**e**) 90 mJ/cm^2 laser were pulsed on BLAST chip without cells on top.

To characterize the effect of hole density and laser energy, five sets of tests were designed and results are shown in Figure 2.20. Pore opening efficiency was calibrated by testing calcein (Invitrogen) uptake after pulsing HeLa cells. Cell viability was measured by propidium iodide (PI, Invitrogen) exclusion 90 minutes after laser pulsing. The images from one set of calibration tests are shown in Figure 2.21. The hole densities in Figure 2.20 are arranged in the same sequence of Figure 2.18 for easier to do a comparison.

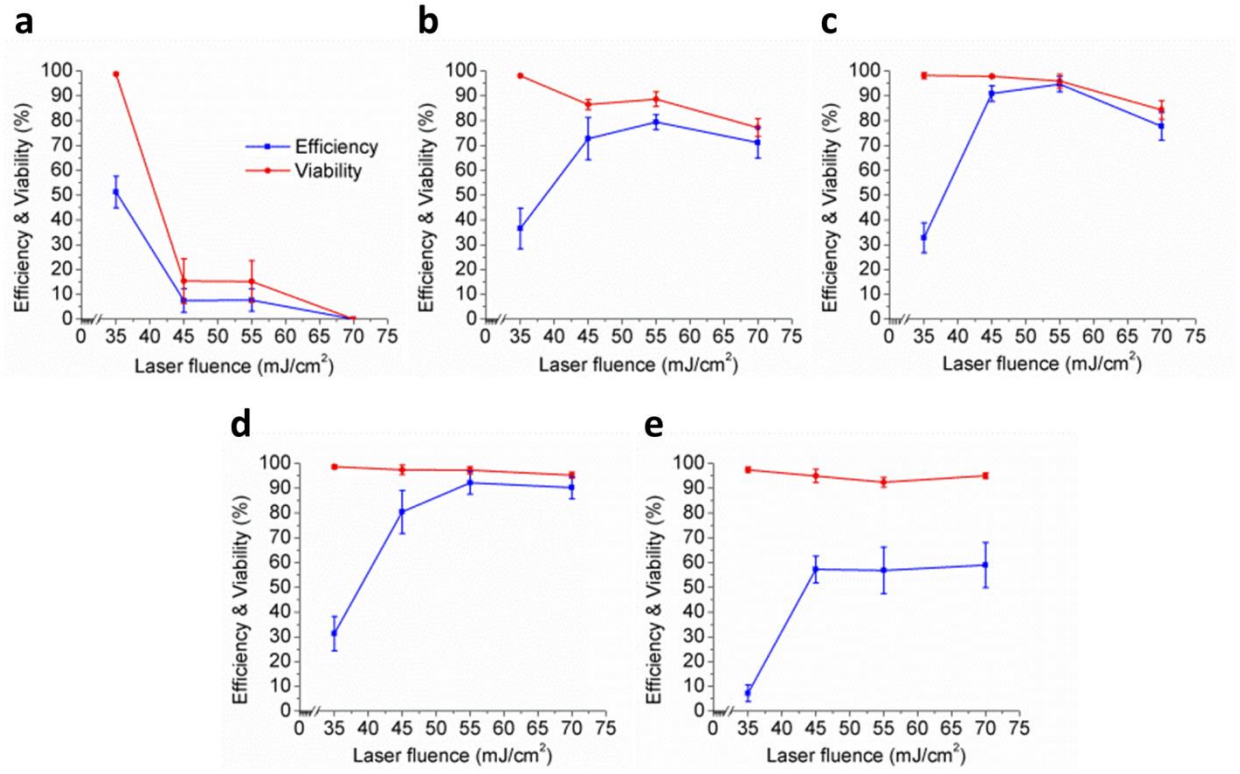

Figure 2.20 | Membrane pore opening efficiency and cell viability. The hole density on the silicon chip varies from (**a**) 1,154,700 (**b**) 513,200 (**c**) 288,700 (**d**) 184,800 (**e**) 128,300 holes/cm^2. Both laser pulse energy and density of holes are critical parameters to control to obtain optimal delivery conditions.

In Figure 2.20 (a), each cell contacted 6.22 holes on BLAST chip and it was difficult to keep cells alive even at low laser energy condition. In contrast, the chip with very low hole density (0.12 holes/10μm^2) can maintain very high cell viability (> 90%) for whole range of laser energy. However, its highest delivery efficiency was below 60% because around 40% cells cultured on the chip did not contact any delivery hole (Fig. 2.18 (e)). The optimized delivery condition for HeLa cells is the BLAST chip with 0.29 or 0.18 holes per 10 μm^2 area at 55 mJ/cm^2 laser pulse energy (Fig. 2.20 (c) and (d)). The efficiency and cell viability approach to 94.7% and 95.9% for 0.29 holes/10μm^2; 92.2% and 97.2% for 0.18 holes/10μm^2. To summarize

these experimental results from Figure 2.18 and 2.20, we can conclude that the best condition for BLAST delivery is opening 1 – 2 holes on each cell.

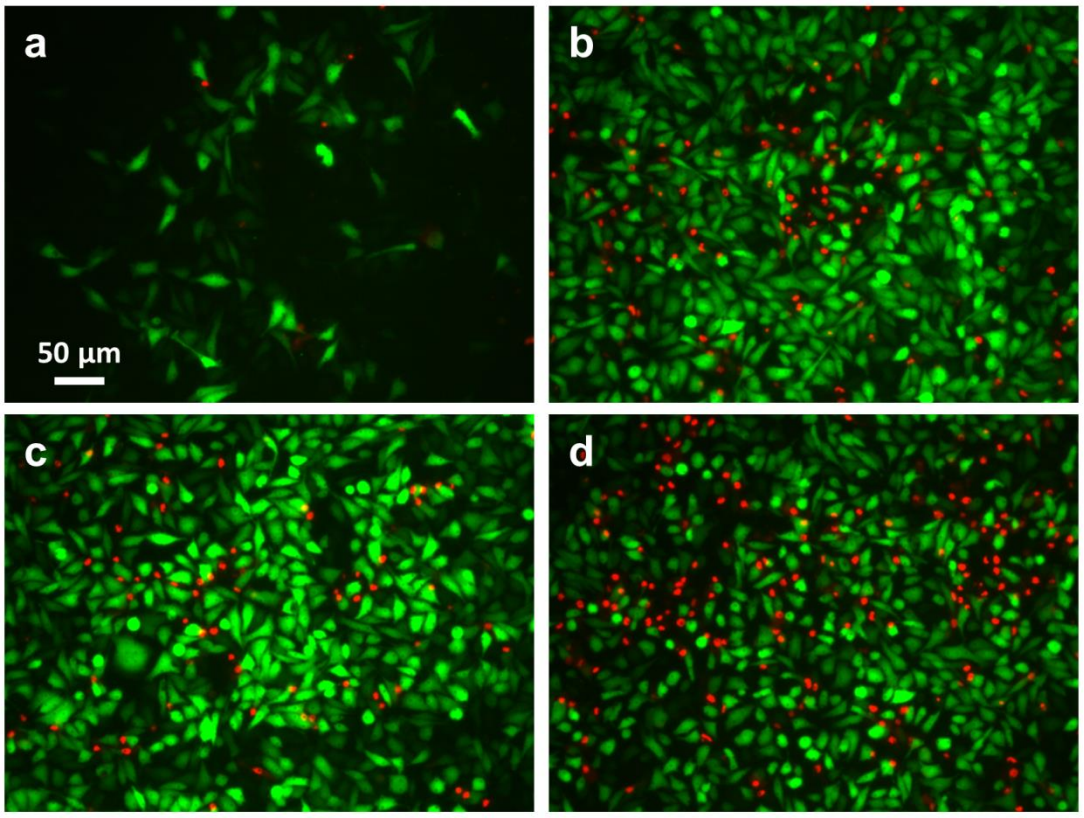

Figure 2.21 | Images showing membrane pore opening efficiency and cell viability. Different laser energies (**a**) 35, (b) 45, (c) 55 and (d) 70 mJ/cm^2 were pulsed on BLAST chip with 288,700 holes/cm^2. Cells: HeLa, calcein delivery (green) and PI viability test (red).

2.5.2 Pumping delay time

Cell membrane resealing starts immediately after transient pores are generated[97]. Large cargo delivery is challenging since these transient pores shrink very quickly, impeding the diffusion of large sized cargo through the pores, a relatively slow process. Therefore active, not diffusion based, cargo delivery is timed to occur before the cell membrane reseals. To measure

the transient opening timeframe for large cargo delivery, we delivered a micron-sized bacterium, green fluorescence protein (GFP)-expressing *Francisella novicida*, into HeLa cells at various delay time intervals between laser pulsing and active fluid pumping (Fig. 2.22). These HeLa cells were incubated for 12 hours at 37^{o}C after delivery to allow the GFP-expressing bacteria to replicate extensively in the cytosol such that infected cells were completely filled with green fluorescent bacteria. As expected, delivery efficiency decreased with increasing delay time. With no delay, the average delivery efficiency across the entire chip is ~58%, whereas with a 10 second delay, the efficiency drops to ~20% (Fig. 2.22).

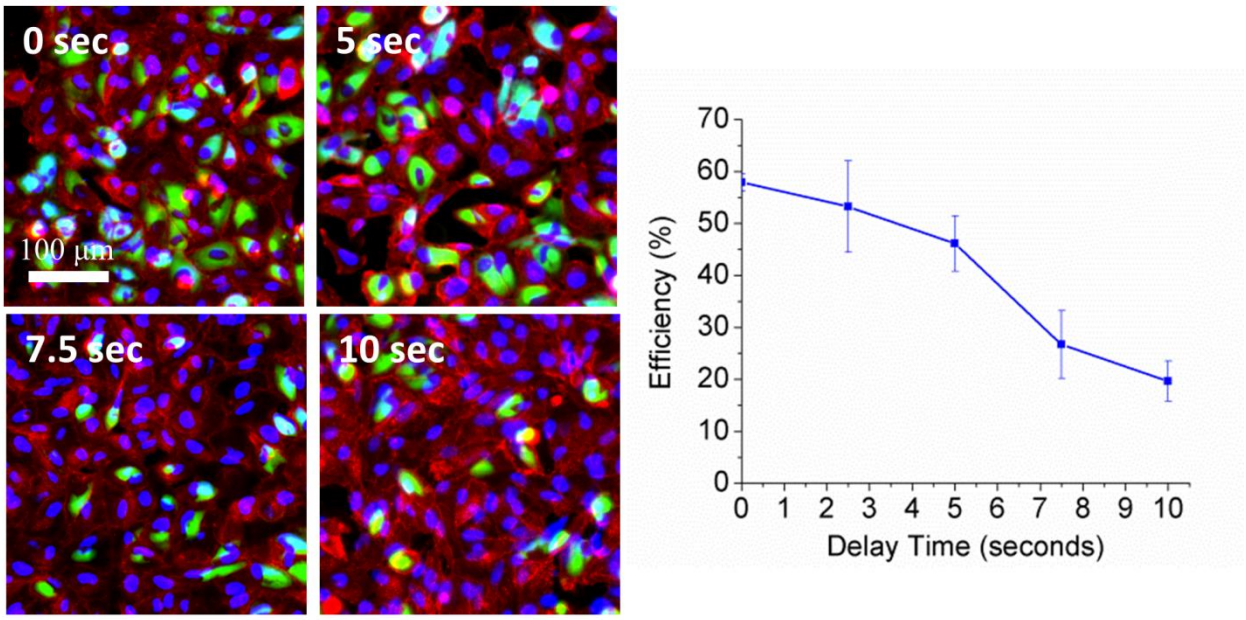

Figure 2.22 | Characterization of the transient window for large cargo delivery. Live bacteria**,** *F. novicida*, expressing green fluorescent protein (GFP) were delivered into HeLa cells at a delay time of 0, 2.5, 5, 7.5 and 10 seconds between laser pulsing and fluid pumping. A 58% delivery efficiency is achieved at 0 delay time. If the delay time is longer than 10 seconds, the delivery efficiency drops to less than 20%.

The delivery of small cargo can tolerate a longer delay time. For example, high efficiency delivery can be maintained for up to several minutes for membrane impermeable calcein dye

(Fig. 2.23), suggesting that a micron-sized pore opened by a cavitation bubble quickly shrinks to exclude the delivery of large cargo but remains permeable to small molecules. Complete membrane resealing takes longer than 10 minutes. Of note, the 40% average efficiency for delivering intracellular bacteria is partially due to the low repetition rate pulse laser used in this study. In our current setup, it takes about 10 seconds to scan the entire 1 cm^2 chip. Many cells in the initially scanned regions have shrunk their pores by the time the pressured delivery is applied, reducing bacterial delivery efficiency.

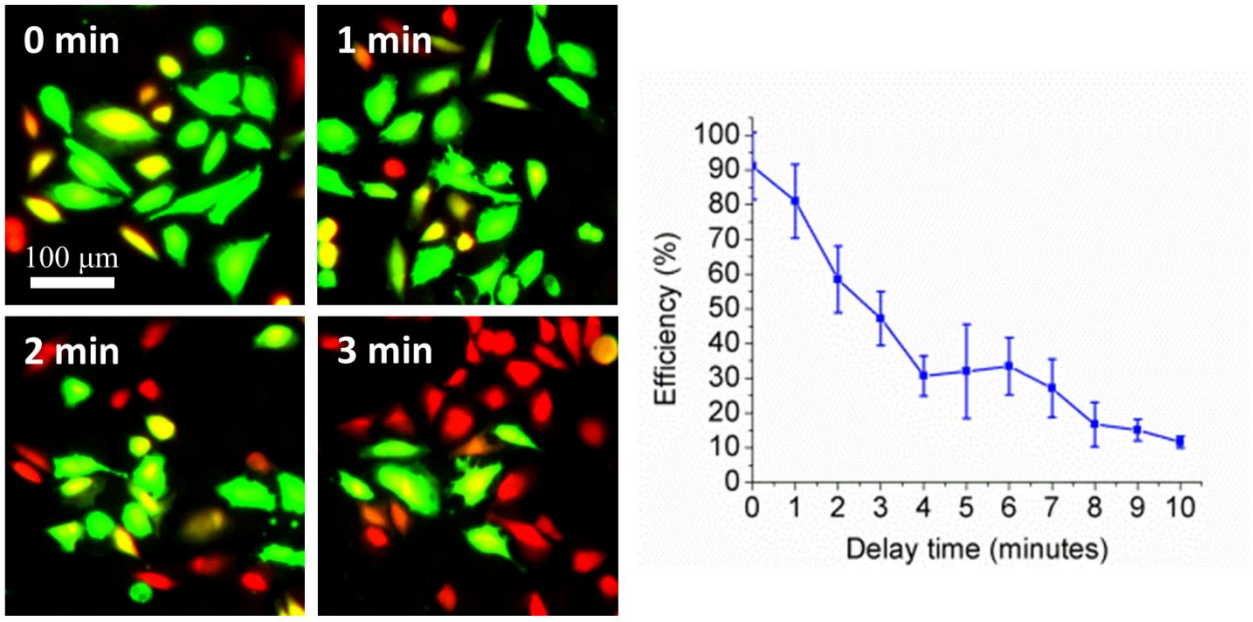

Figure 2.23 | Characterization of the transient window for nanoscale dye delivery. All HeLa cells were stained by WGA 594 (red). Calcein, a polyanionic green fluorescent membrane integrity probe (622 Da), is delivered at different time delays. The cell membrane pores opened by laser induced cavitation bubbles remain permeable for longer than 10 minutes for small molecule delivery before they completely reseal.

2.5.3 Different cell types

BLAST delivery also works well for different cell types, including primary mammalian cells. As shown in Figure 2.24, 40 kDa FITC-dextran (Invitrogen) was delivered into normal

human dermal fibroblasts (NHDFs), peripheral blood monocyte-derived macrophages (PB-MDMs) and renal proximal tubule epithelial cells (RPTECs), and these cells were incubated on the platform for 3 days to check their viability and proliferation.

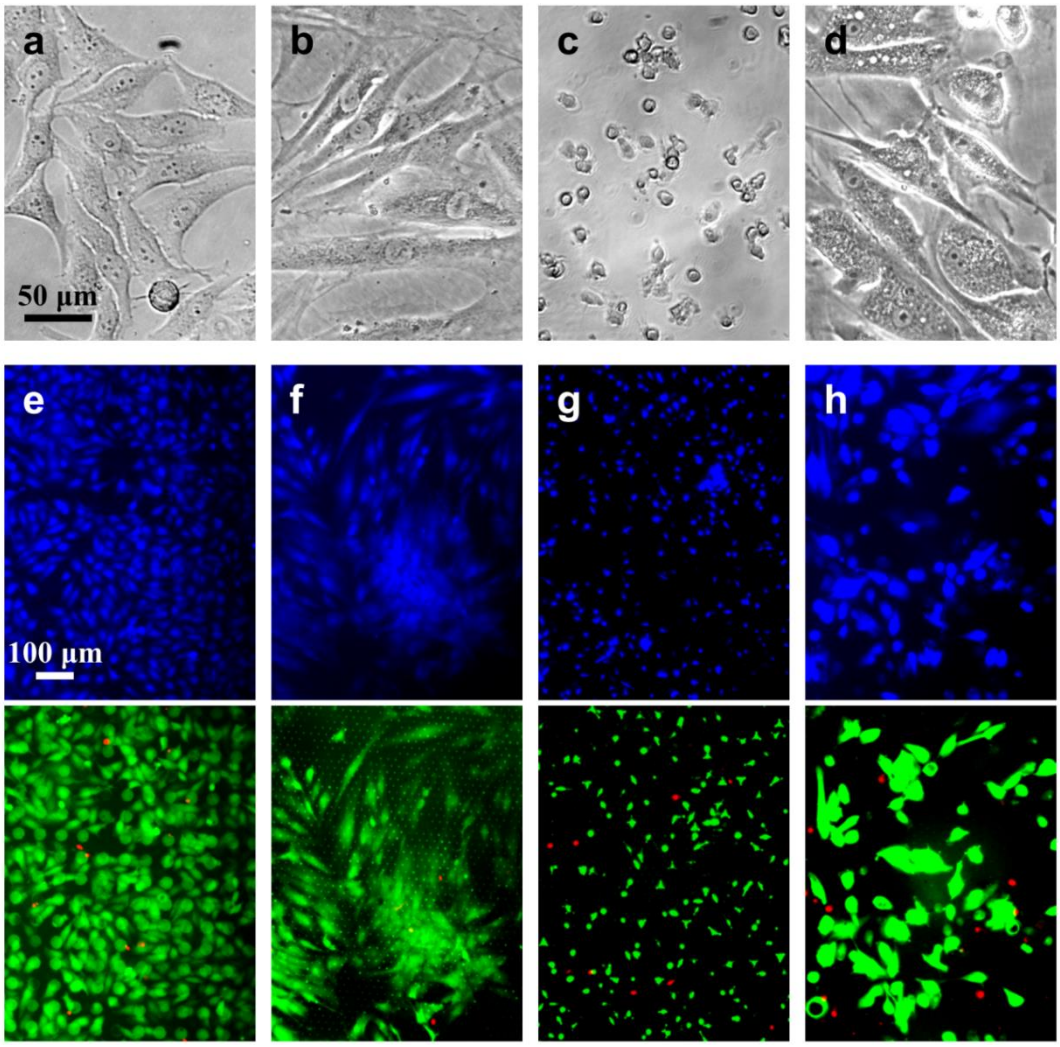

Figure 2.24 | 40kDa FITC-dextran delivered into HeLa and 3 types of primary human cells (3 days after delivery). Bright-field microscopy images of (**a**) HeLa cells, (**b**) normal human dermal fibroblasts (NHDFs), (**c**) peripheral blood monocyte derived macrophages (PB-MDMs), and (**d**) renal proximal tubule epithelial cells (RPTECs). 40kDa FITC-dextran (green) was delivered into (**e**) HeLa cells, (**f**) NHDFs, (**g**) PB-MDMs, and (**h**) RPTECs and incubated on chips for 3 days after delivery. Cells were stained by CellTracker™ Blue CMAC (blue, top row); PI (red) was used to identify the dead cells (bottom row).

All three primary cell lines retained high cell viability (97.7% for NHDFs, 90.7% for PB-MDMs, 95.5% for RPTEC) 3 days after delivery (Fig. 2.25). The delivery efficiencies for NHDFs and RPTECs were 96.6% and 92.1%, respectively. PB-MDMs only approached 60% efficiency, probably because of their smaller size and contact area on the platform compared with NHDF and RPTEC cells (Fig. 2.24).

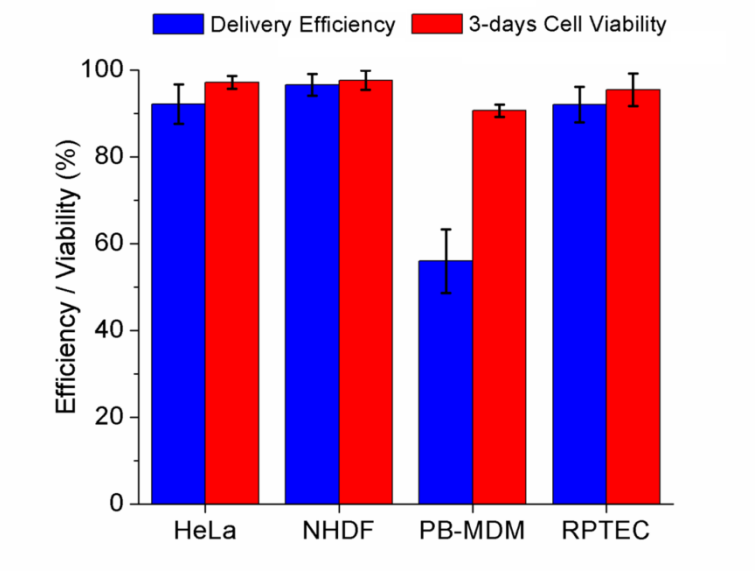

Figure 2.25 | Delivery efficiency and cell viability for 3 different primary cells. FITC-dextran (40 kDa) delivery efficiency and 3-day cell viability for 3 different kinds of primary mammalian cells.

We quantified the proliferation of primary cells after cargo delivery by cell density determinations for cells with and without (control, no laser pulsing and fluid pumping) FITC-dextran delivery and found that BLAST delivery did not affect cell growth (Fig. 2.26). PB-MDMs, which are terminally differentiated cells that do not divide, maintained their original cell density.

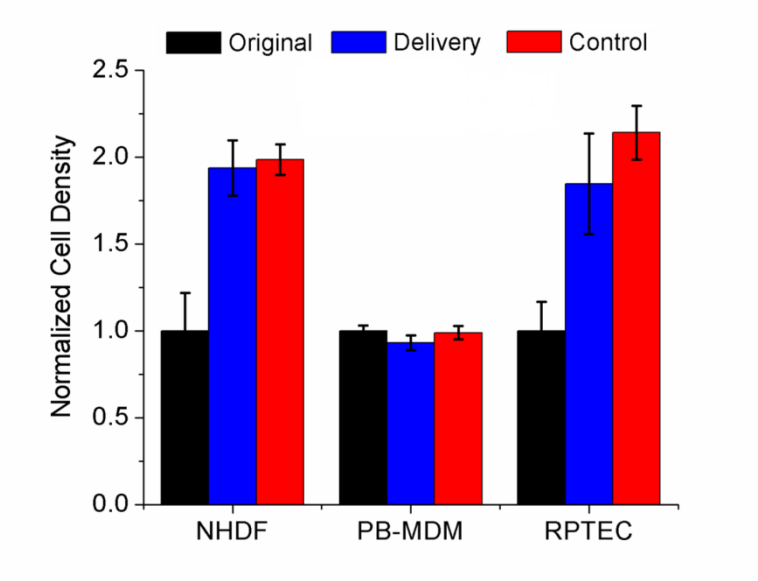

Figure 2.26 | Cell proliferation after BLAST delivery. On-chip 3 day cell densities are compared with their original cell densities (black). FITC-dextran (40 kDa) was delivered into primary cells and cultured on chips for 3 days (blue). Control cells were seeded on chips at the same time and incubated for 3 days without laser pulsing and fluid pumping (red).

2.6 Monitoring of photothermal porated cells

Except the dye diffusion method to estimate the resealing time of photothermal porated cell membrane, an electrical way to monitor the dynamics of membrane-resealing was developed.

2.6.1 Principle

Figure 2.27 illustrates the working principle of the metal microdisk-integrated electrical impedance sensor. A pair of transparent ITO electrodes is used to monitor the response of a target cell. By pulsed laser shining the microdisks on the top of ITO electrodes, micron-sized cavitation bubbles are generated to cut the cell membrane locally. When the pore size is repairable, cell membrane will be resealed over time and the cell remains viable; however, when a cell membrane is severely damaged by large cavitation bubbles, it dies immediately. Schematics of

equivalent circuit models of before and after bubble cutting are shown in Figure 2.27 (b) and Figure 2.27 (c), respectively. Before laser pulsing, the electrical impedance near the microdisk is dominated by the capacitance term because an intact plasma membrane is not electrically conductive and can be considered as a capacitor (Fig. 2.27 (b)). Oppositely, it is dominated by the resistance term after laser pulsing (Fig. 2.27 (c)). Therefore, the electrical impedance can be used to monitor the dynamics of the cell membrane opening and resealing processes.

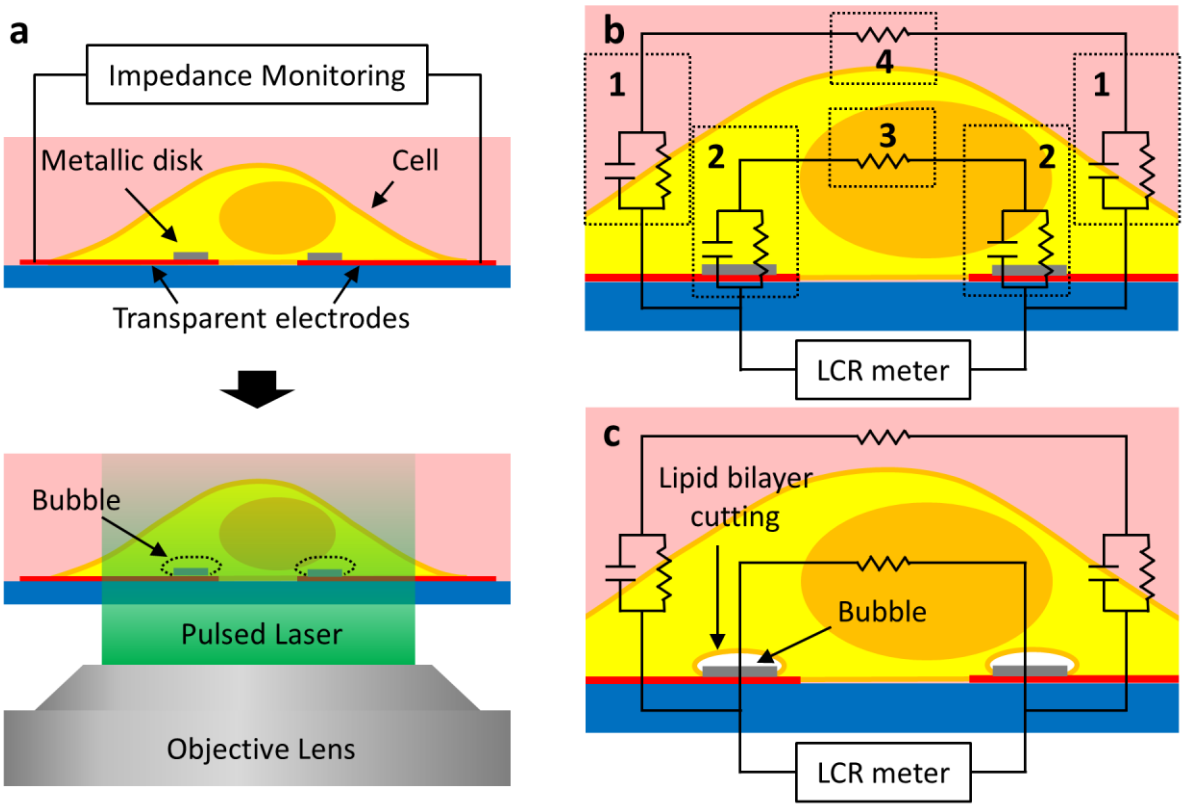

Figure 2.27 | Metallic microdisk-integrated impedance sensor. a, Cells were cultured on the electrode area and contacted both sides of electrodes. Cavitation bubbles were triggered by laser pulse and cut the cell membrane. **b-c,** Simplified equivalent circuit of the target cell (**b**) before and (**c**) after bubble cutting. Equivalent circuit: (1) membrane and medium, (2) membrane, (3) cell interior and (4) medium.

2.6.2 Device design and fabrication

The cross-section view and top view of an impedance sensor are shown in Figure. 2.28. Wires were connected to LCR meter for measuring. The image shows the top view of sensing area with 5 pairs of Ti-coated microdisks located on the top of ITO electrodes.

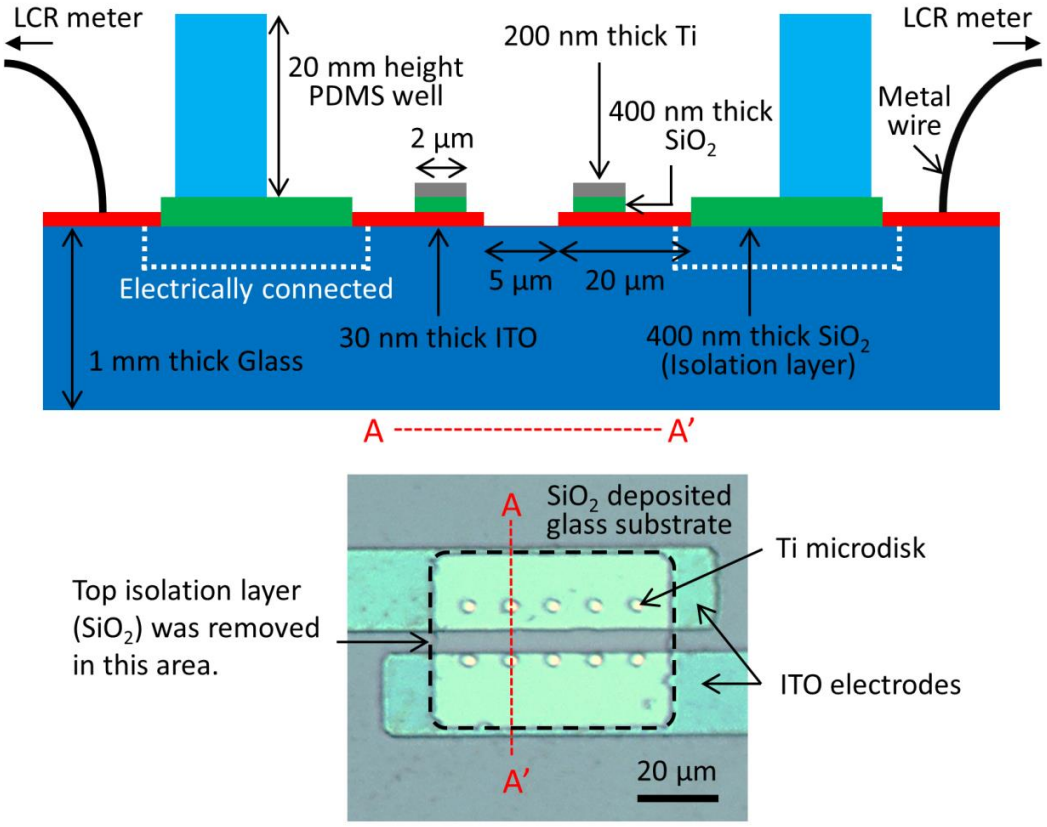

Figure 2.28 | Structure of the microdisk-integrated impedance sensor. Cross section view of the impedance sensor is not drawn to scale.

Fabrication processes for this device are shown in Figure 2.29. It started from a commercial ITO glass substrate. Step 1: A 30 nm thick ITO film on glass was patterned by photolithography and etched by advanced oxide etching. Step 2: A 400 nm thick SiO_2 film was deposited on the entire sensing area by plasma-enhanced chemical vapor deposition (PECVD). Step 3: The SiO_2 layer on the area for wire connection was removed by advanced oxide etching. Step 4&5: A 200

nm thick titanium (Ti) film was coated and patterned on top of the SiO_2 layer to create metallic microdisks with a diameter of 2 μm by lift-off process. Step 6: These Ti disks were also used as deep reactive-ion etching (DRIE) masks to selectively remove the SiO_2 and expose the ITO electrodes for impedance sensing. Step 7&8: Another SiO_2 layer with 200 nm thick was deposited by e-beam evaporation and patterned by a lift-off approach to provide electrical isolation in the area outside the monitored regions to minimize the electrical noise from background. Step 9: A PDMS well with a height of 2 cm and an area of 3 cm^2 was put on the device to build a reservoir for holding cell culture media. Metal wires connected to LCR meter for impedance measuring were soldered on the large contact pads located outside the PDMS reservoir.

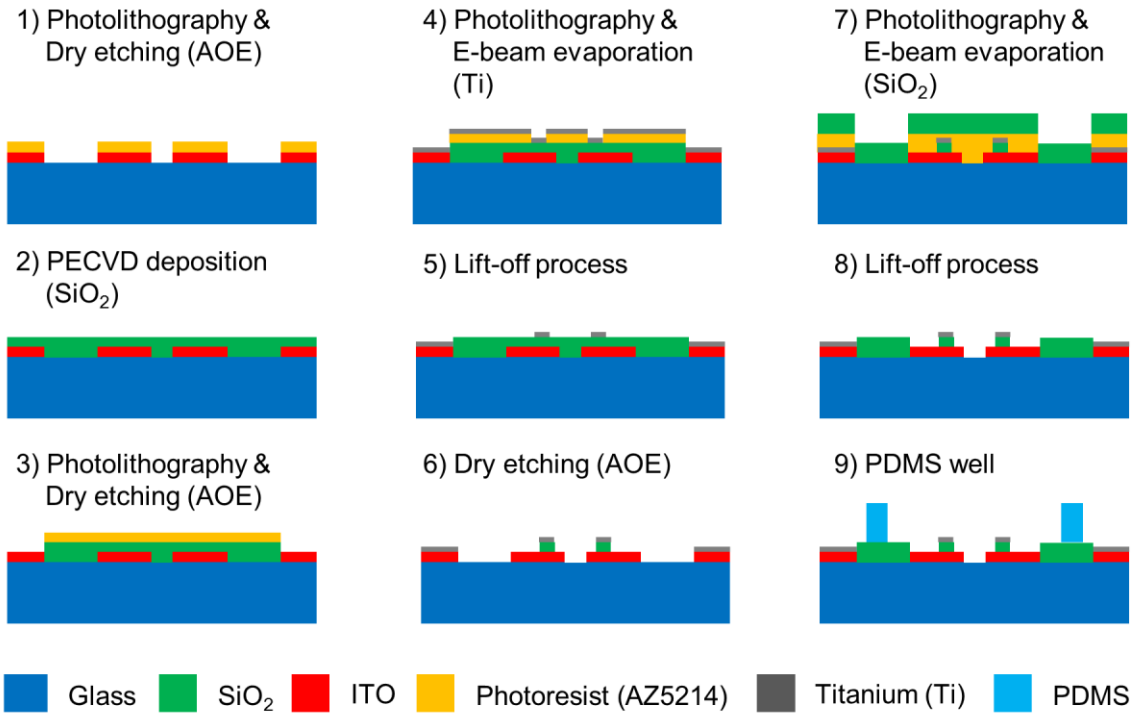

Figure 2.29 | Fabrication procedure of microdisk-integrated impedance sensor.

2.6.3 Resealing time of transient pores

Figure 2.30 shows the measured dynamic impedance of cells severely damaged by a large cavitation bubble excited by a high-energy laser pulsing. The impedance magnitude shifted around 1.26% of the average impedance, which is 10 times larger than the case without cells on electrodes. The impedance angle also changed around 0.0017° after laser pulsing. As shown in the right-hand side of Figure 2.30, these cells were permanently damaged after photothermal poration, and their impedance did not recover 90 min after pulsing due to the uptake of PI fluorescent dye.

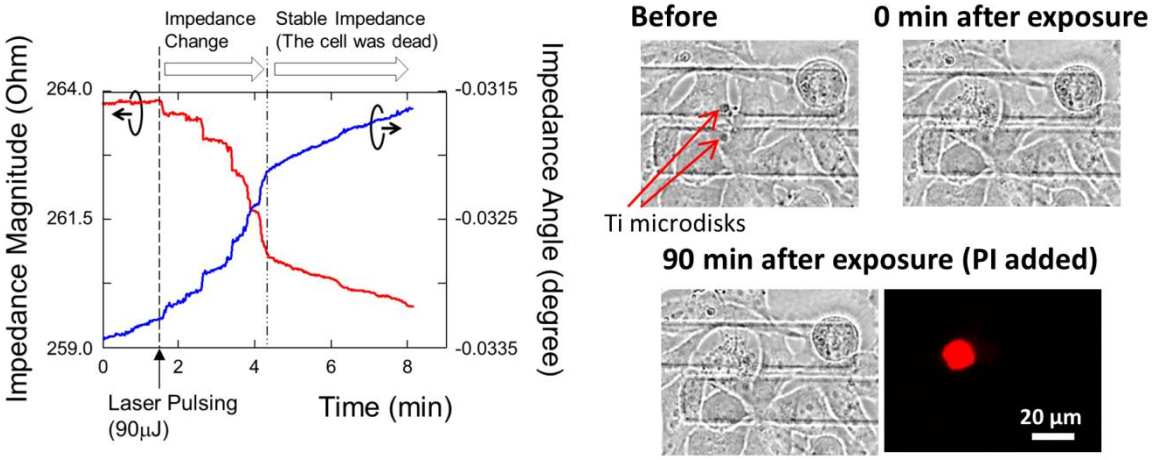

Figure 2.30 | Impedance responses of a cell damaged severely by laser pulsing.

Figure 2.31 plots the impedance responses of cells remaining viable after photothermal poration. The magnitude and the angle of the impedance were changed immediately following laser pulsing. The impedance signal recovered in approximately 2 minutes back to the initial state. The cell images before and after laser pulsing including bright field and fluorescence modes are shown in the right-hand side of Figure 2.31. Before laser pulsing, the culture medium used in this experiment was mixed with 100 μg/mL calcein, a membrane-impermeable green fluorescent dye, to indicate successful pore opening on cell membranes. Cells with transient

pores showed green fluorescence because the nanoscale dye diffused across the pores into the cell cytosol before membrane resealing. After laser pulsing, calcein was washed away and replaced with fresh medium. The images show that cells remained viable and retained the calcein dye for longer than 90 minutes after laser pulsing. This indicates that the cell recovered completely from photothermal poration and the small molecules such as calcein cannot pass through the intact cell membrane. If the cells are not fully resealing, the calcein dye will leak out to the culture medium and no green fluorescent signal can be detected.

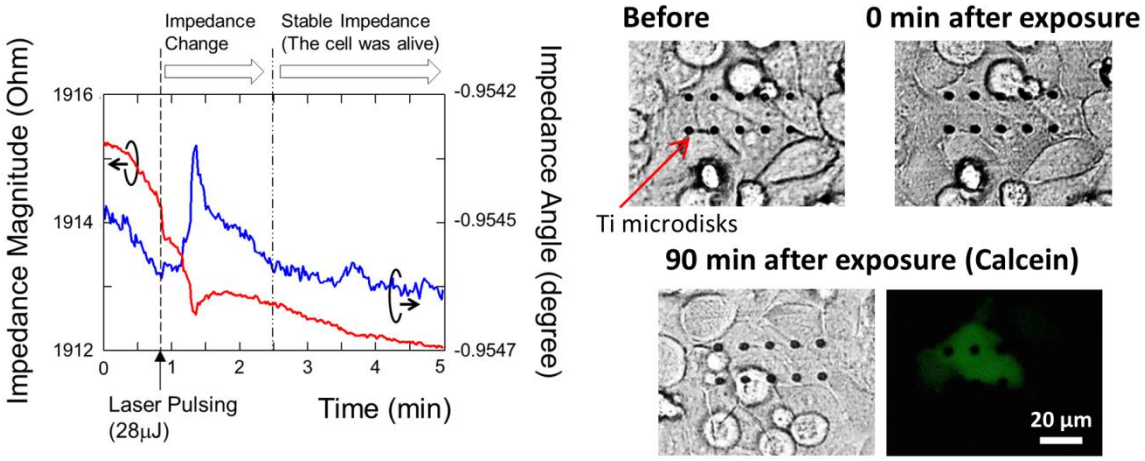

Figure 2.31 | Impedance responses of a living cell irradiated by laser pulsing.

Chapter 3

BLAST Platform for Biological Applications

BLAST platform can deliver broad range of cargo sizes into mammalian cells. Many kinds of samples, such as bacteria, enzymes, antibodies, plasmids, gold particles, magnetic beads and quantum dots, were delivered by BLAST platform and kept functional in the cell cytoplasm. Several interesting phenomena were observed due to this unique technique.

3.1 Bacteria delivery

3.1.1 *Listeria monocytogenes* delivery

We have confirmed that the BLAST platform delivers biologically viable and undamaged cargo directly into the cytosol by studying an escape-incompetent strain of *Listeria monocytogenes* (*L. monocytogenes*) deficient in listeriolysin O and phospholipase C[98]. When the barrier to escape is bypassed by delivering the strain directly into the host cell cytosol, the cytosolic *L. moncytogenes* nucleate actin and form actin comet tails (Fig. 3.1).

L. monocytogenes Δ*hly* Δ*plcB*, strain 10403S, with in-frame deletions of genes encoding the listeriolysin O and the broad-range phospholipase C, was delivered by BLAST platform with laser pulsing into the cytosol of HeLa cells (Fig. 3.1 (a) – (c)) or, as a sham control, in the absence of laser pulsing (Fig. 3.1 (d) – (f)). The cells were washed, incubated at 37^{o}C for 6 hours

in DMEM with 10% FBS and 5 μg/ml gentamicin (which kills any residual extracellular bacteria), and fixed in 4% paraformaldehyde in PBS (detailed protocol shown in Appendix A). DNA of host cells and bacteria (Fig. 3.1 (a) and (d) arrows) were stained with DAPI (Invitrogen). F-Actin was stained with AlexaFluor 488-phalloidin (Molecular Probes) to demonstrate nucleation of actin by cytosolic *Listeria* (Fig. 3.1 (b)). *L. monocytogenes* Δ*hly* Δ*plcB* that nucleate actin to form actin comet tails are observed after BLAST with laser pulsing (Fig. 3.1 (a) – (c)), but not in the absence of laser pulsing (Fig. 3.1 (d) – (e)), confirming that these bacteria, which are unable to escape from host cell vacuoles, were delivered successfully into the cytosol by BLAST.

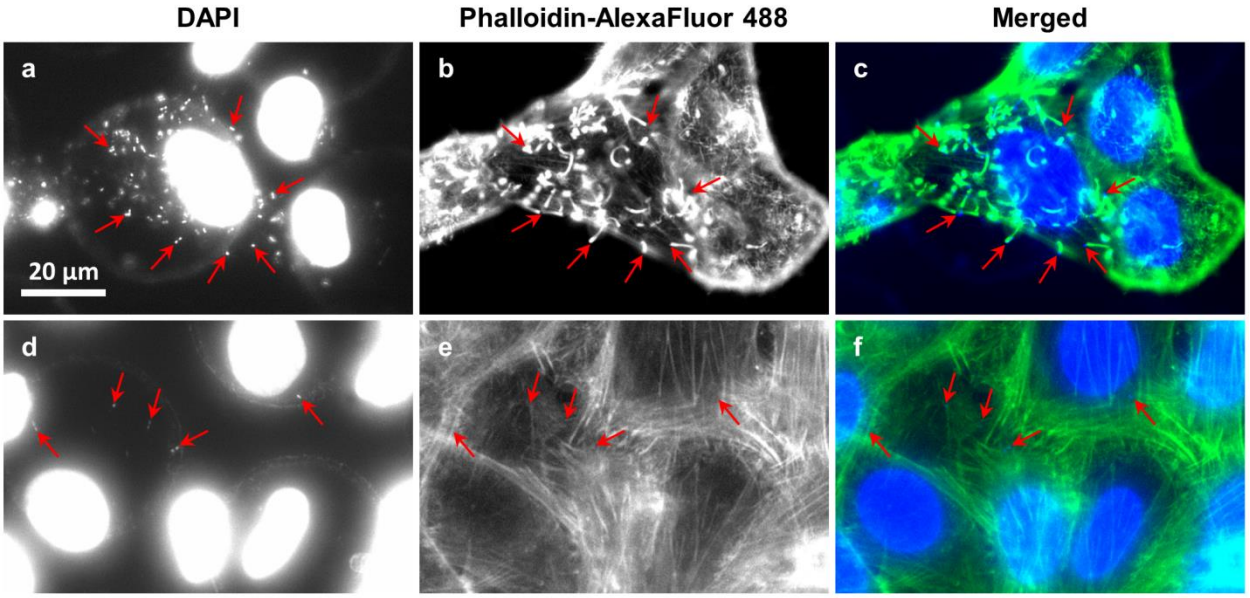

Figure 3.1 | Escape-incompetent *Listeria monocytogenes*, deficient in listeriolysin O and broad range phospholipase C, nucleate actin after BLAST delivery directly into the cytosol of HeLa cells.

We also delivered *L. monocytogenes* into one type of primary cells, NHDFs (Fig. 3.2). *L. monocytogenes-GFP* Δ*hly* Δ*plcB* (green), strain 10403S, with in-frame deletions of genes

encoding the listeriolysin O and the broad-range phospholipase C, was delivered by BLAST with laser pulsing into the cytosol of NHDFs (Fig. 3.2 (a)) or, as a sham control, in the absence of laser pulsing (Fig. 3.2 (b)). The delivered cells were washed, incubated at 37^{o}C for 6 hours in DMEM with 10% FBS and 5 μg/ml gentamicin and fixed in 4% paraformaldehyde in PBS (detailed protocol shown in Appendix B). F-Actin was stained with phalloidin-rhodamine (red) to demonstrate nucleation of actin by cytosolic *Listeria*. *L. monocytogenes-GFP* Δ*hly* Δ*plcB* that nucleate actin to form actin comet tails were observed after BLAST with laser pulsing, but not in the absence of laser pulsing.

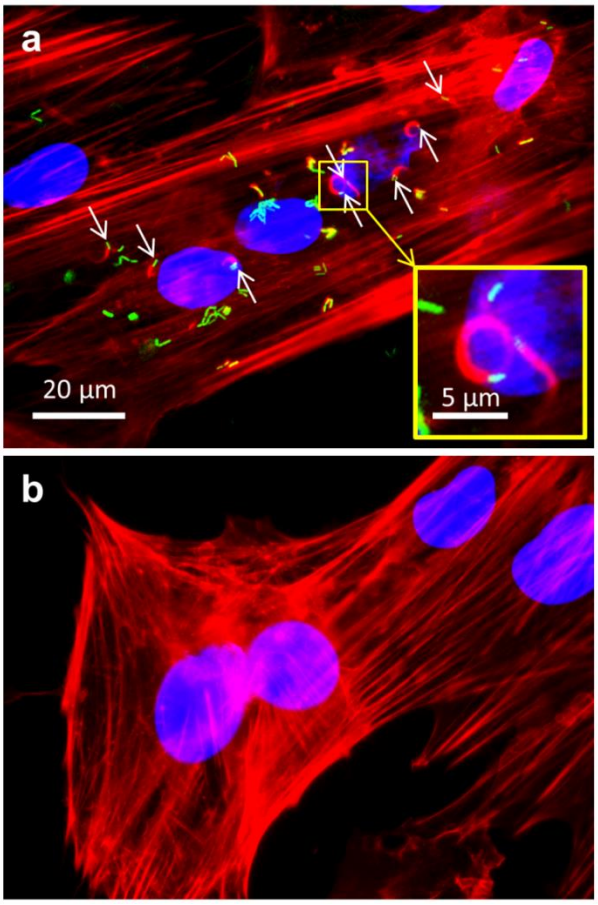

Figure 3.2 | Escape-incompetent Listeria monocytogenes, deficient in listeriolysin O and broad range phospholipase C, nucleate actin after BLAST delivery directly into the cytosol of NHDFs.

3.1.2 *Francisella novicida* delivery

To demonstrate an enabling application of the photothermal platform, we examined the function of *iglC*, a gene within the Francisella Pathogenicity Island (FPI), in intracellular replication of *Francisella*. The high efficiency and nearly simultaneous delivery of bacteria into a population of cells under uniform physiological conditions allows reliable measurements of bacterial intracellular trafficking and growth over time, which is not feasible with current lower-throughput, size-limited methodologies.

Francisella is a non-motile, highly virulent Gram-negative facultative intracellular bacterium that causes a potentially fatal zoonotic disease, tularemia. *Francisella* subverts host cell trafficking by preventing phagolysosomal fusion and escapes into the host cell cytosol, where it replicates[99]. Essential to its virulence and its capacity to escape into the cytosol and replicate intracellularly is a cluster of 17 genes, the FPI, thought to encode a Type 6 Secretion System (T6SS)[90, 100, 101]. Disruption of almost any of the FPI genes prevents phagosome escape and intracellular replication[102]. Because vacuolar escape precedes and appears to be required for intracellular bacterial replication of *Francisella*, it has been impossible to determine whether the FPI is required only for vacuolar permeabilization and bacterial escape into the cytosol or is additionally required for intracytosolic activities such as replication following escape.

HeLa cells are non-phagocytic and inefficiently internalize *F. novicida*. Under the conditions of our assay, less than 0.5% of HeLa cells internalize *F. novicida* in the absence of laser pulsing. However, BLAST delivers a high percentage of *F. novicida* into HeLa cells (Fig. 3.3).

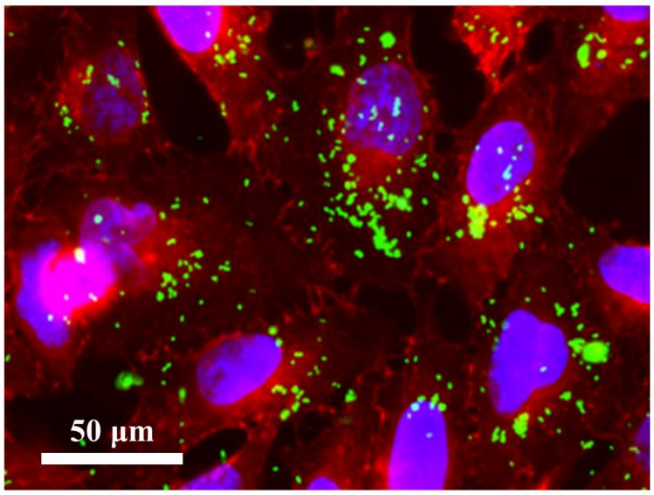

Figure 3.3 | Micron-sized GFP-*F. novicida* (green) were delivered into HeLa cells. The cell nuclei and membranes were stained by DAPI (blue) and WGA 594 (red), respectively.

3.1.3 *Francisella novicida* mutant strains

F. novicida Utah 112 was grown in trypticase soy broth supplemented with 0.2% cysteine or on chocolate agar. When needed, kanamycin and hygromycin were included in the *F. novicida* cultures at 20 µg/mL or 200 µg/mL, respectively. *F. novicida* was chemically transformed with the suicide plasmid pMP590-FnΔ*iglC*-ExC to generate an unmarked in-frame deletion mutant of *iglC* by allelic exchange. The resulting kanamycin resistant clones with plasmid integration were counter-selected on chocolate agar containing 5% sucrose for loss of the integrated plasmid. The clones that were resistant to sucrose and sensitive to kanamycin were screened for deletion of the *iglC* gene by PCR and Western immunoblotting analyses. GFP expressing *F. novicida* strains were generated by introducing pMP633 carrying a codon optimized superfolder gfp (sfGFP; Dr. Francis Nano, University of Victoria) driven by the bacterioferritin (FTL_0617) promoter. For complementation of *iglC*, pMP633BC-*iglC*-sfGFP was introduced into *F. novicida* Δ*iglC* for

bi-cistronic expression of *iglC* and sfGFP.

Bacterial lysates from 1.5 × 10^7 GFP expressing *F. novicida* wild type (Fig. 3.4 lane 1), ΔFPI (Fig. 3.4 lane 2), Δ*iglC* (Fig. 3.4 lane 3), and *iglC* complemented (Fig. 3.4 lane 4) strains were separated by SDS-polyacrylamide gel electrophoresis and transferred to nitrocellulose membrane for probing with monoclonal antibody to IglB (1:1,000; BEI Resources) or polyclonal antibody to IglC (1:1,000), bacterioferritin (Bfr, 1:1,000), or GFP (1:2,000; Assay Designs), as indicated to the right of the Figure 3.4. IglC expression is absent from *F. novicida* ΔFPI and Δ*iglC* strains (Fig. 3.4 lanes 2 and 3) and restored in the *iglC* complemented strain (Fig. 3.4 lane 4).

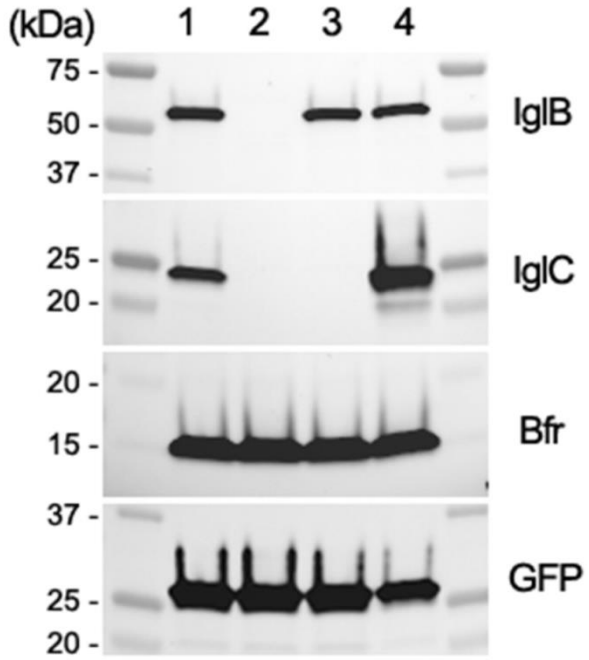

Figure 3.4 | Immunoblot analysis confirms the lack of IglC expression in the *F. novicida* mutant strains. Bacterial lysates from 1.5×10^7 GFP expressing *F. novicida* wild type (lane 1), ΔFPI (lane 2), Δ*iglC* (lane 3), and Δ*iglC* complemented with *iglC* on a plasmid (lane 4) strains were separated by SDS-polyacrylamide gel electrophoresis.

We also confirm that the complementation restores the ability of *F. novicida* Δ*iglC* mutant to multiply intracellularly (Fig. 3.5). Human monocytic THP-1 cells (1×10^5/well) were differentiated with phorbol ester and infected with *F. novicida* expressing sfGFP (1×10^6/well) for 1.5, 6, or 24 hours, as indicated. Human monocytic cell line THP-1 (ATCC TIB202) was maintained in RPMI-1640 supplemented with 10% FBS and penicillin (100 IU)/streptomycin (100 µg/mL). Prior to infection, THP-1 cells were differentiated with 100 nM phorbol 12-myristate 13-acetate for 3 days. Bacteria were pre-opsonized by incubation in 10% AB serum in HBSS at 37℃ for 10 minutes, spun onto THP-1 macrophages at 800 *g* for 30 minutes at 4℃, and incubated at 37℃ for 30 minutes to allow uptake. The infected monolayers were treated with 10 µg/ml gentamicin in DMEM containing 10% FBS for 30 minutes, washed and incubated in DMEM containing 10% FBS and 0.1 µg/ml of gentamicin. At specified time points, the infected monolayers were lysed with 1% saponin in PBS for 5 min, and the serial diluted lysates were plated on chocolate agar for bacterial CFU enumeration.Three *F. novicida* strains were studied: *F. novicida* wild-type, *F. novicida* Δ*iglC*, and *iglC* complemented *F. novicida* Δ*iglC*. The infected monolayers were then fixed with 4% formaldehyde, and the nuclei stained with DAPI. High resolution images of the infected monolayers were acquired by ImageXpress (Molecular Probes) and analyzed by MetaXpress High Content Image Analysis Software. From 1.5 to 24 hours, the number of green fluorescent bacteria per nucleus increased about 10-fold for the *F. novicida* wild-type and complemented *F. novicida* Δ*iglC* strains; in contrast, the number of *F. novicida* Δ*iglC* per nucleus decreased by 3-fold.

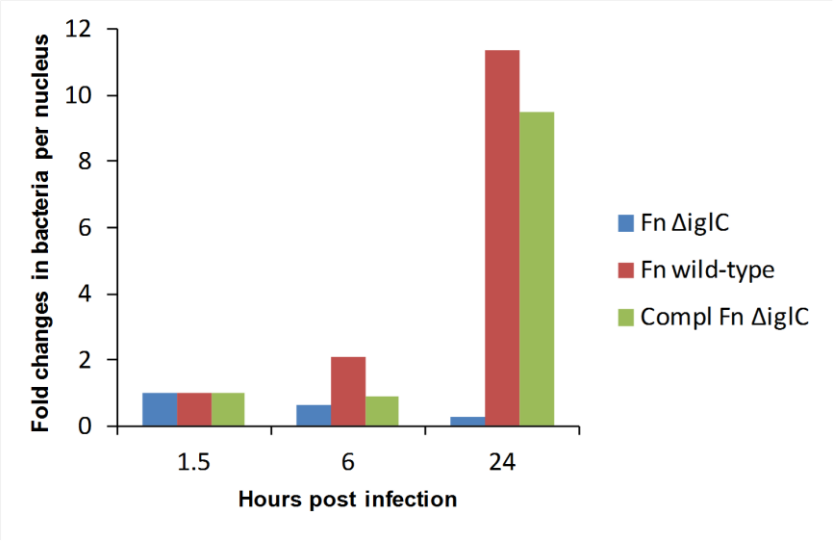

Figure 3.5 | Complementation restores the ability of *F. novicida* Δ*iglC* mutant to multiply intracellularly. From 1.5 to 24 hours, the number of green fluorescent bacteria per nucleus increased about 10-fold for the *F. novicida* wild-type and complemented *F. novicida* Δ*iglC* strains; in contrast, the number of *F. novicida* Δ*iglC* per nucleus decreased by 3-fold.

3.1.4 The *iglC* gene is required for *F. novicida* intracellular growth

Three strains of *F. novicida* – the wild-type, a Δ*iglC* mutant in which the *iglC* gene has been deleted, and a Δ*iglC* mutant complemented with the *iglC* gene - were delivered into HeLa cells (Fig. 3.6 (a) – (c)). HeLa cells are non-phagocytic and inefficiently internalize *F. novicida*, but using BLAST, *F. novicida* were delivered directly into the cell cytosol. After the HeLa cells recovered, they were harvested from the BLAST platform for study of bacterial intracellular trafficking and multiplication over time (detailed protocol shown in Appendix C). We used a modification of the differential digitonin permeabilization assay[103] to identify cytosolic versus vacuolar bacteria, confirming extensive cytosolic localization of the bacteria (Fig. 3.6 (d)), and we assayed bacterial intracellular growth by counting the number of bacteria in HeLa cells over

time (Fig. 3.6 (e)).

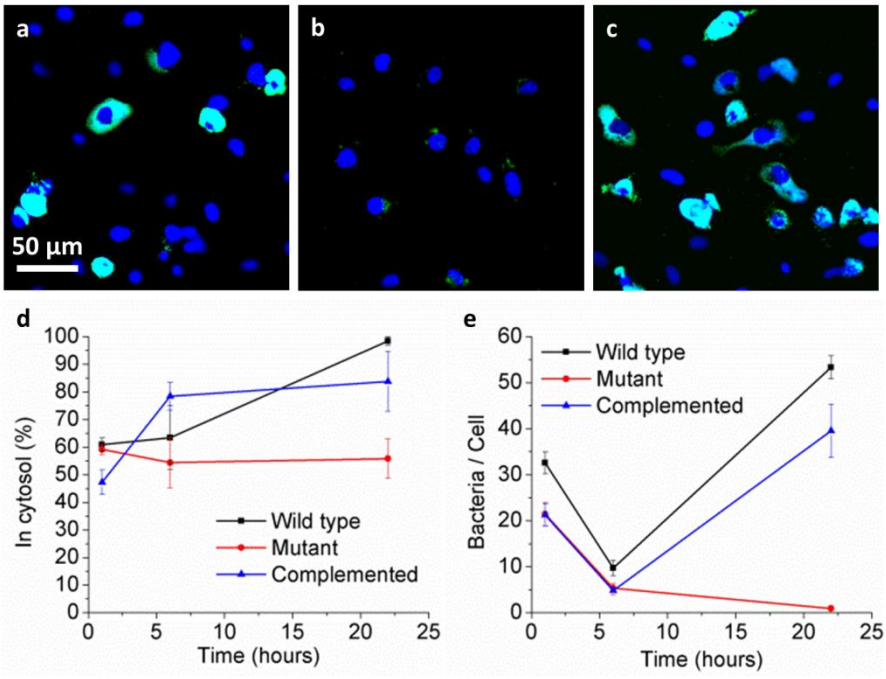

Figure 3.6 | The *iglC* gene is required for *F. novicida* intracellular growth even after cytosolic delivery. GFP-expressing *F. novicida* wild-type (**a**), Δ*iglC* mutant (**b**), and Δ*iglC* mutant complemented with *iglC* (**c**) in the cytosol of HeLa cells at 22 hours after delivery. (**d**) The percentage of these three types of *F. novicida* delivered on the platform were found in the cytosol and not trapped in vacuoles. (**e**) Growth of *F. novicida* wild-type, Δ*iglC* mutant and complemented Δ*iglC* mutant in HeLa cells after cytosolic delivery.

About the differential digitonin permeabilization assay (Fig. 3.7), vacuolar versus cytosolic localization of bacteria was assessed by a modification of the differential digitonin permeabilization method of Chercoun *et al.*[103], which permeabilizes plasma membranes but not bacterial vacuoles. After BLAST delivery of bacteria into HeLa cells, the monolayers were allowed to recover for 30 minutes; stained for 10 minutes with Alexa-Fluor 647 WGA; washed with HBSS; fixed for exactly 1 minute with 4% paraformaldehyde in HBSS; permeabilized for exactly 1 minute with 0.05 mg/mL digitonin in 110 mM potassium acetate, 20 mM HEPES, 2

mM $MgCl_2$, and 15% sucrose (KHM with 15% sucrose); washed twice with KHM containing 15% sucrose; incubated with chicken anti-*F. novicida* antibody (1:1000 dilution, a gift from Dr. Denise Monack, Stanford University) in KHM buffer containing 15% sucrose and 0.1% BSA; washed three times with KHM containing 15% sucrose; fixed for 30 minutes in 4% paraformaldehyde in 75 mM sodium phosphate, pH 7.4; permeabilized thoroughly with 0.1% saponin in PBS; washed with PBS; and incubated with Texas Red-X conjugated goat anti-chicken antibody (Invitrogen) for 90 minutes at room temperature. Monolayers were incubated with DAPI (1 μg/mL), washed with PBS, and viewed by fluorescence microscopy. Green fluorescent bacteria within the WGA-stained host cell borders that stained by the red antibody probe were scored as being cytosolic and those that were not stained by the red fluorescent antibody probe were scored as being membrane bound (vacuolar).

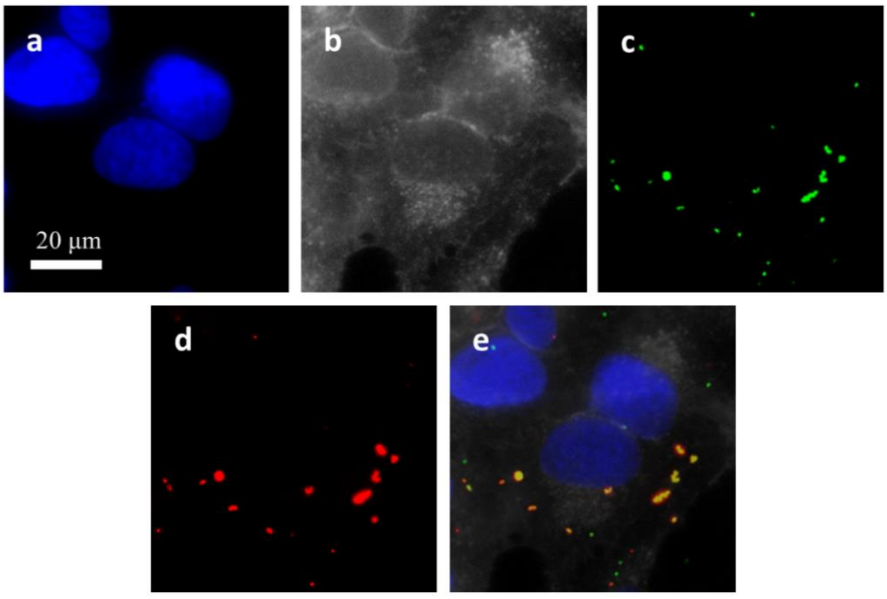

Figure 3.7 | Differential digitonin permeabilization assay for *F. novicida* delivered into HeLa cells. HeLa cells were stained by (**a**) DAPI (blue) and (**b**) WGA 647 (infrared). (**c**) GFP-expressing *F. novicida* (green). (**d**) Texas Red-X conjugated goat anti-chicken antibody (secondary antibody, red). (**e**) Merged image.

Indeed, growth curves over time (Fig. 3.6 (e)) reveal that Δ*iglC* mutant bacteria die inside the HeLa cell cytosol, suggesting that host defense mechanisms of the HeLa cells are able to kill the FPI mutant bacteria. In contrast, wild-type bacteria, which replicate intracellularly, appear immune to these host defenses. The BLAST platform delivers objects directly into the cytosol and as many as 50% of the bacteria are found in cell vacuoles (Fig. 3.6 (d)) within these non-phagocytic cells, suggesting that reuptake of the bacteria into vacuoles by an autophagic process occurs, as shown recently by Chong *et al.* for *F. tularensis* mutants that are escape competent but impaired in cytosolic replication[104]. However, autophagy does not explain the absence of growth for the ~50% of FPI mutants that remain cytosolic. Indeed, Chong *et al.* demonstrated that autophagy played only a minor role in killing of *F. tularensis* that are escape competent but defective in cytosolic replication[104] and Chiu *et al.* showed that an inducer of autophagy was effective in killing *F. novicida* at times when the bacteria are vacuolar but not when they are cytosolic[105]. Additional host defenses such as reactive nitrogen, superoxide, and nutritional restrictions may be responsible for the failure to grow and death of the Δ*iglC* mutants within the HeLa cell cytosol. We have obtained similar results using a strain in which the entire FPI has been deleted (Fig. 3.8).

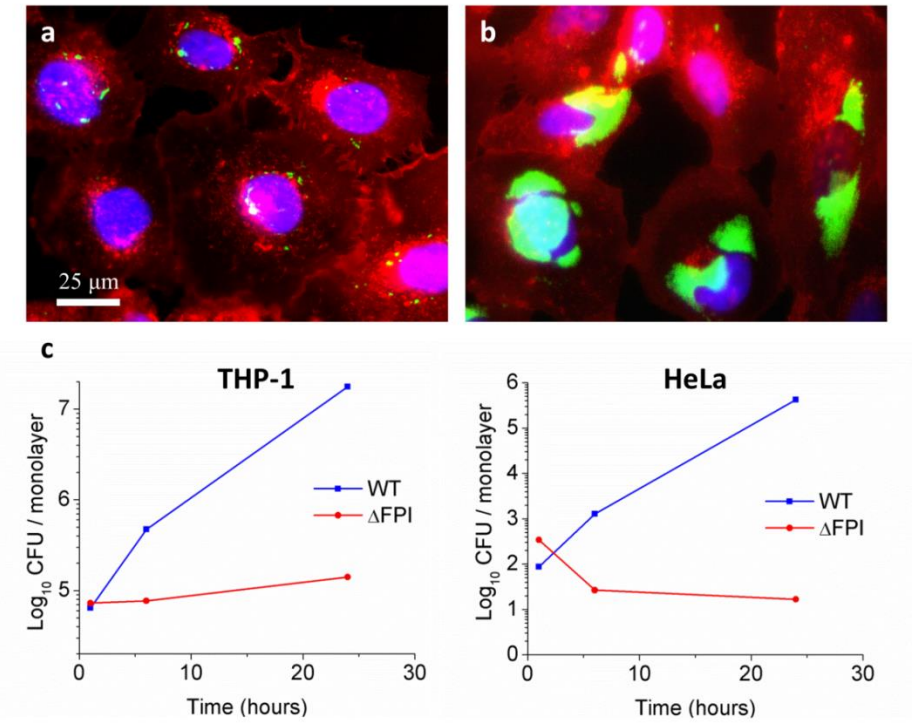

Figure 3.8 | Francisella Pathogenicity Island is required for cytosolic replication. GFP-expressing *F. novicida* (**a**) ΔFPI mutant and (**b**) wild-type in the cytosol of HeLa cells at 22 hours after delivery. (**c**) The ΔFPI strain is not able to multiply either in macrophages (THP-1), in which it is unable to escape from the phagosome, or in HeLa cells, even when delivered directly into the cytosol.

Previously, IglC has been known to be critically important in phagosome permeabilization, but our data indicate that IglC is also required for *Francisella* cytosolic replication even after phagosome escape. We hypothesize that the FPI-encoded secretion apparatus secretes effectors that are essential both for phagosome permeabilization and for counteracting host defenses against cytosolic bacteria. Moreover, our data indicate that the host cell cytosol is not a permissive environment, but instead requires specialized adaptations to permit cytosolic replication of a pathogen. The development of the BLAST tool with its capacity for massively parallel cytosolic delivery of bacterium sized cargo promises to greatly facilitate the

identification of the bacterial genes and pathogenic mechanisms that permit cytosolic pathogens to overcome host defenses and to replicate in the hostile cytosolic environment.

3.2 Enzyme delivery

To confirm that BLAST delivers biologically active and undamaged cargo directly into the cell cytosol, we delivered the bacterial enzyme β-lactamase (29 kDa, Sigma) by BLAST into NHDFs, and evaluated its delivery and functional activity by incubating the cells with the esterified β-lactamase substrate, CCF4-AM[106] (detailed protocol shown in Appendix D).

When CCF4-AM enters the cytosol, endogenous esterases convert it to CCF4, which can be detected by fluorescence resonance energy transfer (FRET). Excitation of CCF4 at 408 nm wavelength leads to efficient FRET and emission of green fluorescence at 530 nm wavelength. Bacterial β-lactamase that has been delivered by BLAST into the cell cytosol cleaves CCF4 into two separate fluorophores and the FRET effect is lost, with the emission fluorescence changing from green to blue at 460 nm wavelength.

Fig. 3.9 presents fluorescence images of CCF4-loaded cells at 5 hours after β-lactamase delivery. β-lactamase at 50 Units/mL and 1 Unit/mL in PBS were delivered into NHDFs using BLAST under the condition of fluid pumping with or without laser pulsing. NHDFs into which more enzyme was delivered show a higher blue-to-green fluorescence intensity ratio. This result shows that the enzyme remains functional after BLAST delivery.

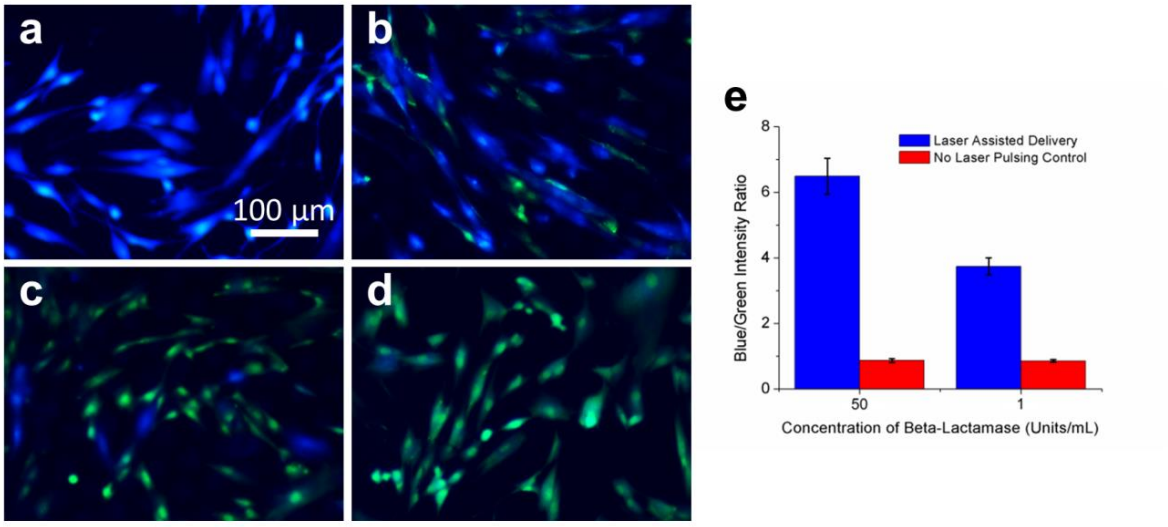

Figure 3.9 | BLAST delivered β-lactamase enzyme is functional inside NHDFs. β-lactamase at 50 Units/mL (**a, c**) or 1 Unit/mL (**b, d**) in PBS were delivered into NHDFs using BLAST under the condition of fluid pumping but with (**a, b**) or without (**c, d**) laser pulsing. (**e**) Blue and green fluorescent intensities for all 4 groups were measured 5 hours after β-lactamase delivery. A higher blue-to-green fluorescence ratio means more β-lactamase was delivered into cells and remained functional, and thus able to cleave CCF4 molecules.

3.3 Antibody delivery

Delivering antibody into cells has lots of biological applications due to its property of specific binding. For instance, Lane *et al.* injected anti-Plk1 antibodies into HeLa cells by microinjection and found that protein Plk1 is required for progression through mitosis[107]. However, labor-intensive microinjection is the most efficient method to delivery antibody due to its big size.

The antibody, Mouse anti-α tubulin with Alexa Fluor 488 (Invitrogen), was delivered into NHDFs by BLAST platform (Fig. 3.10). Mouse anti-α tubulin was prepared to 100 µg/mL in PBS and bonded on the cytoskeleton after delivery into cells. In order to get high quality images,

unbonded fluorescent antibodies need to be washed away. After 5 hours incubation, delivered cells were fixed by 4% paraformaldehye in PBS for 15 minutes at room temperature and permeabilized by 0.1% Saponin in PBS for 15 minutes at room temperature. And then cell samples were rinsed by PBS three times to remove background fluorescence. The clear cytoskeleton structure of NHDFs is shown in Figure 3.10.

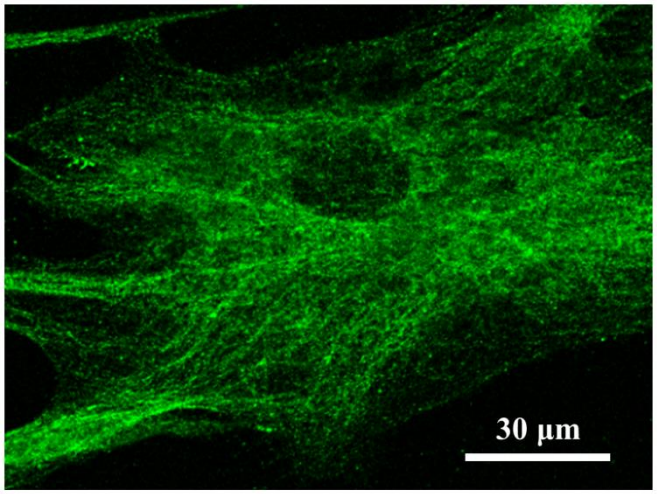

Figure 3.10 | Antibody delivered into cells by BLAST platform. Mouse anti-α-tubulin monoclonal antibody with Alexa 488 conjugate was delivered into NHDFs, labeling the cytoskeleton (green). After 5 hours incubation, cells were fixed and permeabilized to remove background fluorescence.

Another antibody, anti-FLAG, was delivered into THP-1 cells to determine whether anti-FLAG antibody inhibits intracellular replication of *F. novicida* that express FLAG-VgrG (*F. novicida*-FLAG-VgrG). There are two control experiments designed for this test, one is delivering IgG (control antibody) by BLAST platform (Fig. 3.11 (b) and (e)) and another is delivering anti-FLAG without laser pulsing (Fig. 3.11 (c) and (f)). After antibody delivery, *F. novicida*-FLAG-VgrG was incubated with BLAST delivered THP-1 cells for 90 minutes to become infected. The conditions at two time points, 1 hour and 22 hours after antibody delivery, were observed to check the effect of anti-FLAG. Moreover, no antibody signal (red fluorescence)

shown in Figure 3.11 (c) and (f) means that bubble cutting is critical for antibody delivery.

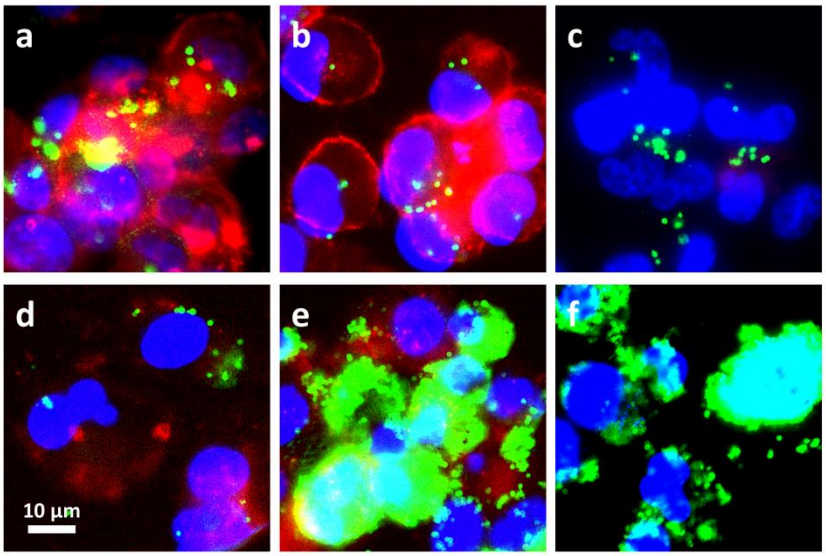

Figure 3.11 | Antibody delivered into THP-1 to inhibit intracellular replication of *F. novicida*. Images show (**a-c**) 1 hour and (**d-e**) 22 hours after delivering (**a**, **d**) anti-FLAG, (**b**, **e**) IgG and (**c**, **f**) anti-FLAG without laser pulsing (control) into THP-1. Green: *F. novicida*, Red: antibody, Blue: DAPI (nuclei).

Statistic analysis of intracellular growth for each group is shown in Figure 3.12. At beginning (1 hour after delivery), the percentage of heavily infected cells for each group is no obviously different. At 22 hours after delivery, the heavily infected cells for both of control groups, IgG delivery and no laser delivery, jump to around 40-50%. In contrast, the anti-FLAG delivered THP-1 cells have less than 20% for heavily infected by *F. novicida*-FLAG-VgrG. Hence, we can conclude that the delivered anti-FLAG antibody can block the function of VgrG proteins and successfully inhibit the intracellular replication of *F. novicida*-FLAG-VgrG in THP-1 cells.

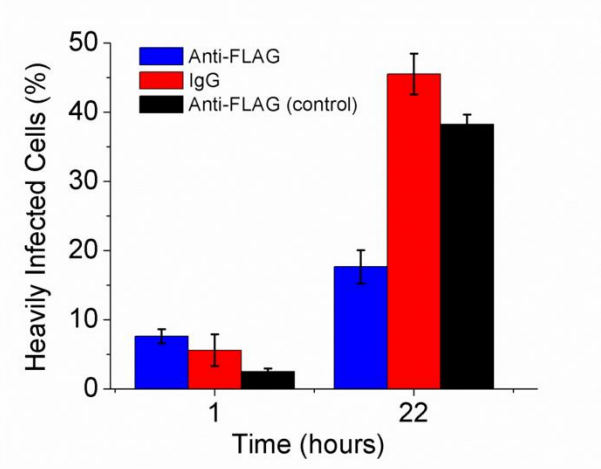

Figure 3.12 | Anti-FLAG antibody inhibits the intracellular growth of FLAG-VgrG expressing *F. novicida*.

3.4 Functional particles delivery

The BLAST platform is also powerful to deliver a wide range of man-made functional particles, such as polystyrene beads, magnetic beads, gold particles and quantum dots, into cell cytosol.

Micron-sized polystyrene beads can be used as carriers for plasmids, proteins or other bio-molecules and are widely used in many different kinds of biological applications. Waleed *et al.* delivered plasmid-coated polystyrene beads into MCF-7 cancer cells by the combination of femtosecond laser and optical tweezers[61]. In this research, 1 μm polystyrene beads were delivered successfully and the green fluorescent protein was detected after 72 hours. For our BLAST platform, 2 μm green fluorescent polystyrene beads (FluoSpheres) modified by carboxylate were concentrated to 10^{10} beads/mL in PBS and delivered into HeLa cells. Fig. 3.13 shows the fluorescent beads inside the cells around 2 hours after delivery.

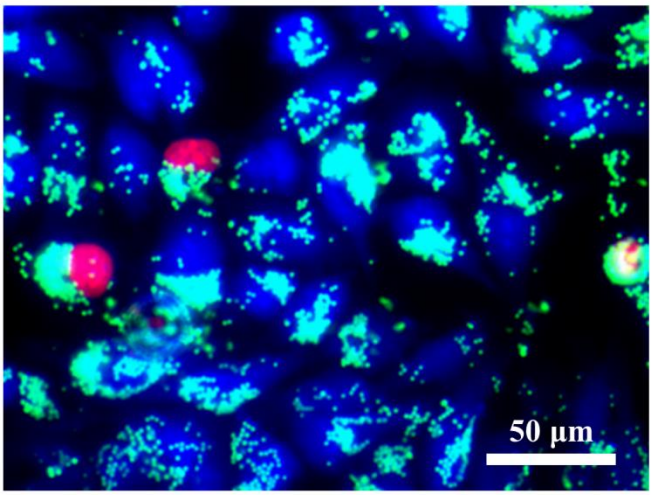

Figure 3.13 | 2 µm polystyrene beads delivered into HeLa cells by BLAST platform. 2 µm green fluorescent polystyrene beads were delivered into HeLa cells. Cell membranes were stained by WGA 350 (blue) and propidium iodide (red) was used to identify dead cells.

For the long-term observation, delivered cells were released from BLAST chip and cultured in a petri dish at 37°C. More than 30 hours after delivery, these cells were still healthy based on their morphology and continued to grow (Fig. 3.14). It proves that BLAST platform can deliver at least 2 µm size cargo into cell cytosol without effecting the cell proliferation.

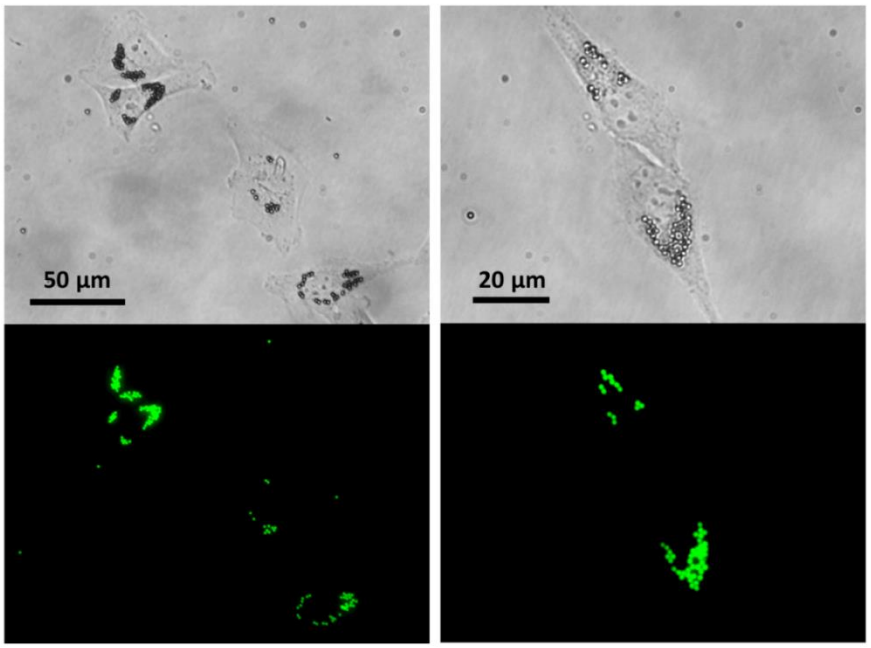

Figure 3.14 | 30 hours after 2 µm polystyrene beads delivered into HeLa cells. 2 µm polystyrene beads delivered HeLa cells were released from BLAST chip and replated in a petri dish for long-term observation. At 30 hours after delivery, cells were still healthy and kept growing.

Magnetic nanoparticles have several applications in medical diagnosis and therapy such as magnetic resonance imaging contrast enhancement, magnetic field assisted radionuclide therapy or as colloidal mediators for cancer magnetic hyperthermia[108]. 200 nm red fluorescent magnetic beads (Chemicell) modified by streptavidin were diluted to 2×10^{10} beads/mL in PBS and delivered into HeLa cells by BLAST. At 2 hours after beads delivery, cells were released from the BLAST chip and replated on a micro-magnet patterned chip[109] for 6 hours incubation at 37°C. The magnetic beads inside cells were attracted by the nearby magnetized ferromagnetic element when an external magnetic field was applied (Fig. 3.15).

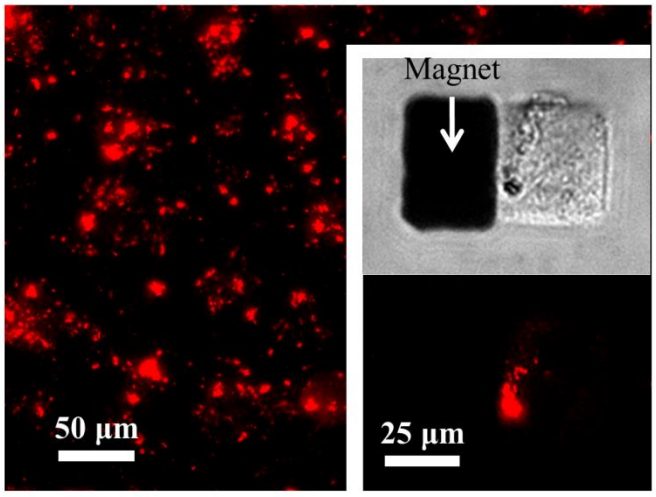

Figure 3.15 | 200 nm magnetic beads delivered into HeLa cells by BLAST platform. 200 nm magnetic beads (red) were delivered into HeLa cells and attracted by a nearby micromagnet.

BLAST is also a promising delivery platform for gold particles, which have become an attractive material for various biomedical applications such as live cell monitoring and drug delivery[110] because of their tunable surface plasmon resonance peaks. 100 nm gold particles (nanoComposix) with PEG-coating were prepared at 5×10^9 particles/mL in PBS and delivered into HeLa cells on BLAST chip. To see the nano-sized particles, delivered cells were observed under a dark-field microscope (Fig. 3.16).

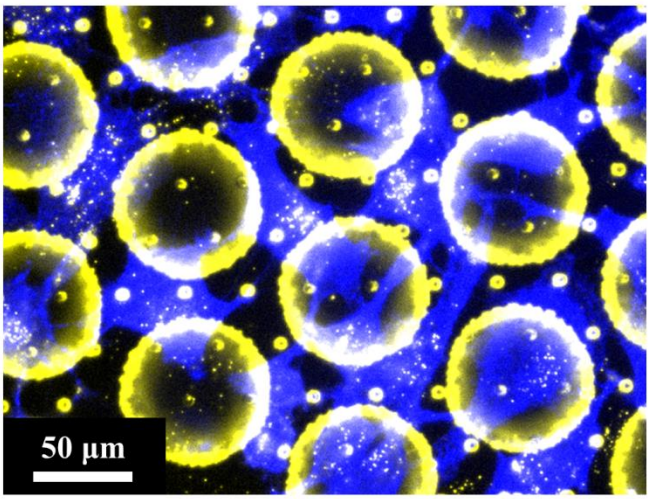

Figure 3.16 | 100 nm gold particles delivered into HeLa cells by BLAST platform. 100 nm gold particles were delivered into HeLa cells and observed under a dark-field microscope. The dark-field image was painted in yellow and merged with the cell membrane image (stained by WGA 350, blue).

Modified quantum dots (QDs) could be utilized as probes to label intracellular structures and have the potential for applications such as high-resolution cellular imaging, long-term observation of cell trafficking, cancer cell targeting, and diagnostics[89, 111]. Derfus *et al.* found that QDs delivered by liposome complexes and electroporation have serious aggregation issue and only microinjection can keep the delivered QDs as monodisperse nanoparticles[112]. However, the throughput is very low for microinjection. BLAST platform is a great solution for efficient QDs delivery. As shown in Figure 3.17, CdSe(core)/ZnS(shell) QDs (Ocean NanoTech) with PEG-coating were delivered into HeLa cells at a concentration of 8 µM.

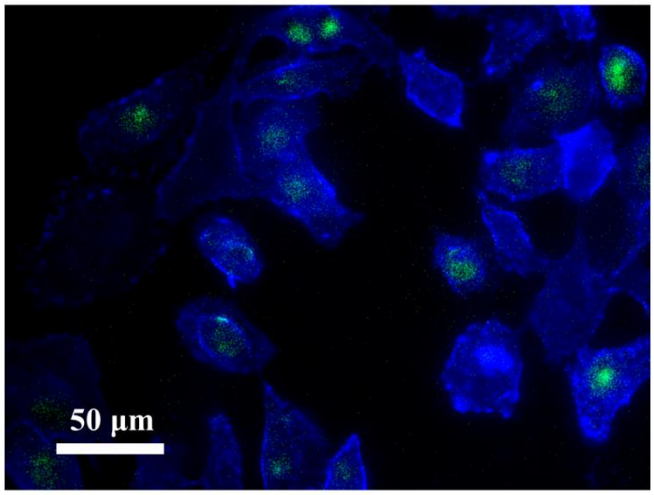

Figure 3.17 | Quantum dots delivered into HeLa cells by BLAST platform. CdSe (core)/ZnS (shell) quantum dots (green) were delivered into HeLa cells. The cell membranes appeared blue due to the WGA 350 staining.

3.5 Plasmids delivery

Delivering plasmids into cells, called cell transfection, is an important technique to study the function of genes and develop the gene therapy. The size of plasmids is around tens of nanometer and it is definitely in the delivery range of BLAST platform. Green fluorescent protein (GFP)-expressing plasmids, pmax GFP (3,486 bp), at a concentration of 50 µg/mL were prepared for delivery. Figure 3.18 shows the HeLa cells had GFP expression at 24 hours after plasmids delivered by BLAST platform. It means the delivered plasmids still kept their function and integrated with target cell DNA to produce green fluorescent proteins. However, the delivery efficiency for plasmids with GFP expression is less than 5%. Wang *et al.* also faced the same issue for cell transfection using bare plasmid DNAs by their technique[69]. The possible reason for low efficiency is that the delivered plasmids degraded fast in cell cytoplasm and most of them had no chance to get inside cell nuclei. Lipid-based membrane can protect DNA from

degradation in cell cytosol. Hence, preparing plasmids packaged by liposomes for BLAST delivery should effectively improve the transfection efficiency.

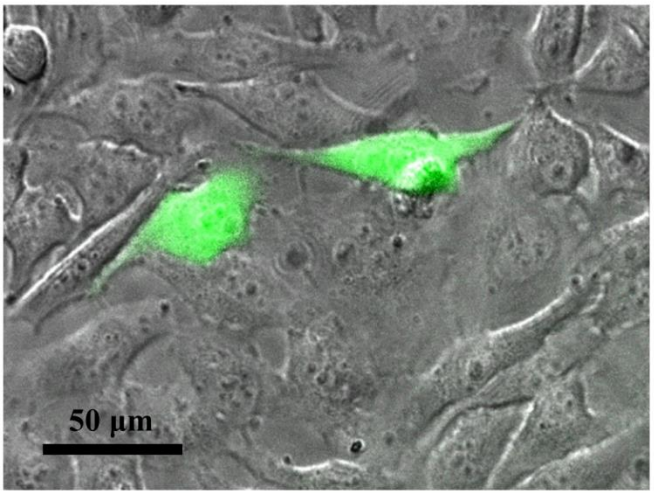

Figure 3.18 | GFP-expressing plasmids delivered into HeLa cells and expressed green fluorescence.

Chapter 4

Other Types of Delivery Platform

BLAST platform is efficient to delivery micron-sized cargo into adherent cells. In order to adapt this technique for more applications, other types of delivery platform were developed for suspension cells and sensitive cell types. Besides, a new design for mass production of BLAST chips was described.

4.1 Bare silicon wafer

For nanoscale molecules delivery, one simple method which is also using photothermal effect was developed. There is no microfabrication for this method. As shown in Figure 4.1, suspension cells or suspended adherent cells were mixed with the sample prepared for delivery. This cell solution was poured on a bare silicon wafer and waited around 10 minutes for cells settled down on the surface. Laser pulses were shined on the silicon substrate underneath the target cells. The silicon substrate was heated up by absorbing laser energy and generated cavitation bubbles which were randomly distributed over the laser-pulsed area. These cavitation bubbles could hit nearby cells and create some pores on cell membrane. The small molecules mixed with target cells would diffuse into cell cytoplasm before the transient pores resealed.

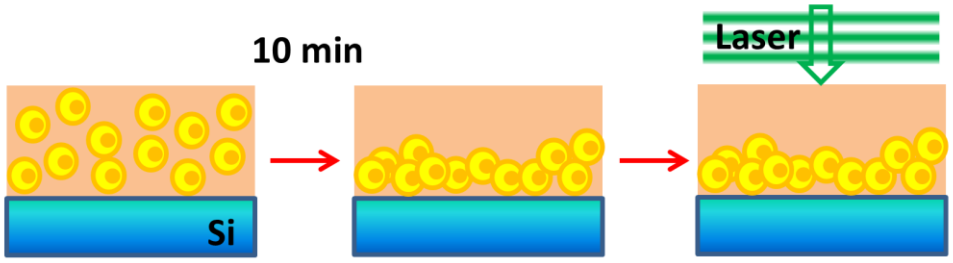

Figure 4.1 | Procedure of cell delivery on a bare silicon wafer by laser pulsing.

To proof this concept, Ramos cells, a kind of suspension cell, were mixed with 100 µg/mL calcein and dropped on the surface of a bare silicon wafer. After 10 minutes, different laser pulsing energy were applied to different groups of target cells and these treated cells were collected by pipette suction. Collected cell samples were washed several times to remove background calcein and PI was added in each sample for viability test. The results are shown in Figure 4.2.

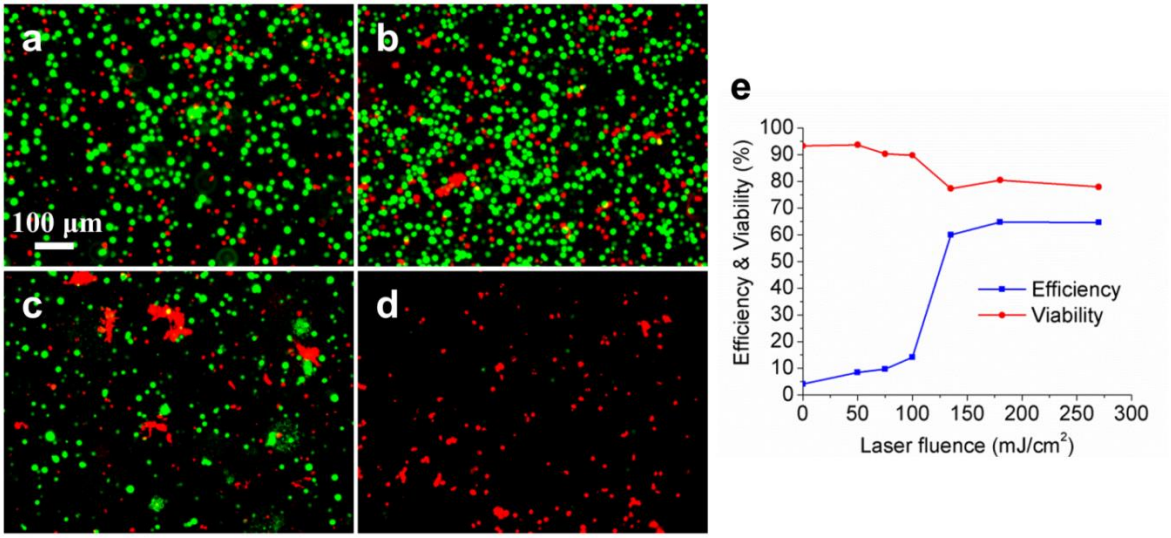

Figure 4.2 | Dye delivery efficiency and cell viability for bare silicon platform. (**a**) 270, (**b**) 180, (**c**) 100 and (**d**) 0 mJ/cm2 laser pulses were shined on cell-loaded bare silicon wafer. Cells: Ramos, calcein delivery (green) and PI viability test (red).

The delivery efficiency jumps up around 100-150 mJ/cm^2 as the threshold energy to induce

cavitation bubbles on the silicon substrate. Multiple laser pulsing would be helpful to improve the molecule uptake efficiency. But it is not easy to approach high cell viability because the bubbles are not controlled very well. The advantage of this method is easy to use and low cost. However, there is no active flow to drive cargo into cells. This diffusion-based platform cannot be used for large cargo delivery.

4.2 Cell-on-substrate BLAST platform

For some specific applications or extremely sensitive cell types, it is not convenient to culture cells on BLAST chips shown in Figure 4.3 (a). Hence, another type of BLAST platform, called cell-on-substrate type, shown in Figure 4.3 (b) was developed. In this platform, cells can be cultured on any kind of transparent substrate, such as cover glasses, petri dishes, etc. And then the cell-cultured substrate is flipped over and located on the top of BLAST chip. These target cells would gently contact the delivery holes on BLAST chip by controlling the thickness of spacing structure. Compared with regular BLAST platform, the mechanisms of membrane opening and cargo driving are totally the same.

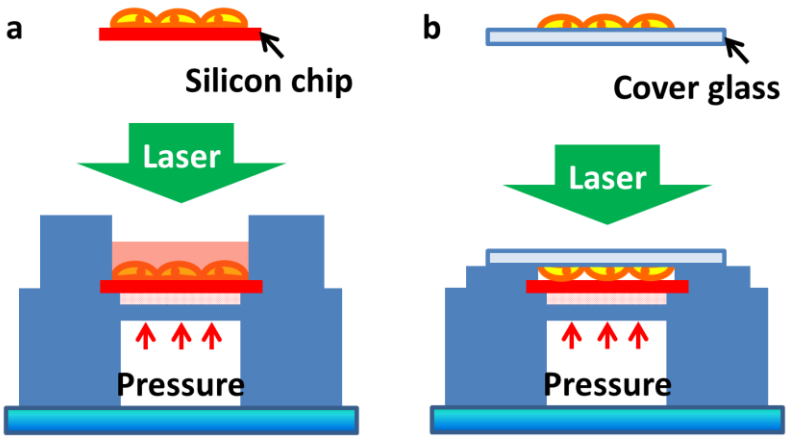

Figure 4.3 | Two types of BLAST platform. Two designs of (**a**) cell-on-chip and (b) cell-on-substrate were tested for cargo delivery.

The experimental results for cell-on-substrate BLAST platform are shown in Figure 4.4. HeLa cells were cultured on a 24 × 40 mm cover glass. For the delivering sample preparation, 200 nm polystyrene beads with the concentration of 2.3×10^{12} beads/mL were loaded in sample storage camber and covered by a non-cell-cultured BLAST chip. Three conditions, laser pulsing with fluid pumping, pumping only and laser pulsing only, were tested and shown in Figure 4.4. There was almost no beads uptake for the cases of pumping only and laser pulsing only. It shows again the importance of membrane cutting with active flow driving for large cargo delivery.

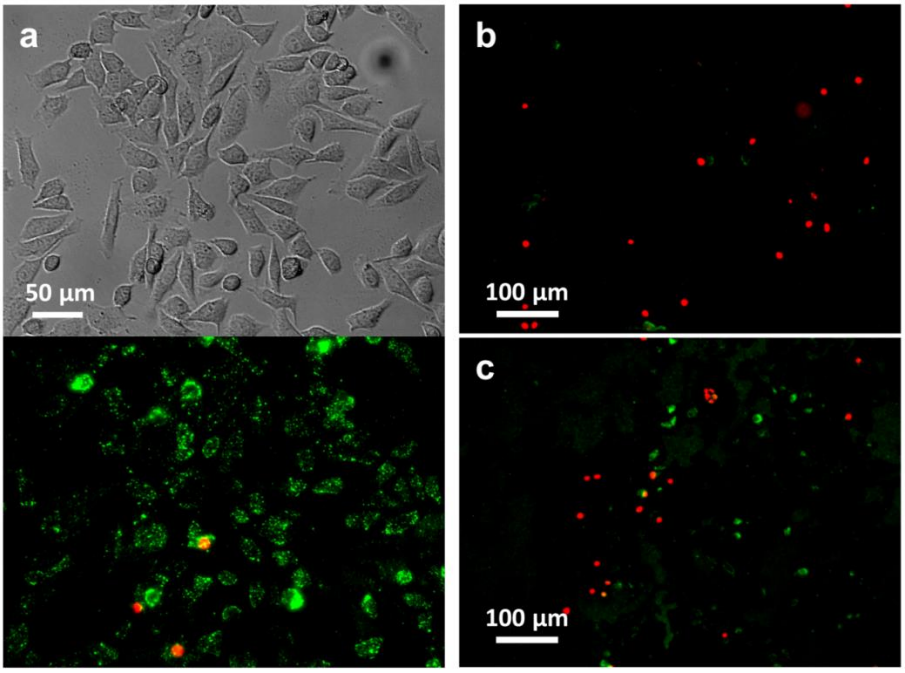

Figure 4.4 | 200 µm polystyrene beads delivered into HeLa cells by cell-on-substrate BLAST platform. The green fluorescent beads were delivered with (**a**) laser pulsing and fluid pumping, (**b**) fluid pumping only and (**c**) laser pulsing only. PI for viability test (red).

Compared with cell-on-chip BLAST, the total amount of delivered cargo in each cell by cell-on-substrate method is much less under the same condition. The possible reason is the driving flow issue explained in Figure 4.5. The regular BLAST (cell-on-chip) has no problem for

fluid pumping because the cells are free to expand when the flow driven into cell cytoplasm (Fig. 4.5 (a)). In contrast, the cells delivered by cell-on-substrate BLAST are confined in a small gap and the space for cell expansion is limited. The liquid is incompressible and has no way to leak out because these cells are sandwiched between two large area substrates. Hence, pumping issue is a critical limitation for cell-on-substrate BLAST platform.

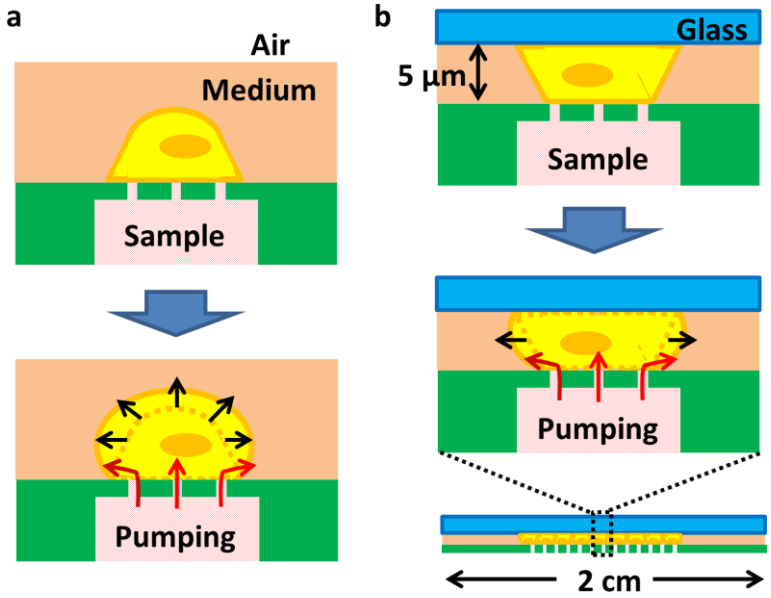

Figure 4.5 | Pumping issue for cell-on-substrate BLAST platform. Schematic pumping flows for (**a**) cell-on-chip and (**b**) cell-on-substrate delivery platform are analyzed.

4.3 BLAST platform for non-adherent cells

The regular BLAST platform does not work well for suspension cells which cannot adhere on the surface of BLAST chip. A new platform for non-adherent cells delivery was developed to serve all kinds of cell types (Fig. 4.6). As shown in Figure 4.6 (a) and (b), a Transwell membrane (Corning), which is a 10 µm thick porous polymer thin film with 1 µm pores randomly

distributed, was used to trap the suspension cells on the chip. To avoid cells smashed by the stress, a well structure worked as a spacer and aligned cells with delivery holes was fabricated on the regular BLAST chip by photolithography process (Fig. 4.6 (c)). AZ 5214 (AZ Electronic Materials), a photoresist, was used as the material of the well structure and its thickness was controlled by the spin-coating process (Fig. 4.6 (e)). To demonstrate the function of new platform, Ramos cells were loaded on BLAST chip with well structure. As shown in Figure 4.6 (d), the size of well structure was designed to accommodate one cell in each location. The delivery hole was located in the center of the well and contacted the target cell with automatic alignment.

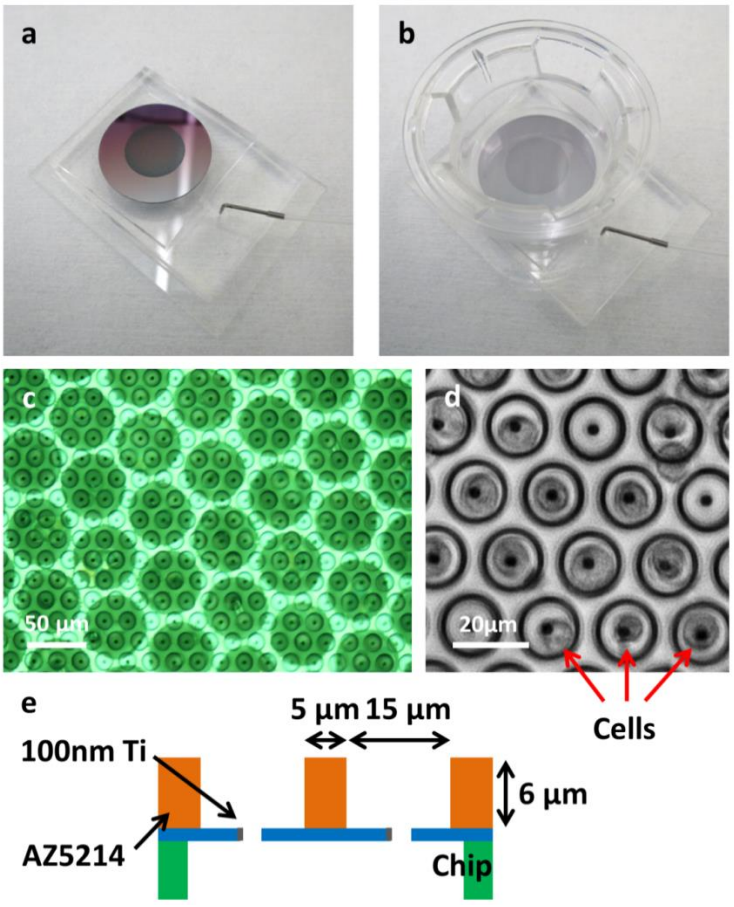

Figure 4.6 | BLAST platform for non-adherent cells. (**a**, **b**) Porous membrane for cell trapping was covered on BLAST chip. (**c**) Well structure on the chip. (**d**) Ramos cells loaded in well structure. (**e**) Dimensions for on-chip well structure.

The test results for non-adherent cells delivery are shown in Figure 4.7. Ramos cells were stained by Calcein-AM (Invitrogen) before loading into well structure. 10 µL PI solution with the concentration of 5 µg/mL was added in sample storage chamber and assembled with well-structure BLAST chip. Loaded cells would be pushed down to contact the delivery holes when covered by the porous membrane. Membrane with 1 µm pores was selected because the liquid would be passed through but cells would be trapped. As shown in Figure 4.7 (b), some of the Ramos cells labelled by solid circles had PI uptake (color turned to red) when a laser pulsed in whole field of view. The low delivery efficiency may be caused by nonuniform trapping for large area. Better trapping mechanism can improve the cells contact with the delivery holes and increase the chance of cargo delivery.

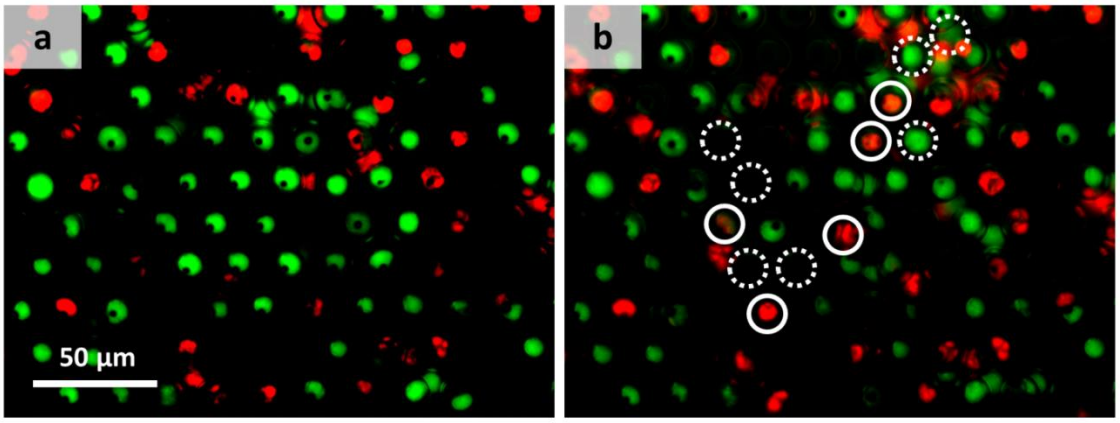

Figure 4.7 | Dye delivered into non-adherent cells. The images show (**a**) before and (b) after PI (red) delivered into Ramos cells. Cells were stained by Calcein-AM (green) before test. Delivered cells are labelled by solid circles.

4.4 SOI BLAST chips for mass production

Regular BLAST chips need to be fabricated one by one due to some critical designs for optimized performance. A new type of BLAST chips fabricated on silicon on insulator (SOI)

wafers was designed to satisfy the requirement of mass production. The most critical challenge for mass production is the uniformity for large area etching, especially the step of DRIE process. DRIE process was used to etch the through-chip channels (300 μm in depth) and any slight variation of etching rate in different locations would cause serious structure collapse because of long-time etching. To improve etching quality for large area, enlarging the etch opening for each single channel is the easiest way. However, the 1.5 μm thick SiO_2 thin film stood on channel structure would be fragile when channel size becomes too large (discussed in Ch 2.3.2). Hence, the thin film was replaced by 10 μm thick silicon layer to strengthen the chip structure shown in Figure 4.8. The SOI wafer with 10 μm device layer was used for new chip fabrication. Besides, the design of honeycomb pattern can further strengthen the supporting structure and maximize the delivery area.

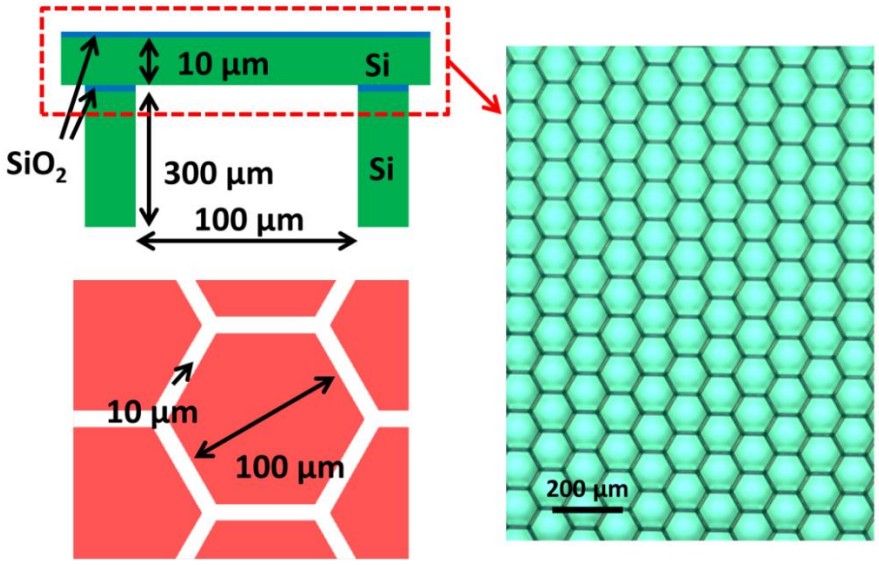

Figure 4.8 | Design of BLAST chips fabricated by SOI wafers.

The improvement in uniformity for large area etching allowed us to fabricate more BLAST chips on each single wafer. As shown in Figure 4.9 (a), a 4-inches SOI wafer can accommodate 9 BLAST chips. Most of the fabrication steps are followed the regular BLAST procedure described

in Chapter 2.2.1. The finished SOI BLAST chip is shown in Figure 4.9 (b) and (c). Mass production can not only save fabrication time but also cut down the cost. The cost of SOI BLAST chip is only 10% regular BLAST one. The only drawback for this design is the potential clogging issue due to the 7 times longer delivery holes (from 1.5 μm to 10 μm in length).

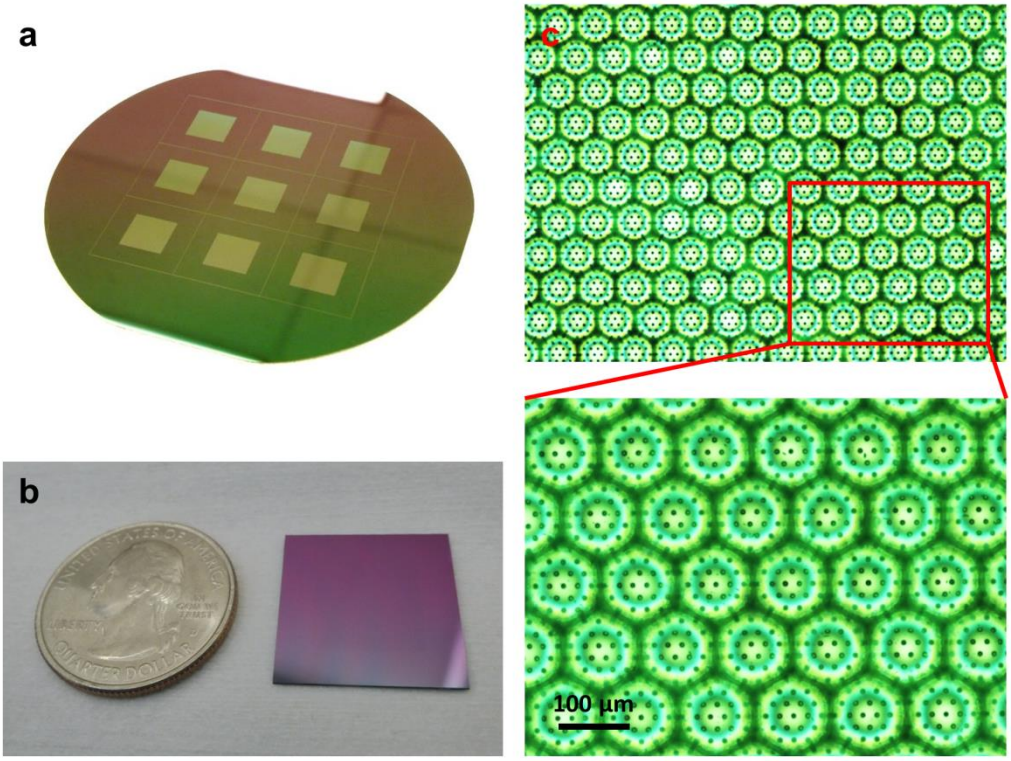

Figure 4.9 | Images for SOI BLAST chips. (**a**) 9 BLAST chips on a 4" SOI wafer. (**b**) A SOI BLAST chip. (**c**) Zoom in the top surface of SOI chip.

Chapter 5

Discussions and Conclusions

The challenge of delivering large cargo into mammalian cells derives from the slow diffusion of large cargo coupled with the fast resealing time of transient membrane pores. BLAST is the first platform that can deliver a wide variety of cargo types, ranging in size up to micron-sized cargo, into mammalian cells with high delivery efficiency, high cell viability, and high throughput. BLAST provides a physical approach for reliably puncturing mammalian cell membranes in contact with metallic nanostructured thin films using short laser pulse illumination. Our data show that a small pulse energy, 55 mJ/cm^2, efficiently opens pores in the plasma membranes of a variety of mammalian cells, including primary cells such as NHDFs, PB-MDMs, and RPTECs, and the HeLa cancer cell line. This cell-type independent membrane opening capability coupled with cargo-type independent, pressure flow driven delivery technology renders BLAST a powerful and versatile platform for delivering a variety of cargo up to a few micrometers in size into a wide spectrum of mammalian cell types.

Furthermore, BLAST delivers all cargo directly into the cell cytosol, avoiding cargo entrapment in endosomes, and BLAST maintains cargo functionalities. This was demonstrated for β-lactamase substrate cleavage in NHDFs and by showing that escape-incompetent *L. monocytogenes* delivered into NHDFs form comet tail-shaped actin bundles in the cytosol.

Both experiments provide direct evidence that cargo is delivered intact, directly into the cytosol.

Massively parallel and nearly simultaneous delivery of cargo into cells under the same physiological conditions using BLAST allows statistically reliable analysis of delivered cargo and the interactions of the cargo with cells over time. Transient membrane pore resealing time studies shown in Figure 2.22 and 2.23 takes advantage of this unique capability. A laser beam programmed to scan across the entire chip to open cell membranes sequentially with known delay time is followed by uniform pressured delivery across the entire chip. The delivery efficiencies in different zones on the chip show the effect of delay time between laser pulsing and fluid pumping under the same delivery conditions, such as cargo concentration, pulse energy, fluid pressure, and incubation time. A single experiment using a single chip can produce sufficient data for statistical analysis.

The study of the intracellular lifestyle of bacteria in live cells shown in Chapter 3.1 was made possible with BLAST. That bacteria can be delivered into 100,000 host cells at one time allows separation of the infected cells into multiple subgroups for study of various subsequent phenomena over time after delivery, such as bacterial localization and intracellular multiplication performed in this study. Although the bacterial delivery experiment was intended only for demonstrating the utility of BLAST, this study unexpectedly discovered that IglC is not only important for phagosome permeabilization, but also required for cytosolic replication after phagosome escape. Such a study is nearly impossible using conventional pipette-based delivery approaches since they do not provide the throughput required for reliable statistical analysis and the cells are not infected simultaneously, making it difficult to perform studies over time for fast occurring events, such as the re-packaging of bacteria into vacuoles after delivery.

Compared with existing techniques, the BLAST mechanism has several important

advantages. As a physical method to disrupt membranes, cargo is delivered into the cytosol directly without any exogenous materials, chemical carriers, or involvement by endocytotic pathways. In contrast to electroporation, electrical fields, which may damage target material or cause cytotoxicity, are not required. The use of sharp glass tips to penetrate cell membranes with conventional microinjection has a deleterious effect on cell viability, especially when using micron-sized pipet tips. With BLAST, laser induced cavitation bubbles generate ultrafast and localized flow to puncture the membrane near the titanium-coated area. This rapid motion should cause less mechanical perturbation to the rest of the cell membrane and results in negligible cell death due to the membrane cutting and cargo delivery processes.

Because of the dimensions of the cargo storage chamber, BLAST delivery to 100,000 cells requires only 10 μL of sample and a cargo concentration in the range of 10^9 to 10^{10} particles/mL that may be adjusted depending on the desired cargo per cell ratio. The small amount of sample required is particularly advantageous for applications involving precious biological samples or man-made micro-devices. The design of the ultra-thin membrane (1.5 μm in thickness) supported by thicker large channel structures (50 μm in diameter) circumvents clogging issues that often plague sharp tip pipet-based injection tools.

Different cell lines may require individualized designs for platform delivery holes and patterns, including experimentally determined size and distribution density, to achieve optimized delivery efficiency and cell viability. In our fabrication process, only one photolithography step needs to be customized for specific platform delivery hole designs. Therefore, the BLAST platform is readily adaptable to a variety of cell lines due to the flexible design of the most critical parameters.

The fabrication of BLAST utilizes standard microfabrication processes. Typical

research-focused universities and similarly focused industrial entities could manufacture the platform chips and enable their usage. Individuals and entities versed in the general art of microfluidic platform generation would not find these platforms challenging to replicate. As for operating the platform, this is equally enabled by simple steps used in almost all biologically focused research or industrial labs worldwide.

The BLAST platform has potential to be a powerful research tool due to its ability to deliver a wide range of cargo sizes and types. Quantum dots, plasmids, gold particles, magnetic beads, and bacteria have all been delivered successfully into the cytosol (Chapter 3). Modified quantum dots could be utilized as probes to label intracellular structures and have the potential for applications such as high-resolution cellular imaging, long-term observation of cell trafficking, cancer cell targeting, and diagnostics[111]. Gene therapy based on the technique of DNA transfection into target cells is under continuous development for clinical use[113]. BLAST is also a promising delivery platform for gold particles, which have become an attractive material for various biomedical applications such as live cell monitoring and drug delivery[110] because of their tunable surface plasmon resonance peaks. Magnetic nanoparticles have several applications in medical diagnosis and therapy such as magnetic resonance imaging contrast enhancement, magnetic field assisted radionuclide therapy or as colloidal mediators for cancer magnetic hyperthermia[108]. The ability to deliver live bacteria directly into the host cell cytosol, bypassing the phagocytic and vacuolar processes, allows studies to determine whether genes required for uptake or vacuolar escape are or are not required for subsequent steps, such as cytosolic replication or cell-to-cell spread, thus providing a valuable tool for dissecting the virulence mechanisms of intracellular pathogens[88].

Finally, the BLAST platform is a versatile tool with the potential to yield new discoveries in

the fields of cell biology and cell engineering. Its applications are not limited to the delivery of large biological molecules or organelles. Man-made, micron-sized intracellular devices are being developed for future research in cell engineering and intracellular delivery of such devices could prove problematic without a high throughput large cargo cell transfer mechanism[114-119]. BLAST is currently the only potential approach for delivering these micromachines into live cells without vacuole trapping.

Appendix A

Materials

1. *L. monocytogenes* Δ*hly* Δ*plcB* and Δ*hly* Δ*mpl* will be grown overnight in BHI at 30 ^{o}C.
2. HeLa cells to be plated onto 4 good chips and 4 not-so-good chips so that the cells will be ready for BLAST on Tuesday, Feb. 18, 2014.
3. DMEM with 10% HI-FBS
4. HBSS
5. 4% paraformaldehye in 0.1M PIPES with 6% sucrose
6. 0.1% saponin in PBS,
7. 1 μg/ml DAPI in PBS
8. Glycerol:PBS (90:10 vol/vol)
9. Rabbit anti-Listeria monocytogenes [use at 1:1000]
10. Goat anti-Rabbit Oregon Green
11. Phalloidin-Rhodamine
12. 4 good chips
13. 4 not-so-good chips

General Design:

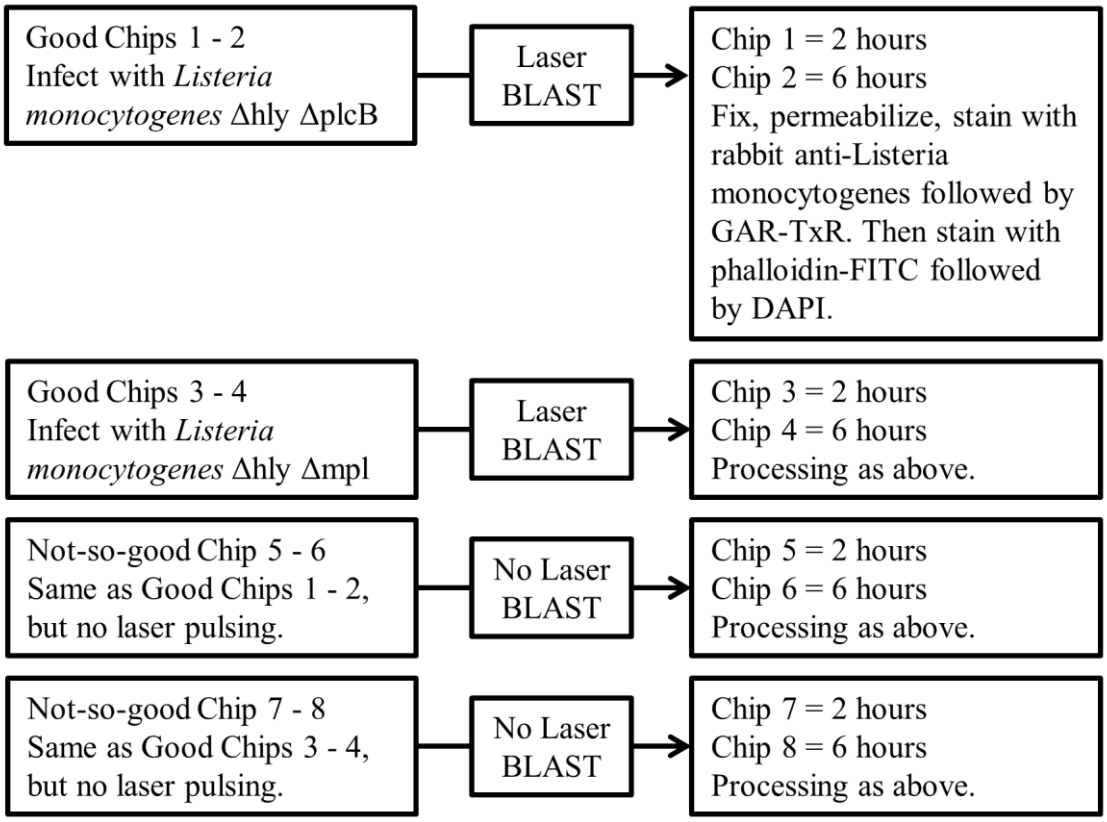

Methods:

1. Inoculate Listeria strains in 10 ml BHI x 2 (two tubes of 10 ml each per strain) the day prior to infection and grow overnight at 30^{o}C.
2. Seed HeLa cells onto BLAST Chips (4 good BLAST chips and 4 not-as-good-BLAST chip [for non-laser treated controls]) one day prior to BLAST infection to an OD of ~1.2.
3. Following day pellet the bacteria at 14,000 g at RT for 1 min in benchtop microfuge, and resuspend in 1 ml HBSS to an OD of 1.0. Wash once and resuspend to OD 1.0 in HBSS.
4. Transfer supernate to a new tube. Determine optical density at 540 nm to ensure OD ~ 1.0 for the Listeria mutant strains.
5. Infect the HeLa cells by Parallel BLAST in HBSS (4 good chips for laser blasting and 4 not-so-good chips as non-laser pulsed controls).

6. Allow cells to recover for 10 min.
7. Wash the cells 4 x with HBSS. Change media to DMEM with 10% HI-FBS.
8. At 60 min after BLAST, change media of the chips to 5 μg/ml gentamicin in DMEM with 10% FBS.
9. At 2 hours (chips 1, 3, 5, 7) or 6 hours (chips 2, 4, 6, 8), replace the medium with freshly prepared pre-warmed (37^{o}C) 4% paraformaldehyde in PBS.
10. Fix for 30 min at room temperature.
11. Wash cells x 2 with PBS.
12. Permeabilize with 0.1% Saponin, 10 mM Lysine in PBS for 30 minutes.
13. Stain with rabbit-anti-Listeria monocytogenes (1:1000) for 1 hour.
14. Wash x 3 with PBS.
15. Stain with Texas Red-conjugated Goat-anti-Rabbit IgG for 1 hour.
16. Wash x 2 with PBS.
17. Stain cells with Phalloidin-FITC (5 ul of methanolic stock per 0.2 ml of PBS). Stain for 15 minutes at room temperature.
18. Wash once with PBS.
19. Stain for 10 minutes with 1 μg/ml DAPI in PBS.
20. Wash x 3 with PBS.
21. Mount with glycerol:PBS (90:10 vol/vol) for viewing.
22. View and take pictures by fluorescence microscope and, if necessary, by Confocal fluorescence microscope.

Appendix B

Materials

1. *L. monocytogenes* Δ*hly* Δ*plcB* (both GFP-expressing and not GFP-expressing) will be grown overnight in BHI at 30^{o}C. These will be used both for BLAST chips and for macrophage infection by regular phagocytosis.
2. *L. monocytogenes* (both GFP-expressing and not GFP expressing) will be grown overnight in BHI at 30^{o}C. These will be used only for the THP-1 macrophage infection by regular phagocytosis.
3. Primary cells, NHDFs, will be plated onto 2 good chips and 2 not-so-good chips so that the cells will be ready for BLAST.
4. DMEM with 10% HI-FBS with and without 5 µg/ml gentamicin
5. HBSS
6. 4% paraformaldehye in PBS
7. 0.1% saponin in PBS
8. 1 µg/ml DAPI in PBS
9. Glycerol:PBS (90:10 vol/vol)
10. Phalloidin-Rhodamine
11. 2 good chips
12. 2 not-so-good chips

General Design:

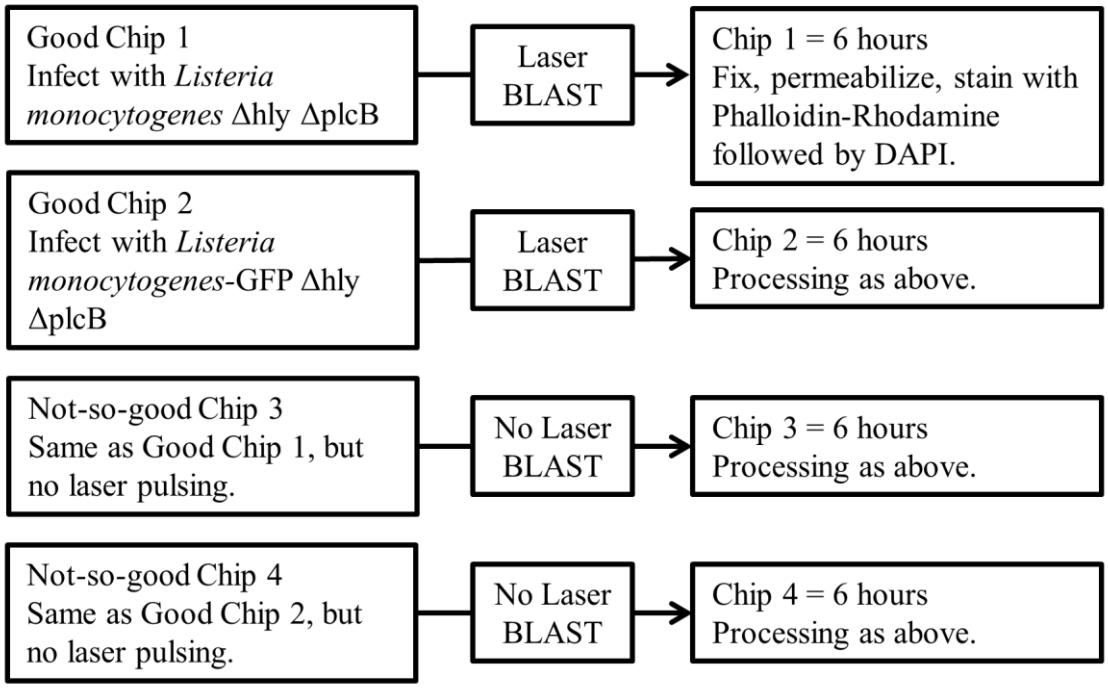

Methods:

23. Inoculate Listeria strains in 10 ml BHI x 2 (two tubes of 10 ml each per strain) the day prior to infection and grow overnight at 30^{o}C to an OD of ~1.2.

24. Seed primary cells, NHDFs, onto BLAST Chips (2 good BLAST chips and 2 not-as-good-BLAST chip [for non-laser treated controls]) one day prior to BLAST infection.

25. Following day pellet the bacteria at 14,000 g at RT for 1 min in benchtop microfuge, and resuspend in 1 ml HBSS. Wash once and resuspend to OD at 540 nm of 2.5 in HBSS.

26. Infect the NHDFs by Parallel BLAST in HBSS (2 good chips for laser blasting and 2 not-so-good chips as non-laser pulsed controls).

27. Allow cells to recover for 10 min.

28. Wash the cells 4 x with HBSS. Change media to DMEM with 10% HI-FBS.

29. At 60 min after BLAST, change media of the chips to 5 μg/ml gentamicin in DMEM with 10% FBS.

30. At 6 hours (all chips), replace the medium with freshly prepared pre-warmed (37^{o}C) 4% paraformaldehyde in PBS.

31. Fix for 30 min at room temperature.

32. Wash cells x 2 with PBS.

33. Permeabilize with 0.1% Saponin, 10 mM Lysine in PBS for 30 minutes.

34. Wash x 2 with PBS.

35. Stain cells with Phalloidin-Rhodamine (5 µl of methanolic stock per 0.2 ml of PBS). Stain for 15 minutes at room temperature.

36. Wash once with PBS.

37. Stain for 10 minutes with 1 µg/ml DAPI in PBS.

38. Wash x 3 with PBS.

39. Mount with glycerol:PBS (90:10 vol/vol) for viewing.

40. View and take pictures by fluorescence microscope and, if necessary, by Confocal fluorescence microscope.

Methods for THP-1 cells in 24-well plates:

1. Infect at OD 0.0005 in DMEM + HI-FBS. Spin plates at 800 g x 30 min at 4^{o}C.
2. Incubate for 30 min at 37^{o}C.
3. Wash plates twice with HBSS and replace with fresh medium with DMEM + HI-FBS.
4. After 30 min at 37^{o}C, replace medium with DMEM+HI-FBS with 5 µg/ml Gent.
5. After 6 hours at 37^{o}C, fix in pre-warmed 4% paraformaldehyde in PBS fixative.
6. Wash x 2 with PBS.
7. Permeabilize with 0.1% saponin with 10 mM lysine in PBS.
8. Stain with phalloidin-rhodamine (5 µl in 200 µl of PBS)
9. Wash with PBS x 2, 0.5 ml per wash.
10. Stain with DAPI, wash with PBS, mount with Molecular Probes Prolong Gold Anti-Fade.

Appendix C

Materials

1. sfGFP-Fn ΔiglC (Fn ΔiglC/pMP633-PbfrSD-sfGFP; Location R2-422). Inoculated in 50 ml TSBC, OD = 10 = "1" = Mutant
2. sfGFP-Fn (Fn/pMP633-PbfrSD-sfGFP; Location L4-233); Inoculated in 50 ml TSBC, OD = 10 = "2" = Parent
3. iglC complemented sfGFP-Fn ΔiglC (Fn ΔiglC/pMP633BC-PbfrSD-iglC_Pomp-sfGFP version 1; Location R2-422); Inoculated in 50 ml TSBC, OD = 10 = "3" = Complemented
4. Parental strain on HeLa no Laser = Control = "4"
5. DAPI in 0.9% NaCl with 20 mM HEPES, pH 7.4
6. WGA AlexaFluor-647 (5 mg/ml stock solution in PBS, dilute 500-fold to get 10 µg/ml working concentration)
7. HBSS with 1 mM $CaCl_2$ and 0.5 mM $MgCl_2$ [50 ml]
8. Accutase [2 ml] to lift HeLa cells from the BLAST chips
9. Chicken anti-Fn
10. Goat anti-IgY-Texas Red
11. DMEM-10% HI-FBS with 10 µg/ml and 0.1 µg/ml gentamicin [50 ml each]
12. HBSS for washing
13. PLL treated 8-well chambered coverglass
14. Digitonin (use at 0.05 mg/ml. Soluble in DMSO at 20 mg/ml = 400x, i.e. final DMSO = 0.25%)

15. KHM buffer with 15% sucrose (7.5 g Sucrose, 10 ml 5x KHM, 35 ml of H_2O)
16. Paraformaldehyde
17. KHM buffer with 15% sucrose and 0.1% BSA
18. THP-1 cells for comparison to verify that Digitonin assay is working properly.
19. 6 good chips (two for each of the 3 strains)
20. 2 not-so-good chips (for use as non-laser controls for the parental strain, one will be at the 30 minute time point and one will be accutase treated to make the 6 hour and 24 hour control time points).

General Design:

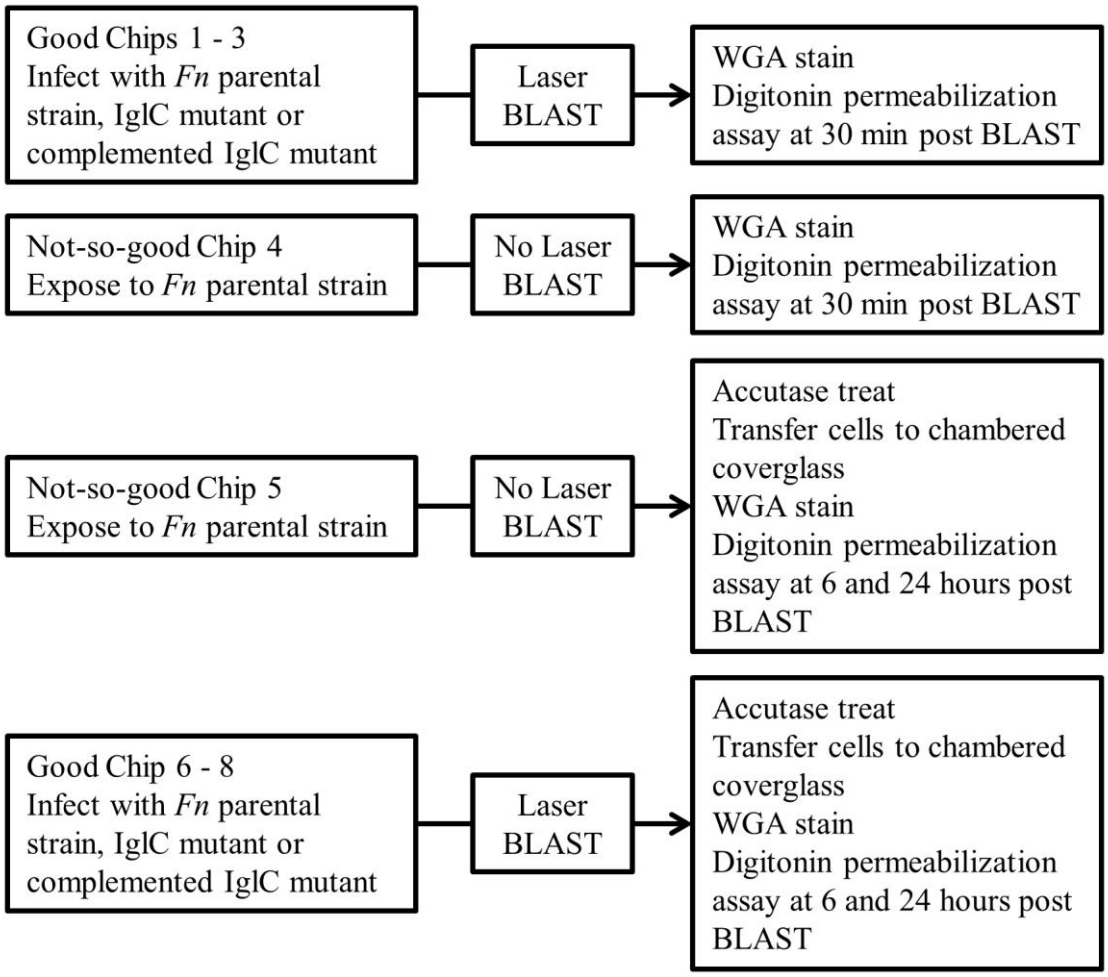

Methods:

1. Coat wells of chambered coverslip with PLL.
2. Inoculate bacteria in 50 ml TSBC with hygromycin.
3. Seed HeLa cells onto BLAST Chips (6 good BLAST chips and 2 not-as-good-BLAST chips [for non-laser treated controls]).
4. Following day pellet the bacteria at 7000xg, 4℃ for 15 min, wash once, and resuspend in 1 ml HBSS.

5. Determine optical density at 540 nm to ensure OD ≥ 10.0.
6. Infect the HeLa cells by Parallel BLAST in HBSS (2 good chips with each of the 3 strains and the 2 not-so-good chips with the parental sfGFP-Fn strain as non-laser blasted controls). For each strain, one good chip will be used for a 30 minute time point and another chip will be accutase treated and used for 6 hour and 24 hour time points on chambered coverglass. For the not-so-good chip, one will be used for the early time point (cells fixed on the chip) and the other chip will be accutase treated and used for 6 and 24 hour time points of the parental strain.
7. Allow cells to recover for 10 min.
8. Change media of the chips to 10 µg/ml Gentamicin in DMEM with 10% FBS.
9. Incubate at 37^{o}C for 30 min.
10. Wash the Chips twice with HBSS containing 1 mM $CaCl_2$ and 0.5 mM $MgCl_2$. Change media of the 6 - 24 hour chips to 0.1 µg/ml Gentamicin in DMEM with 10% FBS.

Procedure for WGA staining and antibody staining for the early time point:

1. After washing the cells twice with HBSS containing 1 mM $CaCl_2$ and 0.5 mM $MgCl_2$ (step #10 above) add WGA-AlexaFluor 647 (10 µg/ml) in HBSS containing 1 mM $CaCl_2$ and 0.5 mM $MgCl_2$. Incubate for 5 min at 37^{o}C.
2. Wash the cells twice with HBSS containing 1 mM $CaCl_2$ and 0.5 mM $MgCl_2$.
3. Fix the HeLa cells for 30 minutes in 0.1 M PIPES, pH 7.4, 6% Sucrose, 4% paraformaldehyde.
4. Wash the cells three times with 0.1 M PIPES, pH 7.4, 6% Sucrose.
5. Incubate cells with 1:250 chicken anti-Fn for 45 min at RT in 0.1 M PIPES, pH 7.4, 6%

Sucrose, with 0.1% BSA.

6. Wash three times with 0.1 M PIPES, pH 7.4, 6% Sucrose.
7. Stain with Goat anti-IgY Texas Red at 1:99 dilution in 0.1 M PIPES, pH 7.4, 6% Sucrose -0.1% BSA for 45 min at room temperature.
8. Wash three times with 0.1 M PIPES, pH 7.4, 6% Sucrose.
9. Stain with DAPI (1 µg/ml) in PBS for 5 min.
10. Wash x 2 with PBS. Mount with glycerol:PBS (90:10 vol/vol) for viewing.
11. View and take pictures by fluorescence microscope and, if necessary, by Confocal fluorescence microscope.

Processing for the 6 - 24 hours chips:

11. 60 min after BLAST, add 0.3 ml of Accutase to each chip.
12. Incubate the chips with the Accutase at room temperature for 5 - 10 minutes to detach the HeLa cells.
13. Wash cells off the chip with 0.5 ml of DMEM with 10% FBS (total volume will be about 0.8 ml, i.e. 0.3 ml of Accutase and 0.5 ml of DMEM-FBS).
14. Transfer the HeLa cells from each chip to one well of each of 2 8-well chambered LabTek coverslip slides (each chip into 2 wells total, one well per slide) about 0.4 ml/well. The wells will be PLL coated prior to use.
15. After 60 min, replace medium with 0.1 µg/ml Gentamicin in DMEM with 10% FBS.
16. Follow above protocol with staining, fixation, and antibody staining etc. after 6 hours and at 24 hours post-BLAST.
17. View by fluorescence microscopy and for each time point and condition, count number of

intracellular bacteria (i.e. within contours of WGA staining and staining green but not red) at each time point and for each condition.

18. THP-1 cells on coverslips will be processed the same at 6 and 24 hour time points after conventional infection of opsonized bacteria. Same three strains in duplicate in each of two 24-well plates, i.e. 6 cover slips/24 wp x 2.

Appendix D

Materials

1. β-Lactamase substrate solution A, CCF4-AM 0.2 mg in 182 µl of DMSO = 1 mM. Rack 8, box B2, -20^{o}C.
2. β-Lactamase enzyme (One unit of β-lactamase hydrolyzes 1.0 µmole of benzylpenicillin per minute at pH 7.0 at 25 ℃.)
3. HBSS
4. Culture medium without Penicillin (or any other β-lactam antibiotic)
5. 3 good and 3 not as good BLAST chips

Methods:

1. Seed cells onto BLAST chips (3 good ones and 3 not as good ones)
2. Dissolve 50 Units β-lactamase in 1 ml of HBSS. Also, do serial dilutions to prepare 10 U/ml and 1 U/ml β-lactamase in HBSS.
3. BLAST into the Chips as described in the table below:

CHIP	Condition	β-lactamase Concentration	Laser pulsing
A	Good	50 U/ml	YES
B	Good	10 U/ml	YES
C	Good	1 U/ml	YES
D	Not as good	50 U/ml	NO
E	Not as good	10 U/ml	NO
F	Not as good	1 U/ml	NO

4. Allow cell membranes to seal and cells to recover for 10 minutes.
5. Wash with HBSS 4-times to wash away non-internalized β-lactamase.
6. Replace last wash with fresh culture medium. Allow cells to recover for 1 - 2 hours. Then add substrate solution.
7. Prepare β-lactamase substrate solution:

   a. Thaw CCF4-AM solution (1 mM).

   b. Add 6 µl of solution A to 60 ul of Solution B (0.1 mM). Vortex.

   c. Add 934 µl of Solution C to the combined A+B solutions (6.6 µM). Vortex = "6X loading solution."

   d. Add 200 µl of "6X-loading solution" to 1 ml of culture medium 1X-loading solution = 1.1 µM
8. Replace cell culture medium with 1X-loading solution.
9. Incubate the cells for 4 - 5 hours at room temp in the dark.
10. View BLAST chips by confocal fluorescence using live imaging. Excite at 410 nm. Detect the non-hydrolyzed fluorescein (via FRET) at 520 nm and detect the hydrolyzed coumarin at ~450 nm.

References

1. Rusk, N. Seamless delivery. *Nat. Methods* **8**, 44-44 (2011).
2. Naldini, L. et al. In vivo gene delivery and stable transduction of nondividing cells by a lentiviral vector. *Science* **272**, 263-267 (1996).
3. Akin, D. et al. Bacteria-mediated delivery of nanoparticles and cargo into cells. *Nat. Nanotechnol.* **2**, 441-449 (2007).
4. Davidson, B.L. & Breakefield, X.O. Viral vectors for gene delivery to the nervous system. *Nat. Rev. Neurosci.* **4**, 353-364 (2003).
5. Thomas, C.E., Ehrhardt, A. & Kay, M.A. Progress and problems with the use of viral vectors for gene therapy. *Nat. Rev. Genet.* **4**, 346-358 (2003).
6. Brown, M.D., Schätzlein, A.G. & Uchegbu, I.F. Gene delivery with synthetic (non viral) carriers. *Int. J. Pharm.* **229**, 1-21 (2001).
7. Thomas, M. & Klibanov, A.M. Non-viral gene therapy: polycation-mediated DNA delivery. *Appl Microbiol Biotechnol* **62**, 27-34 (2003).
8. Glover, D.J., Lipps, H.J. & Jans, D.A. Towards safe, non-viral therapeutic gene expression in humans. *Nat. Rev. Genet.* **6**, 299-310 (2005).
9. Li, S.D. & Huang, L. Gene therapy progress and prospects: non-viral gene therapy by systemic delivery. *Gene Ther.* **13**, 1313-1319 (2006).
10. Mastrobattista, E., van der Aa, M.A.E.M., Hennink, W.E. & Crommelin, D.J.A. Artificial viruses: a nanotechnological approach to gene delivery. *Nat. Rev. Drug Discov.* **5**, 115-121 (2006).
11. Park, T.G., Jeong, J.H. & Kim, S.W. Current status of polymeric gene delivery systems. *Adv. Drug Deliver. Rev.* **58**, 467-486 (2006).
12. Morille, M., Passirani, C., Vonarbourg, A., Clavreul, A. & Benoit, J.-P. Progress in developing cationic vectors for non-viral systemic gene therapy against cancer. *Biomaterials* **29**, 3477-3496 (2008).
13. Felgner, P.L. et al. Lipofection: a highly efficient, lipid-mediated DNA-transfection procedure. *Proc. Natl. Acad. Sci. U. S. A.* **84**, 7413-7417 (1987).
14. De Smedt, S., Demeester, J. & Hennink, W. Cationic polymer based gene delivery systems. *Pharm Res* **17**, 113-126 (2000).
15. Plank, C., Zelphati, O. & Mykhaylyk, O. Magnetically enhanced nucleic acid delivery. Ten years of magnetofection—Progress and prospects. *Adv. Drug Deliver. Rev.* **63**, 1300-1331 (2011).

16. Mehier-Humbert, S. & Guy, R.H. Physical methods for gene transfer: improving the kinetics of gene delivery into cells. *Adv. Drug Deliver. Rev.* **57**, 733-753 (2005).
17. Al-Dosari, M. & Gao, X. Nonviral gene delivery: principle, limitations, and recent progress. *AAPS J* **11**, 671-681 (2009).
18. Escoffre, J.-M., Teissié, J. & Rols, M.-P. Gene transfer: how can the biological barriers be overcome? *J Membrane Biol* **236**, 61-74 (2010).
19. Kim, T. & Eberwine, J. Mammalian cell transfection: the present and the future. *Anal Bioanal Chem* **397**, 3173-3178 (2010).
20. Dean, D.A. & Gasiorowski, J.Z. Nonviral gene delivery. *Cold Spring Harb. Protoc.* **2011**, top101 (2011).
21. Kim, J. et al. Microfluidic approaches for gene delivery and gene therapy. *Lab Chip* **11**, 3941-3948 (2011).
22. Lakshmanan, S. et al. Physical energy for drug delivery; poration, concentration and activation. *Adv. Drug Deliver. Rev.* (2013).
23. Meacham, J.M., Durvasula, K., Degertekin, F.L. & Fedorov, A.G. Physical methods for intracellular delivery: practical aspects from laboratory use to industrial-scale processing. *J. Lab. Autom.* **19**, 1-18 (2014).
24. Somiari, S. et al. Theory and in vivo application of electroporative gene delivery. *Mol. Ther.* **2**, 178-187 (2000).
25. Guignet, E.G. & Meyer, T. Suspended-drop electroporation for high-throughput delivery of biomolecules into cells. *Nat. Methods* **5**, 393-395 (2008).
26. Boukany, P.E. et al. Nanochannel electroporation delivers precise amounts of biomolecules into living cells. *Nat. Nanotechnol.* **6**, 747-754 (2011).
27. Rae, J. & Levis, R. Single-cell electroporation. *Pflügers Arch - Eur J Physiol* **443**, 664-670 (2002).
28. Olofsson, J. et al. Single-cell electroporation. *Curr. Opin. Biotech.* **14**, 29-34 (2003).
29. Khine, M., Lau, A., Ionescu-Zanetti, C., Seo, J. & Lee, L.P. A single cell electroporation chip. *Lab Chip* **5**, 38-43 (2005).
30. Chen, C., Smye, S.W., Robinson, M.P. & Evans, J.A. Membrane electroporation theories: a review. *Med Bio Eng Comput* **44**, 5-14 (2006).
31. Fox, M.B. et al. Electroporation of cells in microfluidic devices: a review. *Anal Bioanal Chem* **385**, 474-485 (2006).
32. Kitamura, K., Judkewitz, B., Kano, M., Denk, W. & Hausser, M. Targeted patch-clamp recordings and single-cell electroporation of unlabeled neurons in vivo. *Nat. Methods* **5**, 61-67 (2008).

33. Valley, J.K. et al. Parallel single-cell light-induced electroporation and dielectrophoretic manipulation. *Lab Chip* **9**, 1714-1720 (2009).
34. Wang, M., Orwar, O., Olofsson, J. & Weber, S. Single-cell electroporation. *Anal Bioanal Chem* **397**, 3235-3248 (2010).
35. Huang, H. et al. An efficient and high-throughput electroporation microchip applicable for siRNA delivery. *Lab Chip* **11**, 163-172 (2011).
36. Movahed, S. & Li, D. Microfluidics cell electroporation. *Microfluid Nanofluid* **10**, 703-734 (2011).
37. Selmeczi, D., Hansen, T., Met, Ö., Svane, I. & Larsen, N. Efficient large volume electroporation of dendritic cells through micrometer scale manipulation of flow in a disposable polymer chip. *Biomed Microdevices* **13**, 383-392 (2011).
38. Xu, Y., Yao, H., Wang, L., Xing, W. & Cheng, J. The construction of an individually addressable cell array for selective patterning and electroporation. *Lab Chip* **11**, 2417-2423 (2011).
39. Adamo, A., Arione, A., Sharei, A. & Jensen, K.F. Flow-through comb electroporation device for delivery of macromolecules. *Anal. Chem.* **85**, 1637-1641 (2012).
40. Chen, S.-C. et al. Delivery of molecules into cells using localized single cell electroporation on ITO micro-electrode based transparent chip. *Biomed Microdevices* **14**, 811-817 (2012).
41. Jain, T., Papas, A., Jadhav, A., McBride, R. & Saez, E. In situ electroporation of surface-bound siRNAs in microwell arrays. *Lab Chip* **12**, 939-947 (2012).
42. Kang, W. et al. Nanofountain probe electroporation (NFP-E) of single cells. *Nano Lett.* **13**, 2448-2457 (2013).
43. Xie, X. et al. Nanostraw–electroporation system for highly efficient intracellular delivery and transfection. *ACS Nano* **7**, 4351-4358 (2013).
44. Kim, H.J., Greenleaf, J.F., Kinnick, R.R., Bronk, J.T. & Bolander, M.E. Ultrasound-mediated transfection of mammalian cells. *Hum. Gene Ther.* **7**, 1339-1346 (1996).
45. Mitragotri, S. Healing sound: the use of ultrasound in drug delivery and other therapeutic applications. *Nat. Rev. Drug Discov.* **4**, 255-260 (2005).
46. Kim, Y.-s., Rhim, H., Choi, M.J., Lim, H.K. & Choi, D. High-intensity focused ultrasound therapy: an overview for radiologists. *Korean. J. Radiol.* **9**, 291-302 (2008).
47. Longsine-Parker, W. et al. Microfluidic electro-sonoporation: a multi-modal cell poration methodology through simultaneous application of electric field and ultrasonic wave. *Lab Chip* **13**, 2144-2152 (2013).

48. Tao, W., Wilkinson, J., Stanbridge, E.J. & Berns, M.W. Direct gene transfer into human cultured cells facilitated by laser micropuncture of the cell membrane. *Proc. Natl. Acad. Sci. U. S. A.* **84**, 4180-4184 (1987).
49. Soughayer, J.S. et al. Characterization of Cellular Optoporation with Distance. *Anal. Chem.* **72**, 1342-1347 (2000).
50. Tirlapur, U.K. & Konig, K. Cell biology: Targeted transfection by femtosecond laser. *Nature* **418**, 290-291 (2002).
51. Clark, I.B. et al. Optoinjection for efficient targeted delivery of a broad range of compounds and macromolecules into diverse cell types. *BIOMEDO* **11**, 014034-014034-014038 (2006).
52. Stevenson, D. et al. Femtosecond optical transfection of cells: viability and efficiency. *Opt. Express* **14**, 7125-7133 (2006).
53. Cui-Ping, Y., Zhen-Xi, Z., Rahmanzadeh, R. & Huettmann, G. Laser-based gene transfection and gene therapy. *IEEE T. Nanobiosci.* **7**, 111-119 (2008).
54. Hellman, A.N., Rau, K.R., Yoon, H.H. & Venugopalan, V. Biophysical response to pulsed laser microbeam-induced cell lysis and molecular delivery. *J. Biophotonics* **1**, 24-35 (2008).
55. Chakravarty, P., Qian, W., El-Sayed, M.A. & Prausnitz, M.R. Delivery of molecules into cells using carbon nanoparticles activated by femtosecond laser pulses. *Nat. Nanotechnol.* **5**, 607-611 (2010).
56. Marchington, R.F., Arita, Y., Tsampoula, X., Gunn-Moore, F.J. & Dholakia, K. Optical injection of mammalian cells using a microfluidic platform. *Biomed. Opt. Express* **1**, 527-536 (2010).
57. Mthunzi, P., Dholakia, K. & Gunn-Moore, F. Phototransfection of mammalian cells using femtosecond laser pulses: optimization and applicability to stem cell differentiation. *BIOMEDO* **15**, 041507-041507-041507 (2010).
58. Stevenson, D.J., Gunn-Moore, F.J., Campbell, P. & Dholakia, K. Single cell optical transfection. *J. R. Soc. Interface* **7**, 863-871 (2010).
59. Wu, T.-H., Kalim, S., Callahan, C., Teitell, M.A. & Chiou, P.-Y. Image patterned molecular delivery into live cells using gold particle coated substrates. *Opt. Express* **18**, 938-946 (2010).
60. Compton, Jonathan L., Hellman, Amy N. & Venugopalan, V. Hydrodynamic determinants of cell necrosis and molecular delivery produced by pulsed laser microbeam irradiation of adherent cells. *Biophys. J.* **105**, 2221-2231 (2013).
61. Waleed, M. et al. Single-cell optoporation and transfection using femtosecond laser and

optical tweezers. *Biomed. Opt. Express* **4**, 1533-1547 (2013).

62. Fan, Q., Hu, W. & Ohta, A.T. Laser-induced microbubble poration of localized single cells. *Lab Chip* **14**, 1572-1578 (2014).
63. Li, Z.G., Liu, A.Q., Klaseboer, E., Zhang, J.B. & Ohl, C.D. Single cell membrane poration by bubble-induced microjets in a microfluidic chip. *Lab Chip* **13**, 1144-1150 (2013).
64. Sengupta, A., Kelly, S.C., Dwivedi, N., Thadhani, N. & Prausnitz, M.R. Efficient Intracellular Delivery of Molecules with High Cell Viability Using Nanosecond-Pulsed Laser-Activated Carbon Nanoparticles. *ACS Nano* **8**, 2889-2899 (2014).
65. Shalek, A.K. et al. Vertical silicon nanowires as a universal platform for delivering biomolecules into living cells. *Proc. Natl. Acad. Sci. U. S. A.* **107**, 1870-1875 (2010).
66. Han, S.-W. et al. High-efficiency DNA injection into a single human mesenchymal stem cell using a nanoneedle and atomic force microscopy. *Nanomed. Nanotech. Biol. Med.* **4**, 215-225 (2008).
67. Shalek, A.K. et al. Nanowire-Mediated Delivery Enables Functional Interrogation of Primary Immune Cells: Application to the Analysis of Chronic Lymphocytic Leukemia. *Nano Lett.* **12**, 6498-6504 (2012).
68. Xie, X. et al. Mechanical model of vertical nanowire cell penetration. *Nano Lett.* **13**, 6002-6008 (2013).
69. Wang, Y. et al. Poking cells for efficient vector-free intracellular delivery. *Nat. Commun.* **5** (2014).
70. Park, S., Kim, Y.-S., Kim, W.B. & Jon, S. Carbon nanosyringe array as a platform for intracellular delivery. *Nano Lett.* **9**, 1325-1329 (2009).
71. Daugimont, L. et al. Hollow microneedle arrays for intradermal drug delivery and DNA electroporation. *J Membrane Biol* **236**, 117-125 (2010).
72. Cai, D. et al. Highly efficient molecular delivery into mammalian cells using carbon nanotube spearing. *Nat. Methods* **2**, 449-454 (2005).
73. Peer, E., Artzy-Schnirman, A., Gepstein, L. & Sivan, U. Hollow Nanoneedle Array and Its Utilization for Repeated Administration of Biomolecules to the Same Cells. *ACS Nano* **6**, 4940-4946 (2012).
74. Persson, H. et al. Vertical oxide nanotubes connected by subsurface microchannels. *Nano Res.* **5**, 190-198 (2012).
75. Sharei, A. et al. A vector-free microfluidic platform for intracellular delivery. *Proc. Natl. Acad. Sci. U. S. A.* **110**, 2082-2087 (2013).
76. McNeil, P.L. & Warder, E. Glass beads load macromolecules into living cells. *J. Cell Sci.*

88, 669-678 (1987).

77. Emerson, N.T., Hsia, C.-H., Rafalska-Metcalf, I.U. & Yang, H. Mechanodelivery of nanoparticles to the cytoplasm of living cells. *Nanoscale* **6**, 4538-4543 (2014).
78. Zhang, Y. & Yu, L.-C. Single-cell microinjection technology in cell biology. *BioEssays* **30**, 606-610 (2008).
79. Capecchi, M.R. High efficiency transformation by direct microinjection of DNA into cultured mammalian cells. *Cell* **22**, 479-488 (1980).
80. Laffafian, I. & Hallett, M.B. Lipid-assisted microinjection: introducing material into the cytosol and membranes of small cells. *Biophys. J.* **75**, 2558-2563 (1998).
81. Chun, K. et al. in Micro Electro Mechanical Systems, 1999. MEMS '99. Twelfth IEEE International Conference on 406-411 (1999).
82. Matsuoka, H. et al. High throughput easy microinjection with a single-cell manipulation supporting robot. *J. Biotechnol.* **116**, 185-194 (2005).
83. Wang, W., Liu, X., Gelinas, D., Ciruna, B. & Sun, Y. A fully automated robotic system for microinjection of zebrafish embryos. *PloS one* **2**, e862 (2007).
84. Adamo, A. & Jensen, K.F. Microfluidic based single cell microinjection. *Lab Chip* **8**, 1258-1261 (2008).
85. Truong, H.H. et al. Automated microinjection of cell-polymer suspensions in 3D ECM scaffolds for high-throughput quantitative cancer invasion screens. *Biomaterials* **33**, 181-188 (2012).
86. Wu, T.-H. et al. Photothermal nanoblade for large cargo delivery into mammalian cells. *Anal. Chem.* **83**, 1321-1327 (2011).
87. Wu, T.-H., Teslaa, T., Teitell, M.A. & Chiou, P.-Y. Photothermal nanoblade for patterned cell membrane cutting. *Opt. Express* **18**, 23153-23160 (2010).
88. French, C.T. et al. Dissection of the *Burkholderia* intracellular life cycle using a photothermal nanoblade. *Proc. Natl. Acad. Sci. U. S. A.* **108**, 12095-12100 (2011).
89. Xu, J. et al. Nanoblade Delivery and Incorporation of Quantum Dot Conjugates into Tubulin Networks in Live Cells. *Nano Lett.* **12**, 5669-5672 (2012).
90. Nano, F.E. & Schmerk, C. The Francisella pathogenicity island. *Ann. N. Y. Acad. Sci.* **1105**, 122-137 (2007).
91. Hartland, G.V. Optical studies of dynamics in noble metal nanostructures. *Chem. Rev.* **111**, 3858-3887 (2011).
92. Link, S. & El-Sayed, M.A. Spectral properties and relaxation dynamics of surface plasmon electronic oscillations in gold and silver nanodots and nanorods. *J. Phys. Chem. B* **103**, 8410-8426 (1999).

93. Kotaidis, V., Dahmen, C., von Plessen, G., Springer, F. & Plech, A. Excitation of nanoscale vapor bubbles at the surface of gold nanoparticles in water. *J. Chem. Phys.* **124**, - (2006).
94. Lukianova-Hleb, E. et al. Plasmonic nanobubbles as transient vapor nanobubbles generated around plasmonic nanoparticles. *ACS Nano* **4**, 2109-2123 (2010).
95. Furlani, E.P., Karampelas, I.H. & Xie, Q. Analysis of pulsed laser plasmon-assisted photothermal heating and bubble generation at the nanoscale. *Lab Chip* **12**, 3707-3719 (2012).
96. Lynch, D.W., Olson, C.G. & Weaver, J.H. Optical properties of Ti, Zr, and Hf from 0.15 to 30 eV. *Phys. Rev. B* **11**, 3617-3624 (1975).
97. Yamane, D. et al. Electrical impedance monitoring of photothermal porated mammalian cells. *J. Lab. Autom.* **19**, 50-59 (2014).
98. Marquis, H., Doshi, V. & Portnoy, D.A. The broad-range phospholipase C and a metalloprotease mediate listeriolysin O-independent escape of Listeria monocytogenes from a primary vacuole in human epithelial cells. *Infect. Immun.* **63**, 4531-4534 (1995).
99. Clemens, D.L., Lee, B.-Y. & Horwitz, M.A. Virulent and avirulent strains of Francisella tularensis prevent acidification and maturation of their phagosomes and escape into the cytoplasm in human macrophages. *Infect. Immun.* **72**, 3204-3217 (2004).
100. Barker, J.R. et al. The Francisella tularensis pathogenicity island encodes a secretion system that is required for phagosome escape and virulence. *Mol. Microbiol.* **74**, 1459-1470 (2009).
101. Nano, F.E. et al. A Francisella tularensis pathogenicity island required for intramacrophage growth. *J Bacteriol* **186**, 6430-6436 (2004).
102. de Bruin, O.M. et al. The biochemical properties of the Francisella pathogenicity island (FPI)-encoded proteins IglA, IglB, IglC, PdpB and DotU suggest roles in type VI secretion. *Microbiology* **157**, 3483-3491 (2011).
103. Checroun, C., Wehrly, T.D., Fischer, E.R., Hayes, S.F. & Celli, J. Autophagy-mediated reentry of Francisella tularensis into the endocytic compartment after cytoplasmic replication. *Proc. Natl. Acad. Sci. U. S. A.* **103**, 14578-14583 (2006).
104. Chong, A. et al. Cytosolic clearance of replication-deficient mutants reveals Francisella tularensis interactions with the autophagic pathway. *Autophagy* **8**, 1342-1356 (2012).
105. Chiu, H.C. et al. Eradication of intracellular Francisella tularensis in THP-1 human macrophages with a novel autophagy inducing agent. *J. Biomed. Sci.* **16**, 110 (2009).
106. Qureshi, S.A. β-Lactamase: an ideal reporter system for monitoring gene expression in live eukaryotic cells. *BioTechniques* **42**, 91-95 (2007).

107. Lane, H.A. & Nigg, E.A. Antibody microinjection reveals an essential role for human polo-like kinase 1 (Plk1) in the functional maturation of mitotic centrosomes. *J. Cell Biol.* **135**, 1701-1713 (1996).
108. Mornet, S., Vasseur, S., Grasset, F. & Duguet, E. Magnetic nanoparticle design for medical diagnosis and therapy. *J. Mater. Chem.* **14**, 2161-2175 (2004).
109. Tseng, P., Judy, J.W. & Di Carlo, D. Magnetic nanoparticle-mediated massively parallel mechanical modulation of single-cell behavior. *Nat. Methods* **9**, 1113-1119 (2012).
110. Hu, M. et al. Gold nanostructures: engineering their plasmonic properties for biomedical applications. *Chem. Soc. Rev.* **35**, 1084-1094 (2006).
111. Michalet, X. et al. Quantum dots for live cells, in vivo imaging, and diagnostics. *Science* **307**, 538-544 (2005).
112. Derfus, A.M., Chan, W.C.W. & Bhatia, S.N. Intracellular Delivery of Quantum Dots for Live Cell Labeling and Organelle Tracking. *Adv. Mater.* **16**, 961-966 (2004).
113. Niidome, T. & Huang, L. Gene therapy progress and prospects: nonviral vectors. *Gene Ther.* **9**, 1647-1652 (2002).
114. Gómez-Martínez, R. et al. Intracellular silicon chips in living cells. *Small* **6**, 499-502 (2010).
115. Tasciotti, E. et al. Mesoporous silicon particles as a multistage delivery system for imaging and therapeutic applications. *Nat. Nanotechnol.* **3**, 151-157 (2008).
116. Chen, L.Y. et al. Mass fabrication and delivery of 3D multilayer μTags into living cells. *Sci. Rep.* **3** (2013).
117. Gomez-Martinez, R. et al. Silicon chips detect intracellular pressure changes in living cells. *Nat. Nanotechnol.* **8**, 517-521 (2013).
118. Kucsko, G. et al. Nanometre-scale thermometry in a living cell. *Nature* **500**, 54-58 (2013).
119. Zimmerman, J., Parameswaran, R. & Tian, B. Nanoscale semiconductor devices as new biomaterials. *Biomater. Sci.* (2014).